HEAT TRANSFER IN LEADING AND TRAILING EDGE COOLING CHANNELS OF THE GAS TURBINE BLADE UNDER HIGH ROTATION NUMBERS

A Dissertation

by

YAO-HSIEN LIU

Submitted to the Office of Graduate Studies of
Texas A&M University
in partial fulfillment of the requirements for the degree of

DOCTOR OF PHILOSOPHY

December 2008

Major Subject: Mechanical Engineering

HEAT TRANSFER IN LEADING AND TRAILING EDGE COOLING CHANNELS OF THE GAS TURBINE BLADE UNDER HIGH ROTATION NUMBERS

A Dissertation

by

YAO-HSIEN LIU

Submitted to the Office of Graduate Studies of
Texas A&M University
in partial fulfillment of the requirements for the degree of

DOCTOR OF PHILOSOPHY

Approved by:

Chair of Committee,	Je-Chin Han
Committee Members,	N. K. Anand
	S.C. Lau
	Hamn-Ching Chen
Head of Department,	Dennis O'Neal

December 2008

Major Subject: Mechanical Engineering

ABSTRACT

Heat Transfer in Leading and Trailing Edge Cooling Channels of the Gas Turbine Blade under High Rotation Numbers. (December 2008)

Yao-Hsien Liu, B.S., National Taiwan University;

M.S., Texas A&M University

Chair of Advisory Committee: Dr. Je-Chin Han

The gas turbine blade/vane internal cooling is achieved by circulating the compressed air through the cooling passages inside the turbine blade. Leading edge and trailing edge of the turbine blade are two critical regions which need to be properly cooled. Leading edge region receives extremely hot mainstream flow and high heat transfer enhancement is required. Trailing edge region usually has narrow shaped geometry and applicable cooling techniques are restricted. Heat transfer will be investigated in the leading edge and trailing edge cooling channels at high rotation numbers close to the engine condition.

Heat transfer and pressure drop has been investigated in an equilateral triangular channel (D_h=1.83cm) to simulate the cooling channel near the leading edge of the gas turbine blade. Three different rib configurations (45°, inverted 45°, and 90°) were tested at four different Reynolds numbers (10000-40000), each with five different rotational speeds (0-400 rpm). By varying the Reynolds numbers (10000-40000) and the rotational speeds (0-400 rpm), the rotation number and buoyancy parameter reached in this study

were 0-0.58 and 0-2.3, respectively. 45° angled ribs show the highest thermal performance at stationary condition. 90° ribs have the highest thermal performance at the highest rotation number of 0.58.

Heat transfer coefficients are also experimentally measured in a wedge-shaped cooling channel (D_h =2.22cm, A_c=7.62cm^2) to model an internal cooling passage near the trailing edge of a gas turbine blade where the coolant discharges through the slot to the mainstream flow. Tapered ribs are put on the leading and trailing surfaces with an angle of attack of 45°. The ribs are parallel with staggered arrangement on opposite walls. The inlet Reynolds number of the coolant varies from 10,000 to 40,000 and the rotational speeds varies from 0 to 500 rpm. The inlet rotation number is from 0 - 1.0. The local rotation number and buoyancy parameter are determined by the rotational speeds and the local Reynolds number at each region. Results show that heat transfer is high near the regions where strong slot ejection exists. Both the rotation number and buoyancy parameter have been correlated to predict the rotational heat transfer enhancement.

DEDICATION

To my parents and sister for their endless love, support, and encouragement

ACKNOWLEDGEMENTS

I am very grateful to Dr. J. C. Han for giving me the opportunity to do research in the area of gas turbine heat transfer. He has provided me valuable experience in this area through his teaching and research. I am appreciative that Dr. N. K. Anand, Dr. S.C. Lau and Dr. H. C. Chen have served on my committee and gave me suggestions on my research and dissertation. I also thank all the experienced partners in the lab who always gave me helpful advice and solutions.

NOMENCLATURE

A	projected surface area of a copper plate segment
A_j	cross sectional area of the slot
AR	channel aspect ratio, W:H
Bo_x	local buoyancy parameter, $(\Delta\rho/\rho)_x Ro^2 (R_x/D_h)$
C_D	discharge coefficient
D_h	channel hydraulic diameter
e	rib height
f	friction factor
f_o	fully-developed friction factor in non-rotating, smooth pipe
H	channel height
h	regionally averaged heat transfer coefficient
k	thermal conductivity of the coolant
L	length of the heated portion of the test section
L_e	length of the unheated portion of the inlet part
$\dot{m}_j$	mass flow rate through the j^{th} slot
$\dot{m}_n$	mass flow rate radially at the exit of the n^{th} region
$\dot{m}_{xn}$	local mass flow rate at the n^{th} region
Nu	regionally averaged Nusselt number
Nu_o	Nusselt number for fully-developed turbulent flow in non-rotating smooth pipe

Nu_s	regionally averaged Nusselt number under stationary condition
P	rib spacing
P_i	pressure at the inlet of the test section
P_o	pressure at the outlet of the test section
P_{in}	pressure at the inlet of the slot
P_{exit}	pressure at the exit of the slot
Pr	Prandtl number of the coolant
Q_{net}	net heat transfer
Q_{loss}	external heat loss
R	mean radius of rotation (from the center of rotation to center of heated channel)
R_x	local radius of rotation (from the center of rotation to local region within heated channel)
Re_x	local Reynolds number
Re_i	Reynolds number at the inlet of the test section
Ro_i	inlet Rotation number, $\Omega D_h/V_i$
Ro_x	local Rotation number, $\Omega D_h/V_x$
Ro	Rotation number, $\Omega D_h/V$
$T_{w,x}$	regionally averaged wall temperature
$T_{b,x}$	local coolant bulk temperature
$T_{f,x}$	local film temperature

V	bulk velocity of the coolant in the streamwise direction
V_i	bulk velocity of the coolant at the inlet of the test section
V_x	bulk velocity of the coolant at the local region
W	channel width
β	angle of channel orientation with respect to the axis of rotation
μ	viscosity of the coolant
ρ	density of the coolant
$(\Delta\rho/\rho)_{in}$	inlet coolant-to-wall density ratio, $(T_w-T_{bi})/T_w$
$(\Delta\rho/\rho)_x$	local coolant-to-wall density ratio, $(T_w-T_{bx})/T_w$
Ω	rotational speed

TABLE OF CONTENTS

Page

LIST OF FIGURES

Page

Page

LIST OF TABLES

1. INTRODUCTION

1.1 Gas Turbine Blade Internal Cooling

Internal cooling techniques for gas turbine blades have been studied for several decades. Gas Turbine Heat Transfer and Cooling Technology [1] provides in-depth information about updated cooling techniques. The internal cooling techniques of the gas turbine blade includes: jet impingement, rib turbulated cooling, and pin-fin cooling. Advanced internal cooling techniques are needed to prevent overheating of the turbine blade. Internal cooling is achieved by circulating compressed air in the multi-pass flow channels inside the blade structure. The internal cooling of the gas turbine blade is influenced by the channel aspect ratio, rib turbulator configurations, rotational and flow parameters. The cooling channels are either single-pass (with radial outward flow) or multi-pass (both radial outward and radial inward flow). Coolant is circulated through serpentine passages fabricated on the inside of the gas turbine blade in order to remove heat from the blade surface. Different aspect ratio channels are applicable to different parts of the turbine blade as shown in **Figure 1**.

1.2 Internal Cooling on the Leading Edge - Triangular Channel

The study of the gas turbine blade internal cooling begins from the stationary, rectangular cooling channels with the ribs placed on the walls of the cooling passage. Ribs trip the boundary layer of the coolant flow and enhance heat transfer at the cost of

---

This dissertation follows the style of *ASME Journal of Heat Transfer*.

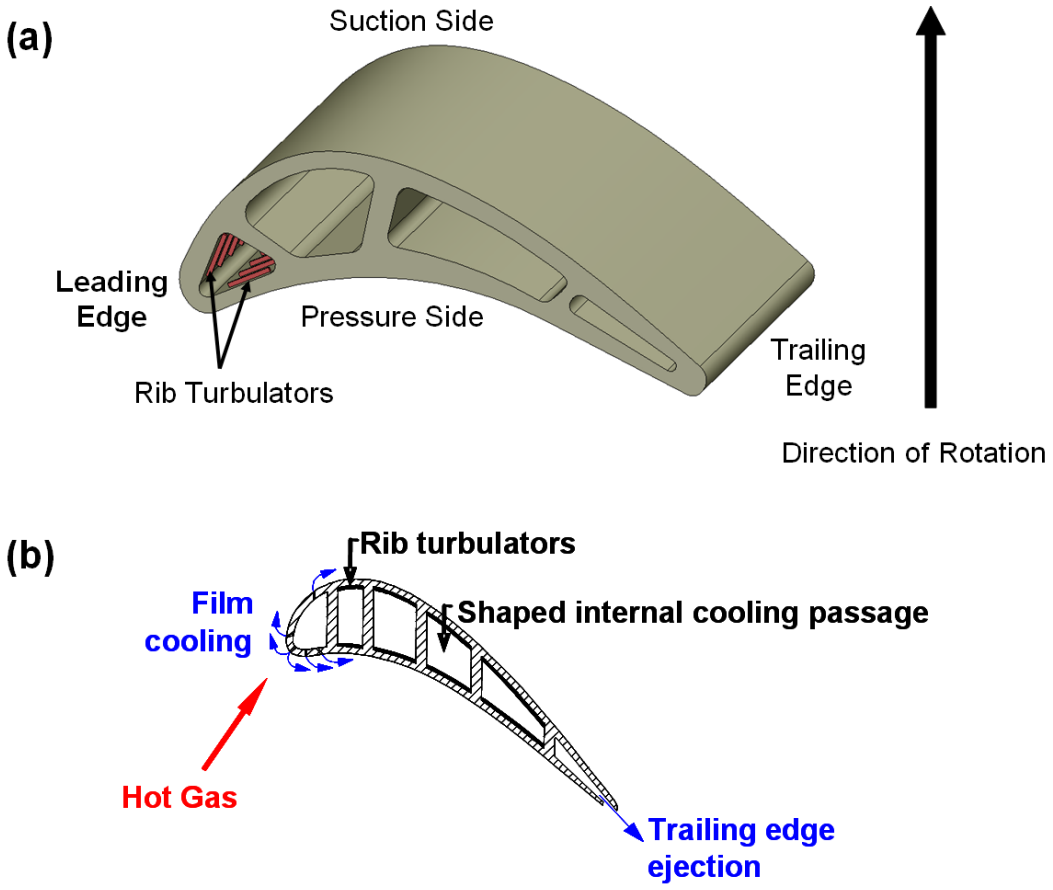

Figure 1: Internal Gas Turbine Blade Cooling Passage for (a) Leading Edge and (b) Trailing Edge

the higher pressure drop. The rib effects in the stationary channel as well as in the rotating channel have been done by several groups. Rib spacing, rib height, rib angle, and the shape of the ribs all affect the heat transfer enhancement. Han [2] measured the heat transfer and friction factor in a square duct with several rib configurations. Han [3] then extended the study to the heat transfer and pressure drop in the ribbed rectangular channels with five different aspect ratios (AR=4:1, 2:1, 1:1, 1:2, and 1:4). The results in the rectangular channel can be compared to the Dittus-Boelter correlation for the turbulent flow in a smooth tube by using the hydraulic diameter of the rectangular channel. Han and Zhang [4] studied the effect of rib-angle orientation on local mass transfer distribution in a three-pass rib-roughened square channel. They concluded that the angled ribs generally provide higher mass transfer coefficients than the transverse ribs and the parallel ribs give higher mass transfer than the crossed ribs. Taslim and Lengkong [5] investigated the staggered 45° angled ribs in a square channel. Three rib spacing-to-height ratios (5, 8.5, and 10), each with three height-to-passage hydraulic diameter ratios (0.133, 0.167, 0.25) were tested. They found out that for the 45° angled ribs in the staggered arrangements, the case for $P/e=10$ and $e/D_h=0.133$ had the best thermal performance. Taslim and Spring [6] used a liquid crystal technique to study the effects of rib profile, spacing, and blockage on the heat transfer coefficients in two rectangular channels with AR=0.5 and 0.55. They found that the sensitivity of the Nusselt number on P/e decreases as e/D_h increases. Liu et al [7] studied the rib spacing effects ($P/e=10$, 7.5, 5, and 3) in a rotating rectangular (AR=1:2) channel. They found out that the very close spacing of $P/e=3$ had the best thermal performance.

Leading edge of the gas turbine blade is a critical region due to high heat load. The triangular cooling channel is normally applied near the leading edge of the turbine blade to fit the blade profile. The measurements are also in good agreement with the correlations developed for the turbulent tube flow with the hydraulic diameter replacing the tube diameter. Metzger and Vedula [8] experimentally measured the heat transfer in triangular channels with angled ribs on two walls. They studied three different rib angles and three different sets of rib orientations. For all the test configurations, 60° angled ribs produce higher heat transfer than the 30° angled ribs, and *P*/e=7.5 rib spacing yield the best thermal performance. Ahn and Son [9] studied the heat transfer and pressure drop in a roughened equilateral triangular channel with *P*/e=4, 8, and 16. They concluded that the *P*/e=8 has the best thermal performance with the Reynolds number from 10000 to 70000. Haasenritter and Weigand [10] performed a computational study of the heat transfer in a rib-roughened triangular channel. The results show good agreement with the experimental data from [8]. Lee et al. [11] measured the heat transfer and pressure drop in a rotating equilateral triangular channel with three different rib arrangements: 45°, 90°, and 135°. They showed that the thermal performance for 45° and 135° angled ribs are very similar and both higher than the 90° ribs. Dutta et al. [12] studied the heat transfer in a two-pass rotating triangular duct. They studied two channel orientations to the direction of rotation. For the radially outward flow in the first pass, the Nusselt number ratios increase with rotation on the trailing wall and reduce on the leading wall. Zhang et al. [13] tested the heat transfer in a triangular duct with full and partial ribbed walls. They found out that the heat transfer coefficients and friction factors in triangular

ducts with partial ribbed walls (90° or 45° ribs) were 10% higher than those with fully ribbed walls.

The entrance geometry also affects the heat transfer distribution inside cooling channels. Kays and Crawford [14] summarized the works that consider the heat transfer in tubes with various entrance conditions. The Nusselt number in tubes with fully developed turbulent flow is also included. The widely accepted Dittus/Boelter – McAdams correlation for the fully developed turbulent flow in circular tubes can also be applied to the flow through channels with non-circular cross section. Wright et al. [15] studied the effect of entrance geometry on the heat transfer enhancement in a rotating rectangular channel (AR=4:1). They showed with the simultaneous development of both the hydrodynamic and thermal boundary layers, the Nusselt number ratios may not reach the fully developed values predicted by the Dittus/Boelter – McAdams correlation. The entrance geometry with re-directed sharp bend by Liu et al. [16] and the sudden contraction by Wright et al. [17] both showed that the heat transfer enhancement is higher than the fully developed flow condition.

In the actual turbine blade, the blade is rotating and the effect of rotation in the cooling channels should be considered. The secondary flow induced by rotation has great impact in the smooth channel as well as in the ribbed channel. Wagner et al. [18] performed heat transfer measurements inside a smooth square channel with radial outward flow in the first pass. The rotation number ranged from 0.00 to 0.48 in their studies. Wagner et al. [19] continued to investigate the heat transfer inside the second and third passage of the smooth square channel. The results from [18, 19] showed that

both the rotation number and density ratio caused large changes in heat transfer for radially outward flow but relatively small changes for radially inward flow. Johnson et al. [20] conducted the heat transfer measurement in a rotating square channel with ribs skewed to the flow and compared the results from the smooth channel. They showed that the heat transfer with skewed ribs is less sensitive to the buoyancy than the heat transfer inside the smooth channel or normal ribbed channel. Fu et al. [21] studied the buoyancy effects in five different aspect ratio channels (AR=4:1, 2:1, 1:1, 1:2, and 1:4) with two channel orientations (90° and 45° or 135°). The rotation numbers varied from 0.0 to 0.3. They showed that increasing the local buoyancy parameter increases the Nusselt number ratio on the trailing surface and decrease the Nusselt number ratio on the leading surface in the first pass for all channels.

The effect of rotation needs to be tested under high rotation numbers in order to simulate the actual engine condition. Zhou et al. [22] investigated the heat transfer in a 4:1 channel under high rotation numbers from 0-0.6. They concluded that there is a critical rotation number where the trend of the heat transfer enhancement begins to reverse. Liou et al. [23] investigated the heat transfer in a rectangular channel (AR=1:2) with 45° angled ribs under high rotation numbers from 0-2. They found out that the 45° staggered ribs generated overall heat transfer enhancement of 1.6-4.3 times higher than the Dittus-Boelter correlation in the Reynolds number range of 5000-15000. Liu et al. [15] also studied the heat transfer in a two-pass rectangular (AR=1:4) channel under high rotation numbers from 0-0.67. They found that the buoyancy parameter is also good to quantify the effect of rotation. Wright et al. [16] conducted the heat transfer

measurements in a wedge-shaped trailing edge channels under high rotation numbers from 0-1.0. It shows that the non-dimensional rotation number and buoyancy parameter not only can be used in the rectangular channel, but also valid in this wedge-shaped channel.

1.3 Internal Cooling on the Trailing Edge - Wedge Channel

Cooling channels near the leading edge could be tall and narrow, and channels closer to the trailing edge are typically wide and short. This wedge-shaped cooling channel is applicable near the trailing edge of the turbine blade. It is necessary to understand the behavior of the coolant through smooth, non-rotating channels before more complicated behavior can be fully interpreted. Turbulent flow through non-rotating, circular tubes has been thoroughly investigated by Kays and Crawford [14]. They summarized the heat transfer in tubes with various entrance conditions. The Nusselt number in tubes with fully developed turbulent flow is also given by Kays and Crawford [14]. The widely accepted Dittus-Boelter - McAdams correlation for fully developed turbulent flow was developed in circular tubes, but this correlation has also been applied to the flow through channels with non-circular cross-sections.

However, the actual turbine blade is rotating. The studies on the non-rotating channel have been extended to the rotating channel by several groups. Wagner et al. [18] show the heat transfer from the leading and trailing walls of a rotating channel are not symmetrical. In other words, in their square (AR=1:1) cooling channel with radially outward flow, the heat transfer from the trailing surface increases with rotation, while

the heat transfer from the leading surface decreases. Johnson et al. [20] extended this study of a square channel to investigate the effect of channel orientation with respect to the direction of rotation. When the channel is oriented non-orthogonally to the direction of rotation, the effect of rotation decreases; in other words, the difference between the heat transfer coefficients on the leading and trailing surfaces is reduced. Dutta and Han [24] confirmed this result in a rotating, square channel.

When the impact of rotation was realized, researchers sought more detailed heat transfer measurements. Park and Lau [25] used naphthalene sublimation to obtain detailed heat/mass transfer distributions in a rotating, two-pass, square channel. The detailed distributions indicated that the Coriolis forces create large spanwise variations on both the leading and trailing surfaces. Bons and Kerrebrock [26] gathered detailed heat transfer coefficient distributions using infrared thermography, and they completed these heat transfer measurements with flow field measurements (particle image velocimetry). In this rotating, single-pass, square channel, they concluded that the reduced heat transfer from the leading wall is the result of the Coriolis force transporting the hot, low momentum wall fluid from the trailing wall to the leading wall.

Cooling channels with different aspect ratios have been applied to different locations of the turbine blade, and the aspect ratio effect should be considered. Azad et al. [27] studied the combined effect of channel aspect ratio and channel orientation. Their finding for a 2:1 (width : height), two-pass channel were similar to a 1:1 channel: in the first pass with radially outward flow, the heat transfer from the leading surface decreased while the trailing surface increased, and the opposite occurs in the second-

pass. Also, the effect of rotation is reduced when the channel is skewed to the direction of rotation.

Channels located near the trailing edge of the blade have an even greater aspect ratio to fit into this narrow region of the blade. Several studies have focused on the effect of rotation in a 4:1 channel. Griffith et al. [28] observed significant spanwise variation in the heat transfer distributions due to rotation. Their results also showed that the channel orientation of the 4:1 channel has a small effect on the trailing surface and a large effect on the leading surface in this one-pass cooling channel. In the 4:1 channel oriented at 135° to the direction of rotation, the heat transfer from all surfaces in the channel is enhanced with rotation. Wright et al. [15] studied the effect of entrance geometry on the heat transfer enhancement in the rotating rectangular channel (4:1). They showed with the simultaneously development of both the hydrodynamic and thermal boundary layers, the Nusselt number ratios may not reach the fully developed values predicted by the Dittus-Boelter – McAdams correlation. Acharya et al. [29] used mass transfer technique to obtain detailed distribution in a two-pass 4:1 channel, and their findings were consistent with Griffith et al. [28]. Zhou et al. [22] considered the effect of rotation in a 4:1 channel with high rotation numbers. They concluded that there is a critical rotation number beyond which the expected heat transfer trends reverse. They also showed that increasing the density ratio increases the heat transfer enhancement. Fu et al. [21, 30] showed how the heat transfer enhancement varied in the smooth channels with five different aspect ratios depending on the channel cross-section, rotation number, and buoyancy parameter. Su et al. [31] performed a CFD study using a Reynolds Stress

Model for rotating rectangular channels (AR=1:1, 1:2, and 1:4). The rotation number ranged 0.0 to 0.28 with the channel at an orientation of 90^{o} relative to the axis of rotation. They concluded that for a large Reynolds and rotation number, the effect of rotation decreases continuously with decreasing aspect ratio.

The channels near the leading edge may have a triangular cross-section, while the channels near the trailing edge may also be triangular or trapezoidal. The heat transfer and friction coefficients measured in smooth equilateral triangles are in good agreement with the established correlations developed for the tube flow with hydraulic diameter of the triangular duct replacing the tube diameter [9, 32]. When the cross-section of the channel changes from an equilateral triangle to a scalene triangle, similar conclusions have been drawn. Obot [33] concluded that the heat transfer coefficients measured in the fully developed region of a scalene triangular duct are comparable to those predicted by the established Colburn equation for fully developed, turbulent flow through a smooth tube. Similar conclusions were drawn by Zhang et al. [34] with their right triangle duct; in their channel with smooth walls, the heat transfer coefficients were adequately predicted with the McAdams correlation while the friction factors could be established with the Blasius equation for turbulent flow through smooth tubes.

The effect of rotation on heat transfer has also been measured in triangular channels. Harasgama and Morris [35] concluded that effect of rotation in a triangular duct with radially outward flow can be estimated by correlations developed for circular tubes. Dutta et al. [12] showed that in the first pass of a triangular channel with radially

outward flow, the heat transfer coefficients on the trailing and side walls are enhanced with rotation, while the heat transfer coefficients on the leading surface decline.

The coolant through trailing edge cooling passages is likely to be extracted for trailing edge ejection, either through the discrete holes or slots, to further protect the trailing edge of the blade. Kumaran et al. [36] studied the heat transfer in a rectangular pin fin channel with short and long ejection holes. They found out that the heat transfer in the pin fin channel with sidewall ejection flow is about 25-30% lower than that with the straight flow. Taslim et al. [37] used a more realistic trapezoidal (wedge-shaped) channel with trailing edge ejection. They showed in a smooth, wedge-shaped channel, the average heat transfer coefficients were adequately predicted with the Dittus-Boelter correlation. They also showed that significant spanwise variation is present in this channel. However, when trailing edge ejection is introduced, this spanwise variation is reduced due to the lateral flow. Hwang and Lu [38] also studied the effect of trailing edge ejection in trapezoidal ducts. They confirmed that the fully developed heat transfer coefficients in the trapezoidal duct (without bleed flow) are comparable to those predicted by the Dittus-Boelter correlation. They also concluded that increase the ejection rate increases the heat transfer coefficients on the narrow side of the channel at the cost of reducing the heat transfer coefficients on the wide side of the channel. Lau et al. [39-41] investigated the heat transfer and pressure drop inside the pin-fin channel with ejection holes. Heat transfer coefficient decreases as the mainstream flow rate decreases. The ejection holes need to be configured so that the much of cooling air can

be forced to flow downstream in the radial direction before exiting the channel through ejection holes.

1.4 Objective

The thermal load near the leading edge of the blade is high and higher heat transfer enhancement is required to protect the components. Ribs will be put on the leading and trailing surfaces. Three rib configurations (45°, inverted 45°, and 90°) will be tested to see the heat transfer distribution. Although the effect of rotation has been studied by several groups, however, most of the data available in the open literature is low rotation number and low buoyancy parameter. The results on the high rotation number and buoyancy parameter are still very limited. The objectives are as follows:

1. Investigate the heat transfer distribution in the equilateral triangular channel under stationary and rotating conditions. Since the thermal load varies near the leading edge of the turbine blade, each surface of the channel is divided into two regions to provide individual heat transfer distribution during the tests.
2. Study the heat transfer and pressure drop inside the triangular channel with three different rib configurations (45°, inverted 45°, and 90°) at high rotation number and high buoyancy parameter.
3. The Reynolds numbers, the rotational speeds, and the density ratios (0.11-0.15) were varied in order to obtain a thorough understanding of the effects from the rotation number and buoyancy parameter. Correlation functions have been generated to predict the heat transfer enhancement for every rib configuration.

Most of the data available for the trailing edge cooling channel is on the rectangular shape. The wedge-shaped channel or trapezoidal channel is a more realistic design for a practical application but the studies on these channels are very limited. Moreover, available heat transfer results for the internal cooling channels are only at low rotation numbers. Effect of rotation on heat transfer in the wedge-shaped channel at high rotation numbers hasn't been thoroughly investigated, especially for the real engine design condition. In the actual blade, the coolant is ejected through the slots to the mainstream flow. In the current study, taper ribs with slot ejection will be tested to see the heat transfer enhancement at high rotation numbers. Based on the data available in the open literature, the objectives are as follows:

1. Study the effect of rotation in the trailing edge cooling channel with slot ejection, especially under high rotation numbers close to the engine condition. Tapered ribs with 45° angle of attack will be used to study heat transfer enhancement.
2. Current study also focuses on detailed heat transfer distribution with the ribs and slot ejection in the streamwise and spanwise directions.
3. With the coolant flow discharged through the slots, the coolant remaining in the cooling passage decreases. The variation of the coolant flow remaining in the channel needs to be determined to investigate the effect on heat transfer enhancement and the effect of rotation.
4. The Reynolds number (10000–40000) and the rotational speed (0-500 rpm) are varied in order to obtain a thorough understanding of the effects of the rotation

number and buoyancy parameter. These two non-dimensional parameters will be tested to quantify the effect of rotation in the smooth channel and ribbed channel.

2. EXPERIMENTAL SETUP

2.1 Rotating Facility

The study of the heat transfer inside the rotating cooling channel is performed in a rotating facility as shown in **Figure 2**. The coolant air comes in from the bottom of the rig through the rotary union into the hollow shaft. The air continues to travel through the hub to a rubber hose and comes into the pressure vessel containing the test section. After the air passes through the heated test section, the air goes through another rubber hose to a copper tubing inside the slip ring. The copper tubing connected to the second rotary union at the top of the slip ring and then expels to the outside. A needle valve is attached to the pipe to adjust the pressure of the flow loop. A motor is used to drive the shaft with a frequency controller to control the rotational speeds from 0 – 400 rpm. A 100 channel slip-ring is used as an interface to transfer the data reading from the rotating test section to the data acquisition system.

The typical rotation number of the aircraft engine is in the range of 0 - 0.25. One method of obtaining the desired range of rotation numbers with the applicable Reynolds numbers is to run the laboratory experiments at increased pressures. With the coolant pressurized above atmospheric pressure, at a given mass flow rate (Reynolds number), the density increases while the coolant velocity decreases. The decreased velocity yields increased rotation numbers. With the air pressurized at 5 times of the atmospheric pressure, the rotation number reached in this study in the triangular channel is shown in **Fig. 2**.

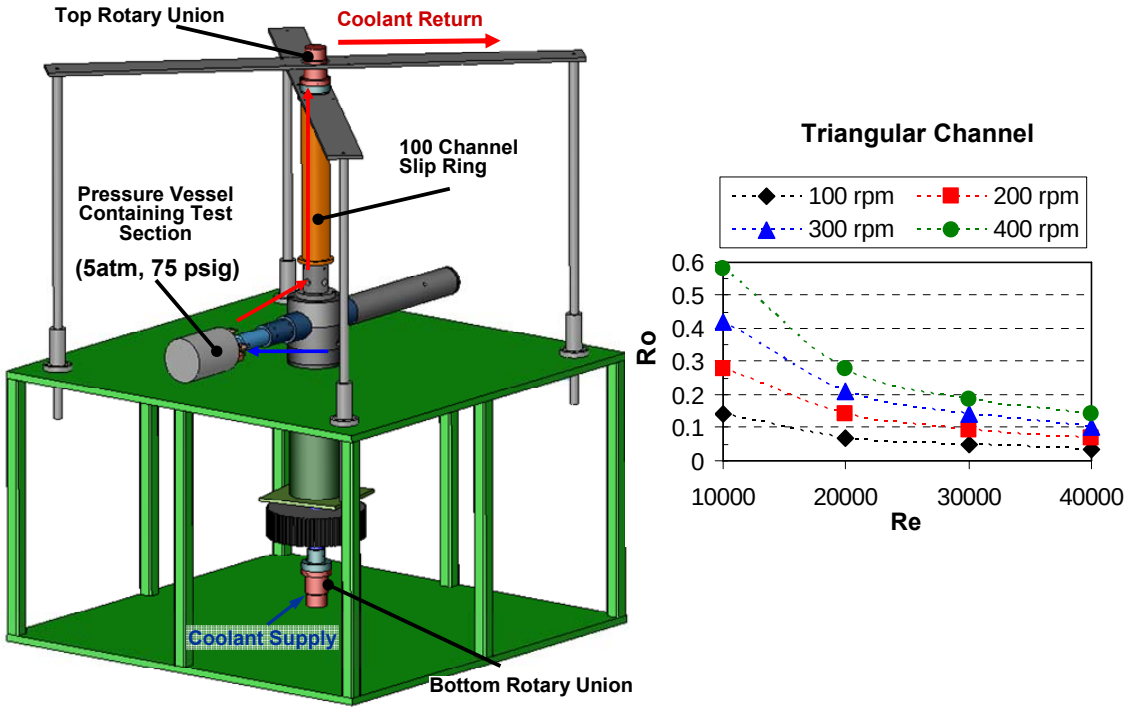

Figure 2: Rotating Facility

2.2 Triangular Test Section with Ribs

The equilateral triangular test section used in the current study is shown in **Figure 3(a)**. The coolant air comes from a 1.27 cm diameter pipe into the inlet part. Two mesh screens are placed on the inlet part to help spread the flow. The thickness of the inlet part is 3.81 cm with the L_e/D_h=2.09. The inlet part has a slot with the same cross section as the triangular test section and is fully attached to the test section parts. The flow goes radially outward into the test section and discharges into the cavity of the pressure vessel then back to the flow loop. Two pressure taps were placed at the inlet and another two pressure taps were placed at the outlet to measure the pressure drop across the ribbed channel.

The equilateral triangular test section consists of three parts: leading, trailing, and the inner walls as shown in **Figure 3(b)**. These three pieces are made of Garolite and the thickness of each piece is 2.54 cm. Two rows of copper plates are instrumented in each wall. The size of each copper plate is 1.35 cm wide by 1.11 cm high and the thickness is 0.476 cm. The copper plates on the leading and trailing surfaces are in staggered arrangement. The gaps between the copper plates are filled with silicon as an insulation layer. A blind hole is drilled in each copper plate and the thermocouple is glued in each hole by the epoxy. Electric resistant heaters are placed beneath the copper plates in each row. In other words, total of six heaters are used to heat up L1, L2, T1, T2, and two inner wall regions. The insulating material of the test section reduces the heat loss from the heaters to the supporting material. In the current study, the ribs are glued on the leading

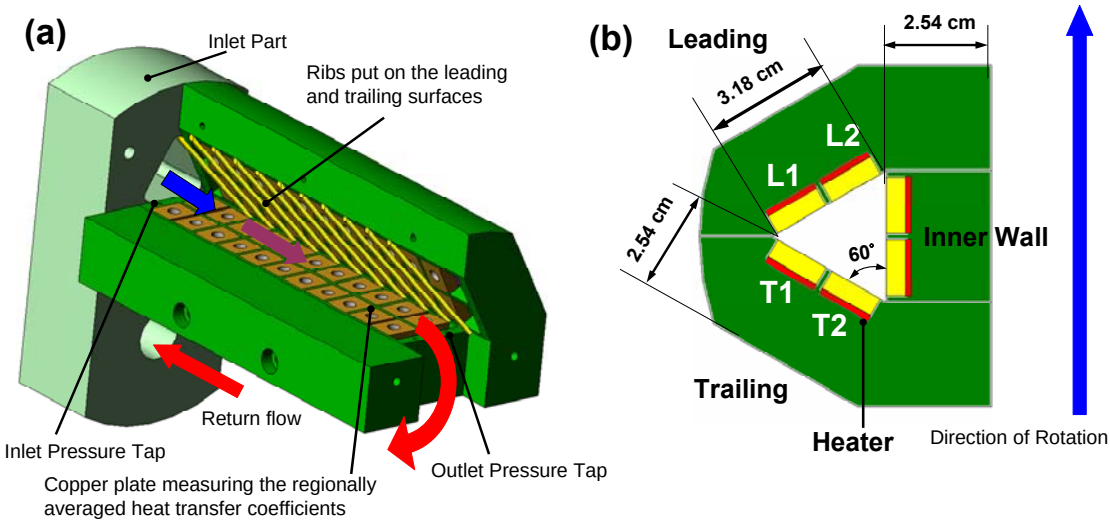

Figure 3: (a) Details of the Triangular Test Section, (b) Cross Sectional View of the Test Section

and trailing surfaces only by the super glue. The square ribs are made of brass with the cross section of 1.59 mm by 1.59 mm. Three different rib configurations are tested with the same *P*/e ratio of 8 and the e/D_h ratio of 0.087. The channel orientation is 90° to the direction of rotation. **Figure 4** shows these three rib configurations (45°angled, inverted 45° angled, and 90° orthogonal). Due to the staggered arrangement of the copper plates, the ribs on the leading surface and trailing surface are also staggered. In order to eliminate the conduction effects caused by the continuous ribs across different surfaces, insulation is filled between the gaps as shown in **Fig. 4**.

2.3 Wedge Test Section with Tapered Ribs and Slot Ejection

For the wedge-shaped channel, four different configurations were tested in the current study. The test begins with a smooth surface where the flow returns through a turn region to the second pass as shown in **Figure 5(a)**. Although only the first pass (radially outward) of the test section is instrumented for heat transfer measurements, a second pass is needed to return the flow, and maintain the desired pressure within the test section. This serves as a baseline test for the wedge-shaped channel. The experiment then extends to the slot ejection case as shown in **Figure 5(b)**. The first pass of the channel is dead ended and thus all the flow discharges through these six slots into the second pass. The flow ejected from the six slots then travels through the second pass back to the flow loop. The length of the unheated entrance region is 4.76 cm. The heated length of the channel is 15.56 cm with a hydraulic diameter of 2.25 cm. This gives an overall heated length-to-hydraulic diameter ratio (L/D_h) of 6.30.

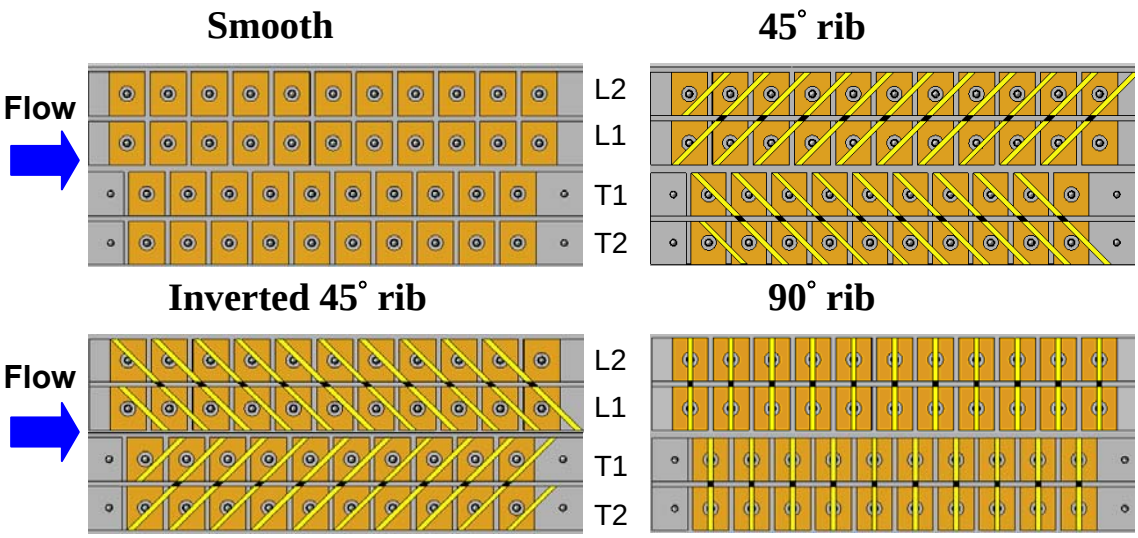

Figure 4: Rib Configurations of the Current Study

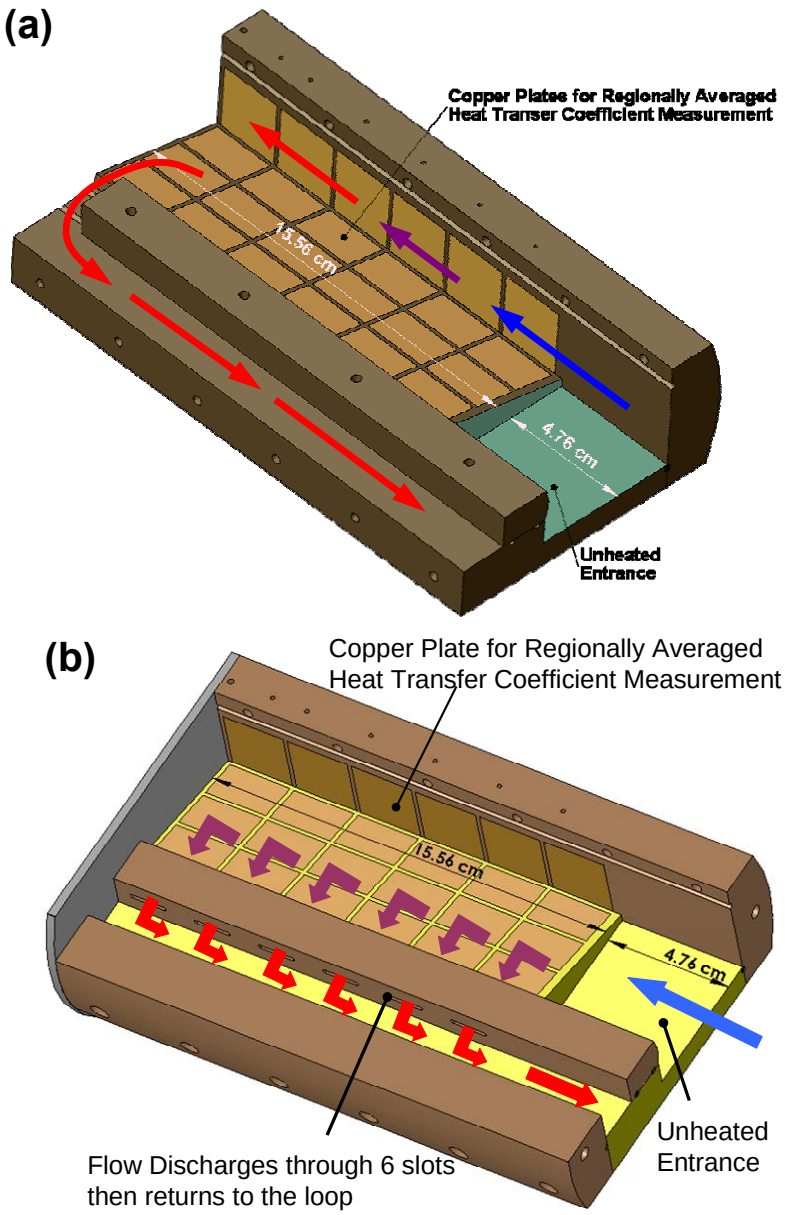

Figure 5: Wedge-Shaped Test Section Details on Smooth Surface (a) without Slot Ejection and (b) with Slot Ejection

The cross-section of the channel is wedge (or trapezoid). The side wall (close to the middle portion of the blade) is 2.54 cm tall, and the cross-section narrows to 0.32 cm near the trailing edge of the blade. The distance from the inner-most side to the outer-most side is 5.28 cm. If the channel were extended to form an isosceles triangle, the apex angle of the triangle would be 23.5°. Six slots were machined at the narrow side as shown in **Figure 6.** The width and the length of each slot are 0.16 cm and 1.27 cm, respectively. The distance between each slot is 1.27 cm. The distance from the center of rotation to the center of the heated channel is 67.8 cm. The air enters an unheated entrance with a rectangular cross-section of 5.38 cm wide by 3.18 cm tall. Two mesh screens are positioned in this entrance region to help spread the flow before it reaches the heated portion of the test section. With this entrance configuration, the air is forced through a sudden contraction before it enters the heated test section. Obviously, with the wedge-shaped cross-section, the contraction ratio is much greater near the outer wall (9.9:1) of the test section than the inner wall (1.25:1).

The mass flow rate ejecting through each slot is influenced by the returning crossflow and thus heat transfer inside the test section is also affected. This strong returning crossflow can be eliminated by discharging the flow into the bigger plenum and then returns to the loop as shown in **Figure 7(a)**. Only the first pass (radially outward) of the test section is instrumented for heat transfer measurements. The first pass of the channel is dead ended and thus all the flow discharges through these six slots into the plenum and then back to the flow loop.

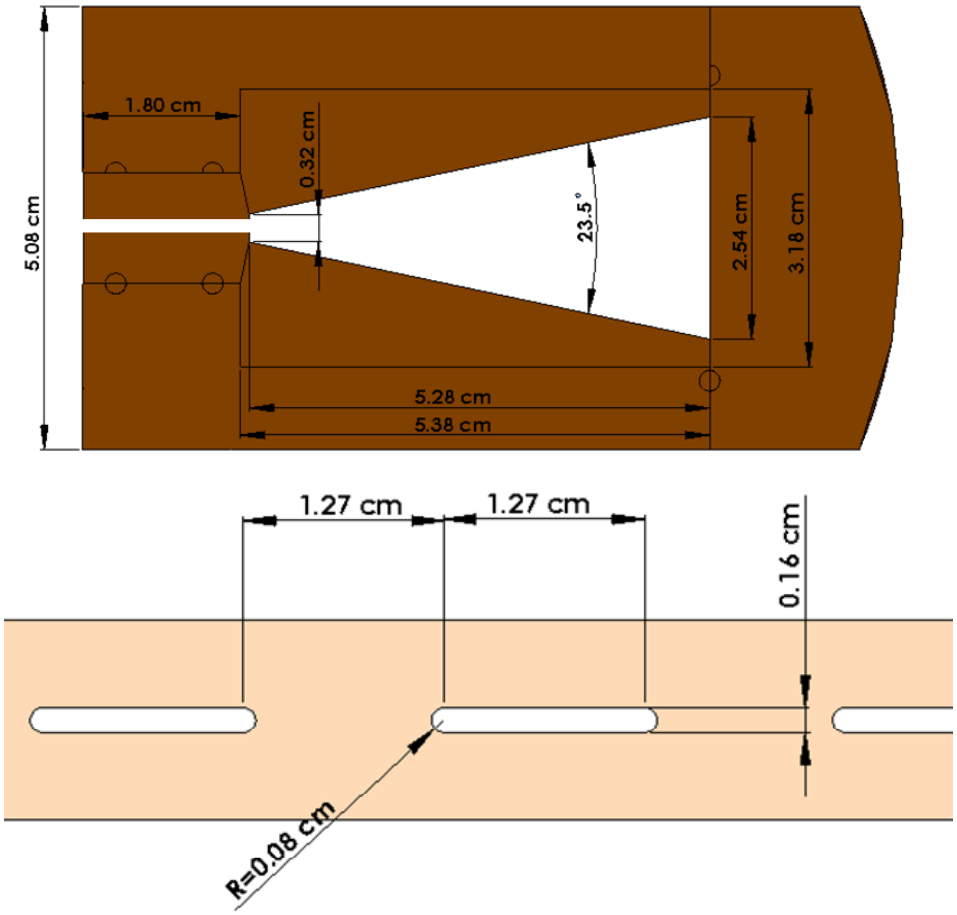

Figure 6: Cross Sectional View of the Test Section with Slot

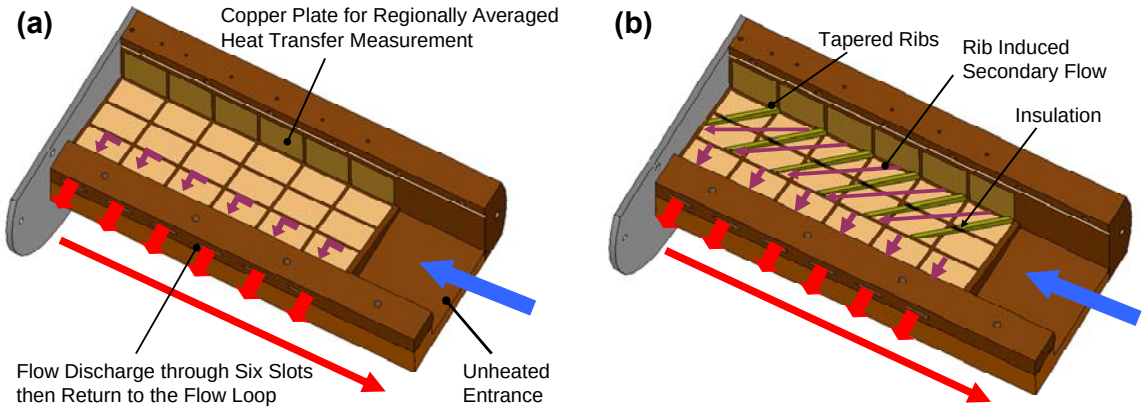

Figure 7: Wedge-Shaped Test Section without Returning Cross Flow for (a) Smooth Surface and (b) Ribbed Surface

Tapered rib turbulators were put on the leading and trailing surfaces of this test section as shown in **Figure 7(b)**. The tapered rib extended from the inner surface to the mid-span to improve heat transfer. In order to eliminate the conduction problem, insulation is filled between the ribs across the copper plate. The cross section view of this ribbed test section is shown in **Figure 8**. Those tapered ribs were in parallel arrangement but staggered on the opposite walls. The angle of attack of this tapered rib is 45° with pitch to maximum height ratio (P/e_{max}) of 8. The maximum rib height to hydraulic diameter ratio (e_{max}/D_h) is 0.143 and the rib height to channel height ratio (e/H) is maintained at 0.125. The length of the rib is 4.75cm with a cross section of 3.18mm by 3.18mm on the wide side and a cross section of 3.18mm by 1.38mm on the narrow side. The ribs are made of brass and are glued to the copper plates by the super glue.

To measure the heat transfer variation across the width (or span) of the channel, both the leading and trailing surfaces are divided into three regions. **Figure 9** shows how these six regions combined with the inner side wall, give a total of seven regionally averaged heat transfer coefficient measurements. Each region consists of a single copper plate with 0.318 cm thickness. Each copper plate has a 0.159 cm blind hole in the backside with thermocouple mounted in the hole with high conductivity thermal epoxy. Six regions are used in the streamwise (flow) direction, so a total of forty-two regions comprise the test section. The outer-most wall (near the trailing edge) is left un-instrumented for the slot ejection in the current study.

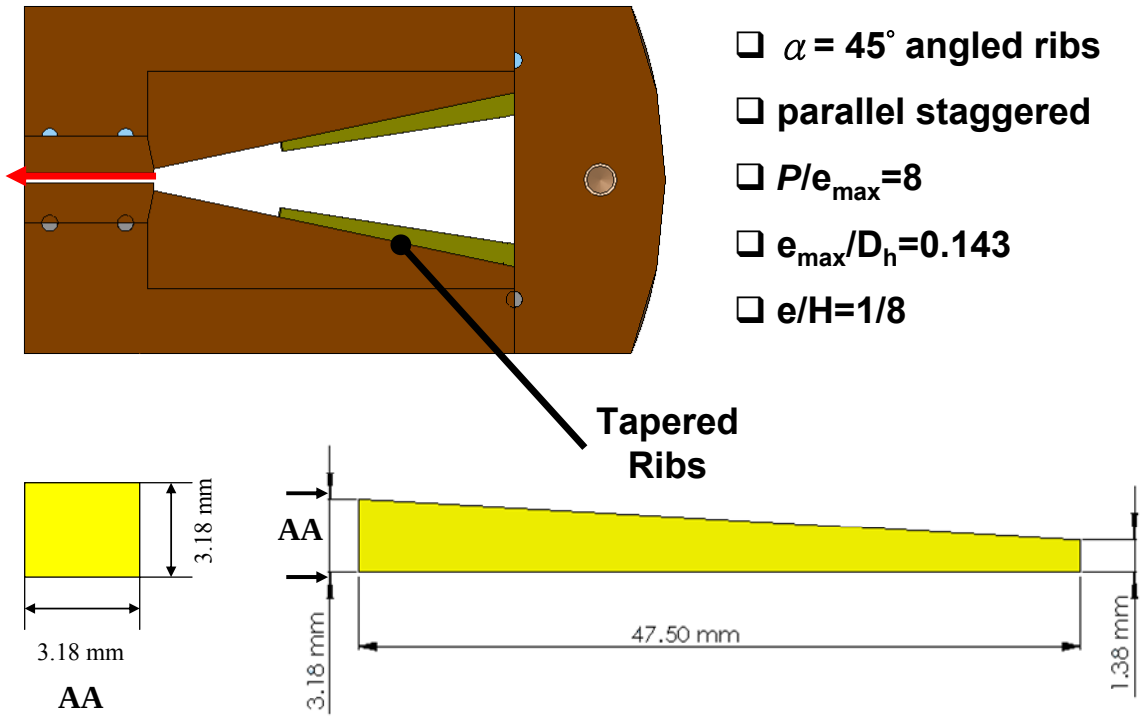

Figure 8: Tapered Rib Configuration

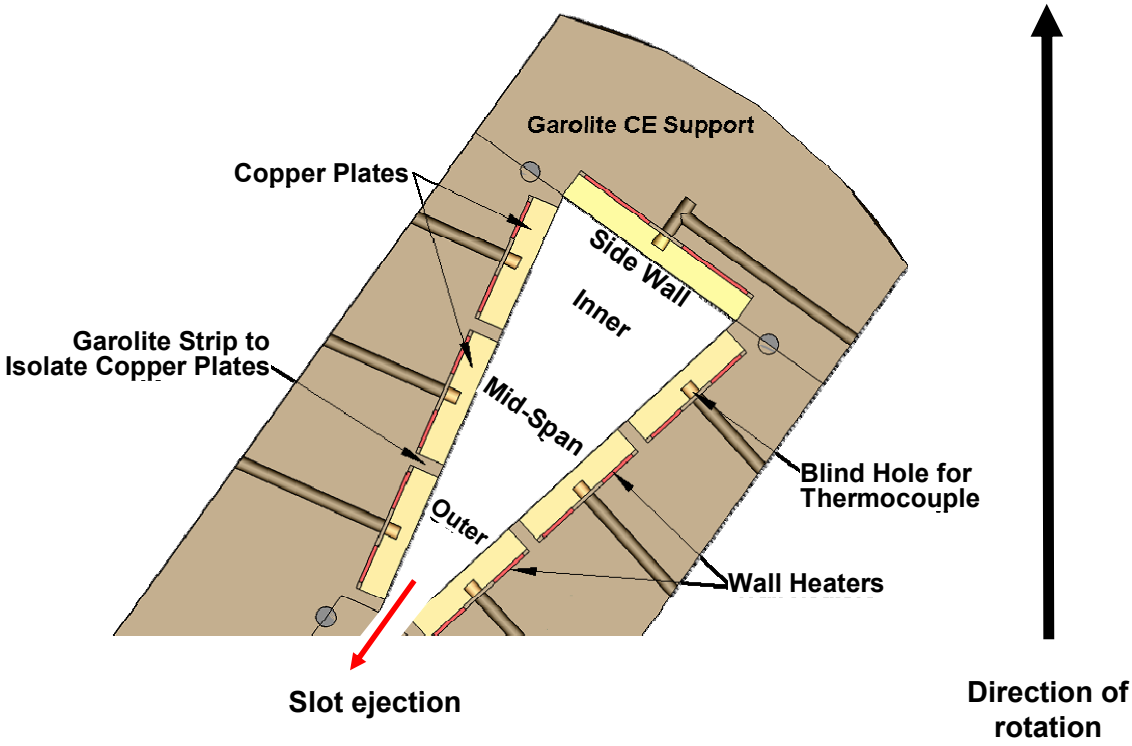

Figure 9: Schematics of the Wedge-Shaped Test Section

Electric resistance heaters are fixed beneath the copper plates. One heater services six copper plates; each spanwise region has an individual heater. In other words, one heater is used to heat all six copper plates of the side wall, and one heater is used for the six plates of the trailing-inner surface, and so on. High conductivity thermal paste is applied to each heater to minimize the contact resistance between the heater and the copper plates. The copper plates are mounted in the test section support structure which is fabricated from grade CE garolite. The insulating material reduces the heat loss from the heaters to the supporting material. The test section is assembled and placed in the pressure vessel. Additional insulating material is used to fill the air gaps between the test section and the wall of the pressure vessel. Pressure taps are instrumented at the inlet and exit of the slots and are connected to inclined manometer for pressure drop measurement.

The coolant air enters the test section at six times the atmospheric pressure; this pressure is maintained for all cases, both stationary and rotating. The Reynolds number at the inlet is controlled at 10000, 20000, 30000, and 40000. The channel is orientated 135° to the direction of rotation. The rotational speed of the channel is varied from 0 to 500 rpm.

3. DATA REDUCTION

3.1 Heat Transfer Measurement

As described with the experimental setup, regionally averaged heat transfer coefficients are measured in the current study. The heat transfer coefficients can be determined from Newton's Law of Cooling as demonstrated in Equation 1.

$$h = \frac{\dot{Q}_{net}}{A\left(T_{w,x} - T_{b,x}\right)} = \frac{\dot{Q}_{in} - \dot{Q}_{loss}}{A\left(T_{w,x} - T_{b,x}\right)} \tag{1}$$

The net rate of heat transfer is determined from the difference of the power supplied to each resistance heater and the heat lost from the test section. The heat loses are determined from a series of calibration where insulation is inserted into the channel. Power is supplied by the heaters, and the power required to reach a series of given temperatures is recorded. With the insulating material placed inside the channel, natural convection is eliminated. The power supplied to the heaters during this calibration is equivalent to the heat lost during the actual cooling trials. Separate heat loss calibrations are required for each rotational speed.

The regional wall temperature ($T_{w,x}$) is measured using the thermocouple fixed in each copper plate. The coolant bulk temperature at a specific location ($T_{b,x}$) in the channel is determined based on the measured inlet and outlet temperatures. With thermocouples placed in the flow in the inlet section and the exit, the inlet and outlet bulk temperatures are known. Therefore, the temperature of the coolant at any location within the channel can be calculated using linear interpolation.

The measured heat transfer coefficients can be represented by the non-dimensional Nusselt number. Although the Nusselt number is useful to extend the results from the laboratory to actual engine, it is often more useful to normalize the Nusselt number in order to quantify the heat transfer enhancement (or declination) due to either the specific channel geometry or rotation. The Nusselt number ratio (Nu/Nu_o) is used to show the heat transfer enhancement relative to fully developed, turbulent heat transfer in a circular tube. This fully developed, turbulent heat transfer can be expressed with the Dittus-Boelter - McAdams correlation for heating. Equation 2 shows this Nusselt number ratio.

$$\frac{Nu}{Nu_o} = \left(\frac{hD_h}{k}\right)\left(\frac{1}{0.023\,\mathrm{Re}^{0.8}\,\mathrm{Pr}^{0.4}}\right) \tag{2}$$

3.2 Friction Factor Ratio and Thermal Performance

In order to measure the friction factor, the pressure difference between the inlet and the outlet must be obtained. The friction factor can be calculated from the pressure drop between the inlet and the outlet of the channel as shown in Equation 3.

$$f = \left(P_i - P_o\right) \Big/ 4\left(\frac{L}{D_h}\right)\frac{1}{2}\rho V^2 \tag{3}$$

The inlet pressure, P_i, is taken as the average of the two pressure measurements at the channel entrance, and the outlet pressure, P_e, is average of the two pressure measurements at the channel outlet.

The frictional losses can then be calculated by dividing the fiction factor by the turbulent friction factor in a smooth tube as given by the Blasius equation. With the

friction factor in a smooth tube defined in equation 4, the friction factor ratio can be expressed in terms of the measured friction factor, and the smooth channel friction factor, as shown in equation 5.

$$f_0 = 0.079\mathrm{Re}^{-0.25} \tag{4}$$

$$f / f_0 = f / 0.079\mathrm{Re}^{-0.25} \tag{5}$$

Based on the heat transfer enhancement (Nu/Nu_o) and the frictional loss penalty (f/f_o), the thermal performance (η) for a given rib configuration can be calculated. Equation 6 shows the thermal performance based on the constant pumping power condition.

$$\eta = (Nu / Nu_0) / (f / f_0)^{1/3} \tag{6}$$

3.3 Local Mass Flow Rate Measurement

The local mass flow rate decreases along the streamwise direction due to slot ejection in the wedge-shaped channel, and the coolant flow remaining in the channel needs to be determined in order to obtain the accurate Nu_o. The estimated mass flow rate through j^{th} slot can be calculated by Equation 3 from Kumaran et al. [36].

$$\dot{m}_j = C_D A_j \left[2\rho \left(P_{in} - P_{exit} \right) \right]^{1/2} \tag{7}$$

C_D is the discharge coefficient, and A_j is the cross-sectional area of the slot. The density is obtained by the pressure and bulk temperature at each location. The pressure is measured by the pressure taps at the inlet and exit of the slot. The bulk temperature is obtained by the linear interpolation of the inlet temperature and outlet temperature of the channel. The sum of the mass flow rate through these 6 slots is equal to the total mass

flow rate at the inlet of the channel. A constant discharge coefficient among these six slots is assumed, so the ratio of the mass flow rate radially into the nth region to the inlet mass flow of the channel can be determined by Equation 8.

$$\frac{\dot{m}_n}{\dot{m}} = 1 - \frac{\sum_{n=1}^{n-1} \dot{m}_j}{\dot{m}} \tag{8}$$

$\sum \dot{m}_j$ is the sum of the mass flow rate through the slots upstream of the nth region at which the value of $\dot{m}_n$ is to be calculated, and $\dot{m}$ is the mass flow rate at the inlet. There are total of 6 regions in the streamwise direction within the channel. The local mass flow rate in each region (at x) of the channel is the average of the radially inlet and radially outlet mass flow in that region as shown in Equation 9.

$$\frac{\dot{m}_x}{\dot{m}} = \frac{\dot{m}_{n-1} + \dot{m}_n}{2\dot{m}} \tag{9}$$

3.4 Uncertainty Analysis

The experimental uncertainty for the presented results was calculated using the method developed and published by Kline and McClintock [42]. Air properties were taken based on the mean bulk air temperature. The estimated uncertainty for the temperature measurements is 0.5 °C.

The uncertainty for the temperature measurement in the triangular channel is 0.3°C. The uncertainty of the Nusselt number ratio is approximately 4.9% for the highest Reynolds number (Re=40000). For the lowest Reynolds number (Re=10000), the

maximum uncertainty is approximately 9.8%. The maximum uncertainty for the friction factor ratio is 9.7% at Re=10000 and drops to 4.8% at Re=40000.

In the wedge-shaped channel, the most uncertainty exists in the measured quantities at the inlet Reynolds number of 10000. The overall uncertainty in the Nusselt number ratio is approximately 16.9% of the presented values. However, at the higher Reynolds numbers, the percent uncertainty of the individual measurements decreases. The overall uncertainty in the Nusselt number ratio decreases to approximately 5.8% of the calculated value at the highest inlet Reynolds number of 40000.

4. RESULTS AND DISCUSSION

4.1 Leading Edge – Triangular Channel

4.1.1 Heat Transfer in Stationary Channel

Heat transfer is influenced by the channel geometry and the flow condition inside the stationary channel. In the current setup, the coolant flow goes through an unheated short entrance (L_e/D_h=2.09) and then into the heated test section. The boundary layer begins to develop along the strewmwise direction and the developing flow condition is expected in this channel. In order to study the heat transfer enhancement, the Nusselt number ratio (Nu/Nu_o) is considered. Nu_o is the Dittus-Boelter correlation using the hydraulic diameter of the triangular channel replacing the tube diameter. When the surface has been roughened with ribs, the ribs trip the flow and the flow reattaches to the hot surface. For the angled ribs, they not only trip the flow but also induced a secondary flow along the rib orientations. Heat transfer will be further enhanced by the rib induced secondary flow as shown **Figure 10**. The secondary flow induced by 45° angled ribs goes from the rib leading region (L1 and T1) towards the rib trailing region (L2 and T2). The strength of this secondary flow decreases along the rib orientation. The secondary flow tends to impinge on the rib leading region (L1 and T1). Therefore, the heat transfer enhancement is higher in the rib leading region (L1 and T1) than the rib trailing region (L2 and T2). For inverted 45° angled ribs, the secondary flow structure is reversed as the rib is inverted. The rib induced secondary flow tends to impinge on the L2 and T2 region and the heat transfer enhancement is higher on the L2 and T2 than the L1 and T1 regions.

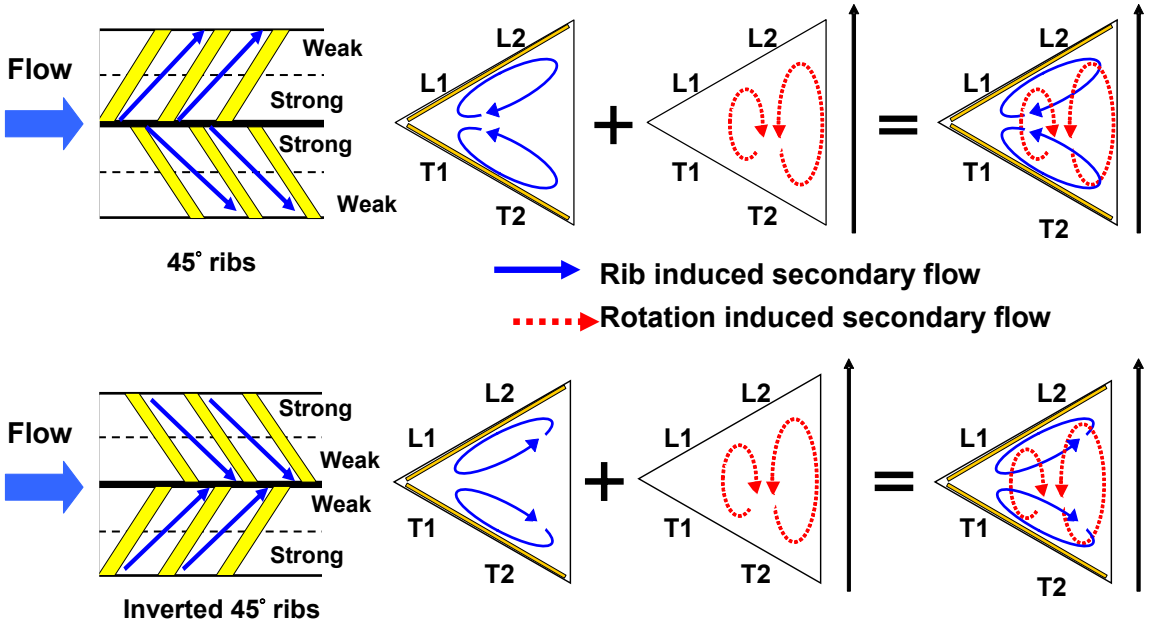

Figure 10: Conceptual View of the Rib and Rotation Induced Secondary Flow

Figure 11 shows the Nusselt number ratio comparisons in the stationary triangular channel with smooth walls and ribbed walls at Re=20000. Each data point of the current study is the average of the two points on the leading or trailing surfaces. The data from Metzger and Vedula [8] was also tested in an equilateral triangle channel with 60° angled ribs with P/e=7.5. An identical smooth channel with L_e/D_h=10.39 was installed upstream of their test section as a flow-developing section. However, the unheated region in the current study is much shorter (L_e/D_h=2.09). The coolant flow is in the developing condition and the boundary layer is much thinner. Therefore, the Nusselt number ratios (Nu/Nu_o) in the current study are higher than the results from Metzger and Vedula [8] but the trends of these two are very similar. As stated in [8], the angled rib

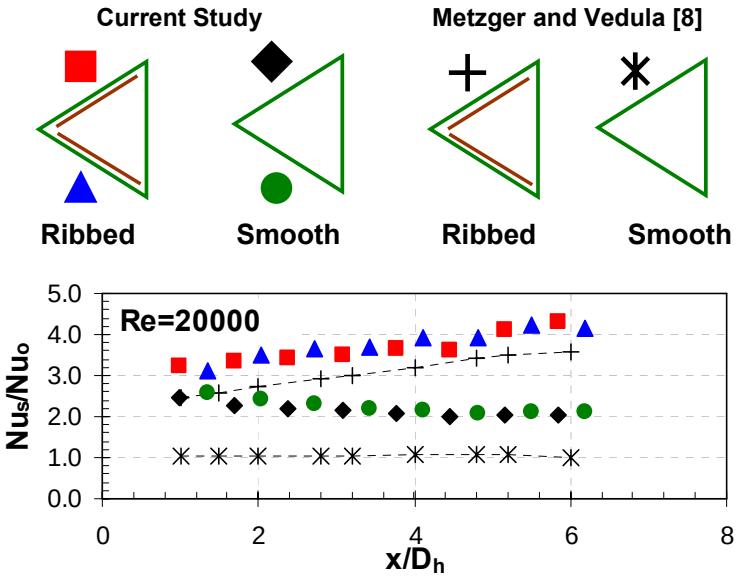

Figure 11: Nusselt Number Ratio (Nu/Nu_o) Comparison in the Stationary Ribbed Channel (Re=20000)

induced secondary flow grows in strength as the flow encounters several additional ribs in the streamwise direction and the heat transfer is enhanced gradually. For the ribbed cases, both results show the Nusselt number ratio increases along the streamwise direction. For the smooth cases, the Nusselt number ratio of the current study shows gradually decreases in the streamwise direction. While the data from Metzger and Vedula [8] maintains the same level due to the fully-developed flow condition.

45° Angled Ribs

Figure 12 shows the Nusselt number ratios (Nu/Nu_o) in the stationary channel with smooth wall and 45° ribbed wall. Four different Reynolds numbers from 10000 to 40000 were reported. The results on the smooth walls will be discussed first. For the smooth case, the heat transfer enhancements on these four regions are very similar due to symmetric geometry. The Nusselt number ratio decreases along the streamwise direction due to the boundary layer development. The Nusselt number ratio decreases from about 3.0 to 2.2 when Reynolds number is 10000. The Nusselt number ratio decreases from 2.3 to 2.0 when Reynolds number is 40000. It shows that the Dittus-Boelter – McAdams correlation can still be applied to the smooth triangular channel with the hydraulic diameter replacing the tube diameter.

For the 45° ribbed channel, the ribs induce flow reattachment and the heat transfer is enhanced at the cost of higher pressure drop. The heat transfer enhancement in the rib leading region (L1 and T1) is higher than the rib trailing region (L2 and T2). The angled rib induced secondary flow grows in strength as the flow encounters several

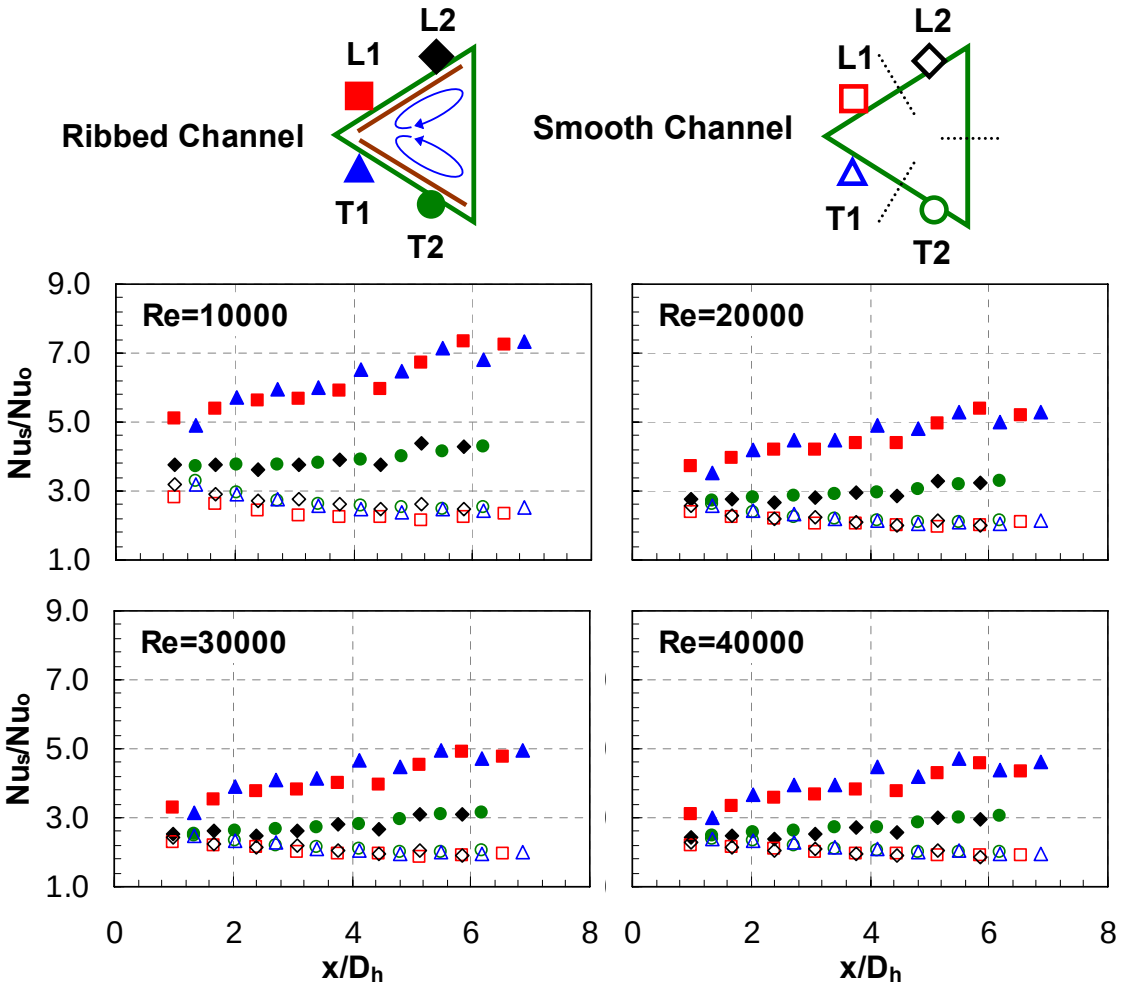

Figure 12: Nusselt Number Ratio in the Stationary Channel with 45° Angled Rib

additional ribs and the heat transfer is increased gradually along the streamwise direction. The Nusselt number ratio increases along the streamwise direction from 5.0 to 7.4 in L1 and T1 region at Re=10000. It increases along the streamwise direction from 3.8 to 4.3 in L2 and T2 region at Re=10000. For the lowest Reynolds number of 10000, the heat transfer enhancement near the rib leading region (L1 and T1) is about 1.7 times higher than the smooth cases near the entrance and 3.5 times higher than the smooth cases near the exit of the channel. While on the rib trailing region (L2 and T2), the heat transfer enhancement from the entrance to the exit is only about 1.3 to 2.0 times higher than the smooth cases at Re=10000. The entire ribbed leading and trailing surfaces both have higher heat transfer enhancement than the smooth cases. However, as the Reynolds number increases from 10000 to 40000, the heat transfer enhancement by the ribs decreases.

Inverted 45° Angled Ribs

For the inverted 45° angled ribs, the rib induced secondary flow is reversed compared to the 45° angled ribs. The rib induced secondary flow now goes along the surface of L2 and T2 surface towards L1 and T1 surface. It tends to impinge on the inner wall and then turn around near L2 and T2 region due to channel geometry. Therefore, the higher heat transfer occurs on L2 and T2 surfaces while the lower heat transfer occurs on L1 and T1 surfaces. **Figure 13** shows the Nusselt number ratios (Nu/Nu_o) in the stationary channel with smooth walls and inverted 45° ribbed walls. It shows the reversed heat transfer trend as compared to the 45° angled rib. Nusselt number ratio

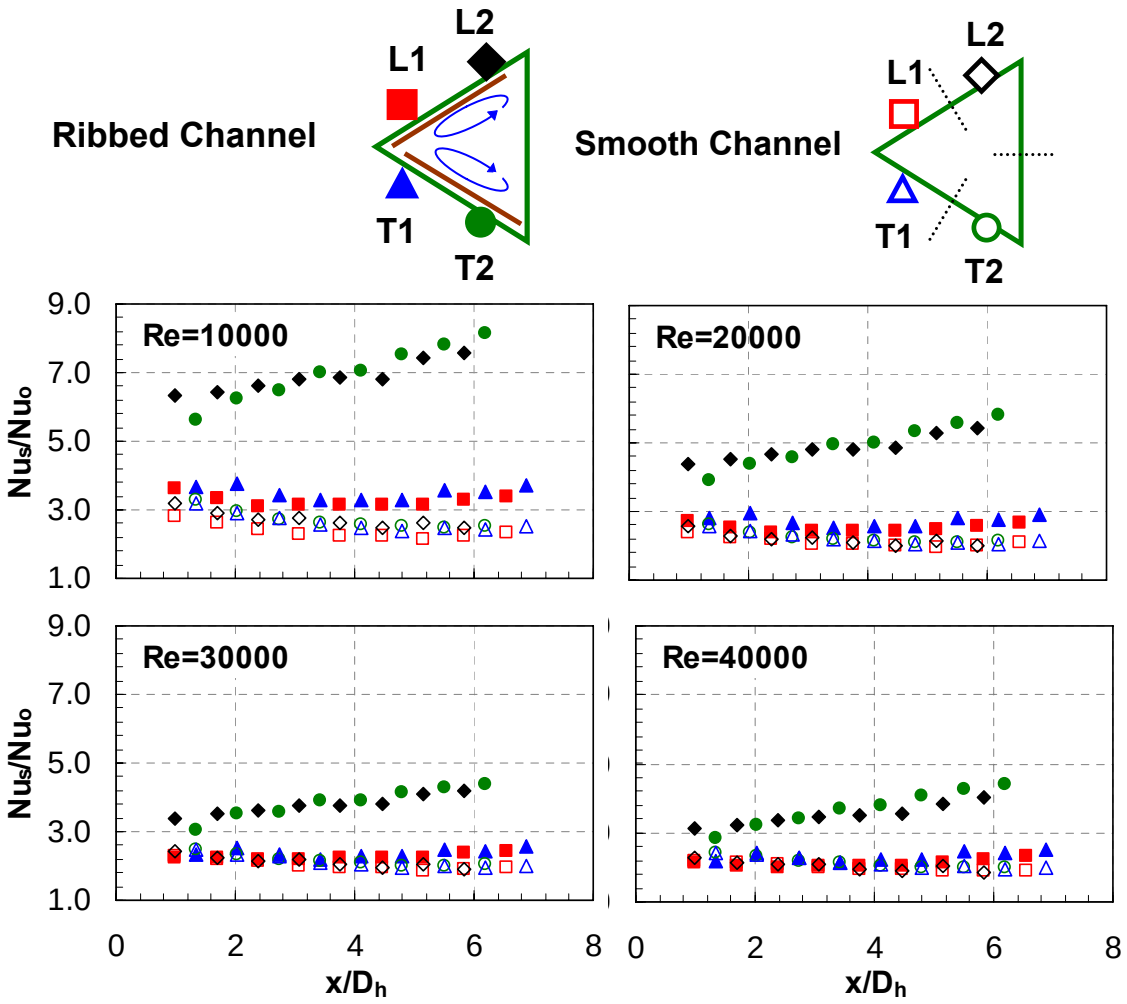

Figure 13: Nusselt Number Ratio in the Stationary Channel with Inverted 45° Angled Rib

(Nu/Nu_o) also increases along the streamwise direction. For Reynolds number of 10000, Nu/Nu_o increases from 6.0 to 8.0 along the streamwise direction on L2 and T2 surfaces. Heat transfer is only slighted altered by the ribs on L1 and T1 surfaces and heat transfer enhancement is smaller than L2 and T2 region. For Reynolds number of 10000, the heat transfer enhancement near L2 and T2 surfaces is about 2 times higher than the smooth case near the entrance while about 3.2 times higher than the smooth case near the exit of the channel. Nusselt number ratio (Nu/Nu_o) increases along the streamwise direction. For L1 and T1 region, heat transfer is only slighted altered by the ribs. The Nu/Nu_o ratio is 1.3 times higher than the smooth case near the entrance and 1.5 times higher than the smooth case near the exit of the channel. When Reynolds number increases, heat transfer enhancement by the ribs decreases. At higher Reynolds number of 40000, the heat transfer enhancement due to ribs is small and the Nusselt number ratios for smooth case and ribbed case are very similar near the entrance of the channel.

90° Orthogonal Ribs

For 90° orthogonal ribs, heat transfer is altered mainly due to ribs tripping the flow and the flow reattachment. There is no rib induced secondary flow along the rib orientation and heat transfer is more uniformly altered across the entire channel. The Nusselt number ratios (Nu/Nu_o) on these four regions are very similar to each other and decrease along the streamwise direction as shown in **Figure 14.** The heat transfer level is lower than the high heat transfer region, but higher than the low heat transfer of the angled rib cases. At Reynolds number of 10000, Nusselt number ratio on the leading

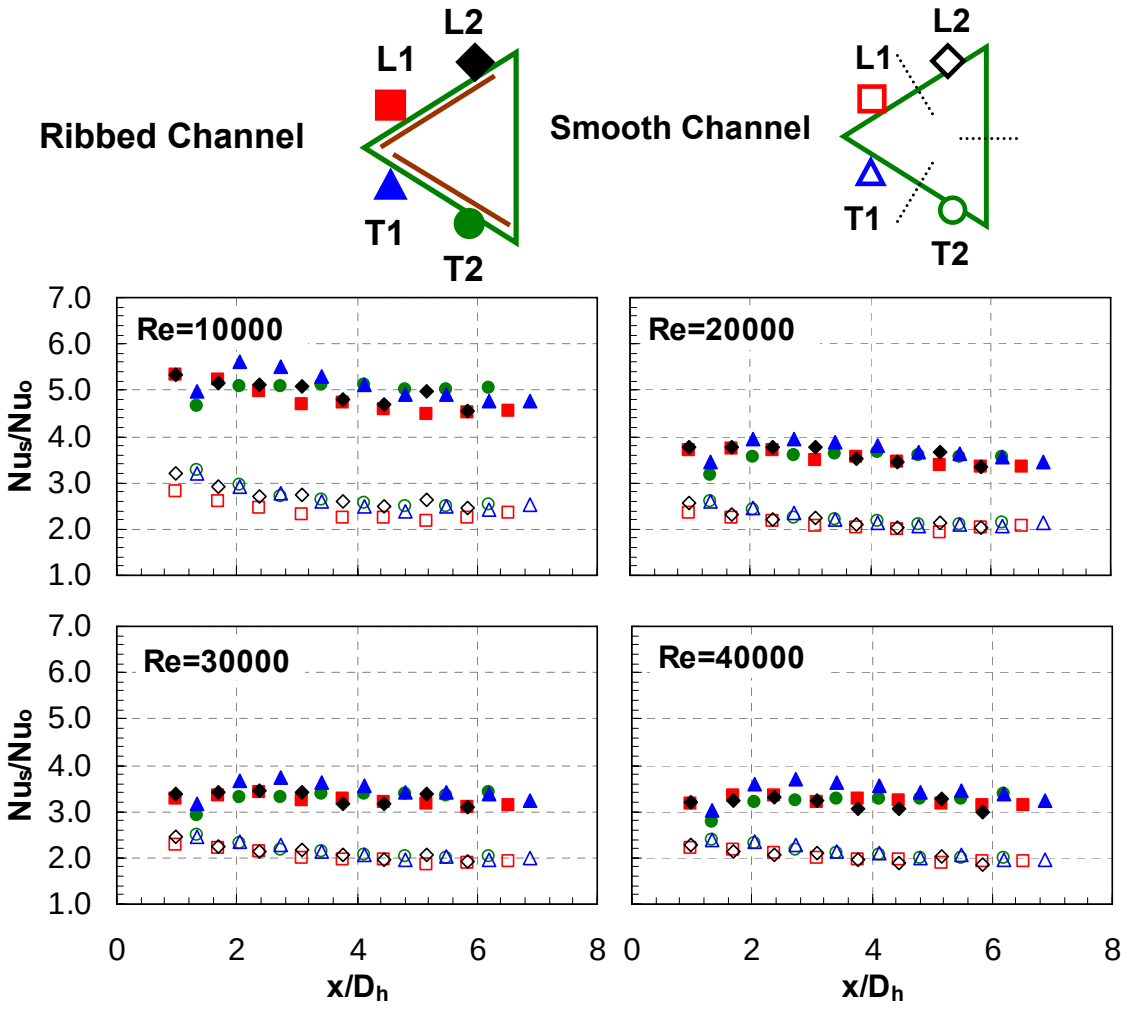

Figure 14: Nusselt Number Ratio in the Stationary Channel with 90° Rib

surface (L1 and L2) decreases from 5.4 to 4.5 along the streamwise direction. On the trailing surface, there is a sudden increase of Nusselt number ratio at the entrance and then gradually decreases along the streamwise direction. The Nusselt number ratio is about 1.7 times higher than the smooth case at Re=10000 and 1.5 times higher than the smooth surface at Re=30000. When Reynolds number increases, the Nusselt number ratio (Nu/Nu_o) decreases for all cases.

4.1.2 Heat Transfer in Rotating Channel

Before the detailed discussion of the rotating results, it is necessary to describe the effect of rotation inside cooling channels. Two counter rotating vortices are generated due to Coriolis force during rotation. For the radially outward flow, rotation increases heat transfer on the trailing surface, while decreases heat transfer on the leading surface. The structure of these two counter rotating vortices varies depending on the channel geometry and the direction of rotation. **Fig. 10** shows this secondary flow pattern in the current triangular channel, which also involves the formation of the two counter rotating vortices. In a ribbed channel, the rib induced secondary flow interacts with the rotating induced secondary flow and the heat transfer behavior is affected by the combined effects from both. **Fig. 10** shows these combined effects of the secondary flow patterns for 45° and inverted 45° angled ribs. The effect of rotation is small and doesn't have significant impact on heat transfer on the rib leading surface (L1 and T1) because rib induced secondary flow dominates. While near the rib trailing surface (L2 and T2),

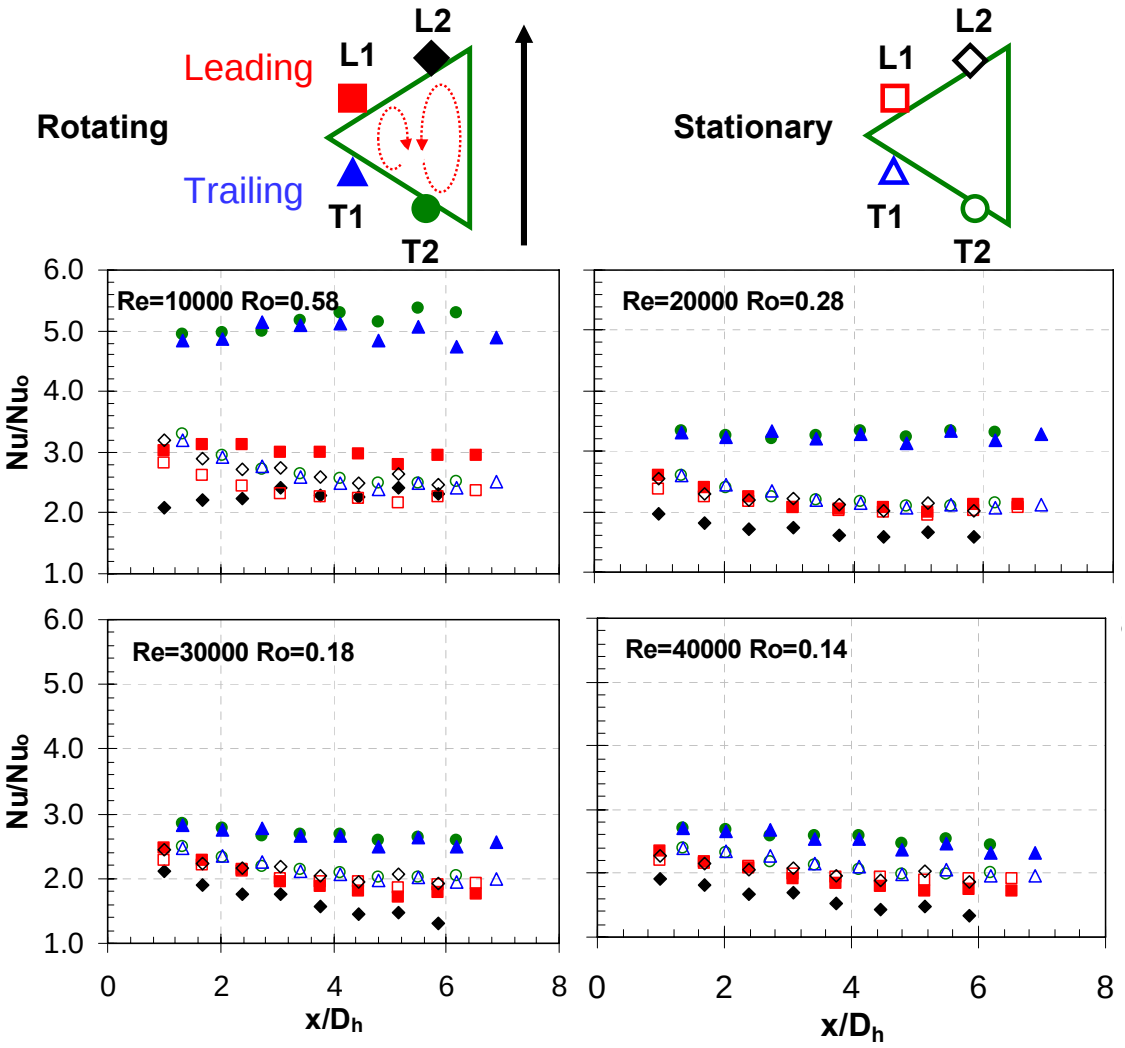

Figure 15: Nusselt Number Ratio Distribution in the Rotating Smooth Channel

the wide space allows the rotation induced secondary flow to develop freely and the effect of rotation is more obvious.

Smooth Channel

Figure 15 shows the Nusselt number ratio distributions with smooth walls. The stationary results and rotating results are plotted in the same figure to study the effect of rotation. Four Reynolds number cases, each under stationary condition and the highest rotational speed (400 rpm) are presented. This figure can clearly show the pure effect of rotation inside this equilateral triangular channel without ribs. The effect of rotation enhances the heat transfer on the trailing surface (both T1 and T2). The Nusselt number ratios (Nu/Nu_o) are very close to each other on T1 and T2 region except there is small deviation near the exit of the channel at Re=10000. On the leading surface, the Nusselt number ratio on the L2 region is smaller than the stationary case. While on the L1 region, the Nusselt number ratio is very close to the stationary case from Re=20000 to Re=40000. The heat transfer enhancement/declination due to rotation decreases when Reynolds number increases. The heat transfer enhancement due to rotation is smallest at the highest Reynolds number of 40000.

45° Angled Ribs

With 45° angled ribs put on the leading and trailing surfaces, the Nusselt number ratio distributions in both the stationary and rotating channels (400 rpm) are shown in **Figure 16**. Near the rib leading region (L1 and T1), the rib induced secondary flow

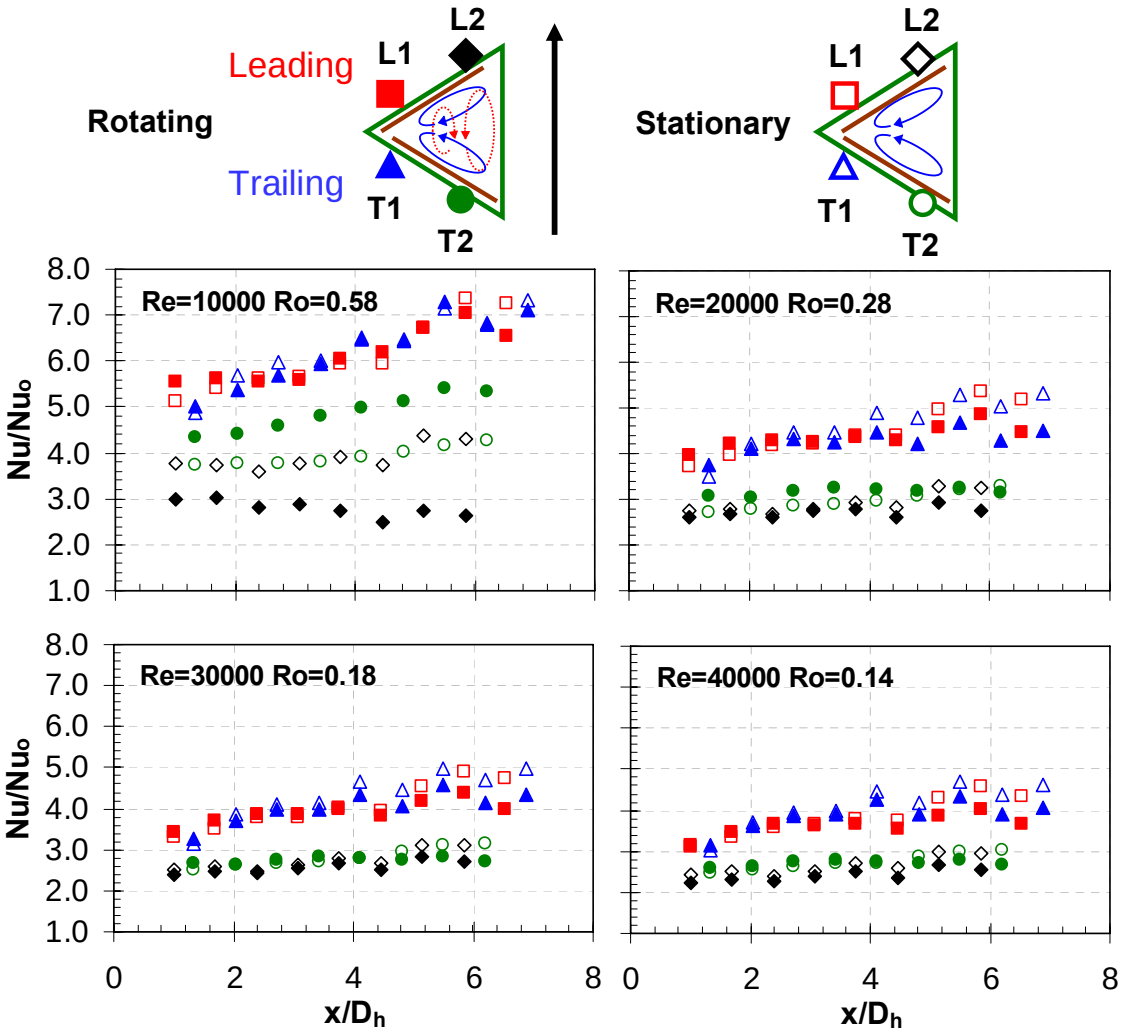

Figure 16: Nusselt Number Ratio Distribution in the Rotating Channel with 45° Angled Rib

dominates over the smaller rotation induced secondary flow. The Nusselt number ratio for the rotating case and the stationary case are similar at the entrance of the channel and starts to diverge towards the end of the channel. For 45° angled rib, it has high heat transfer near these two regions (L1 and T1) and the heat transfer improvement due to rotation is limited. While on the rib trailing region (L2 and T2), the effect of rotation is more obvious and enhances heat transfer on the trailing surface while decreases heat transfer on the leading surface. On the L2 region, the rib induced secondary flow opposes the rotation induced secondary flow and produces lowest heat transfer.

Inverted 45° Angled Ribs

For the inverted 45° angled ribs, the direction of rib induced secondary flow is reversed while the rotation induced secondary flow remains the same. Heat transfer enhancement/declination due to effect of rotation is more obvious than 45° angled ribs as shown in **Figure 17**. On T2 surface, both the rib and rotation induced secondary flows acting together to enhance heat transfer and the highest heat transfer occurs due to the combined effects. Nusselt number ratio (Nu/Nu_o) increases from 6.0 to 11.0 along the streamwise direction at Re=10000. The heat transfer enhancement on L1 and T1 surfaces is obvious and is different from 45° angled ribs. Heat transfer on T1 surface is slightly higher than the L1 surface due to effect of rotation but both higher than the stationary case. Therefore, L1 surface has the lowest heat transfer at Re=30000. However, L2 surface has the lowest heat transfer at Re=10000 due to stronger effect of rotation (higher rotation number).

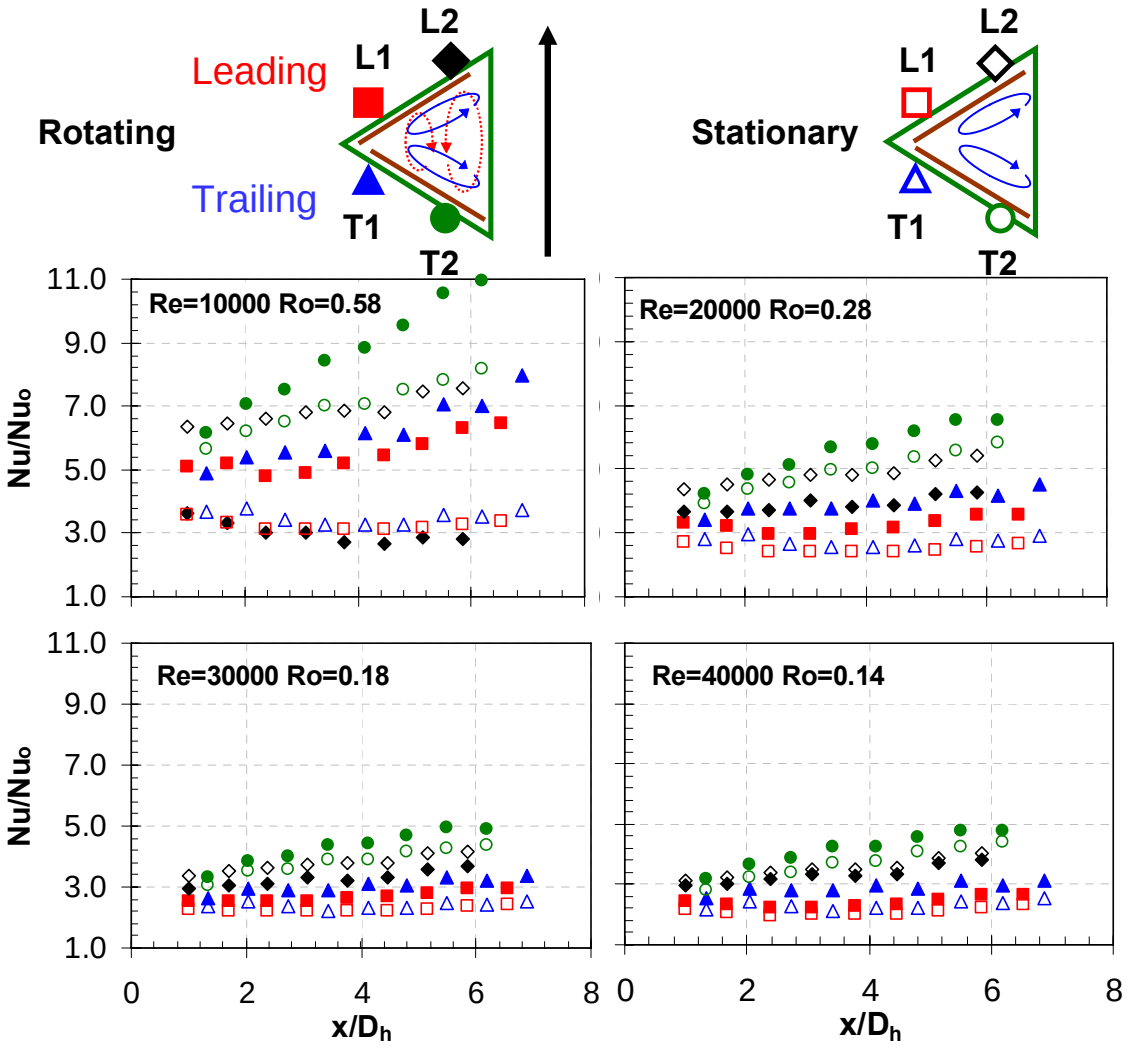

Figure 17: Nusselt Number Ratio Distribution in the Rotating Channel with Inverted 45° Angled Rib

90° Orthogonal Ribs

Figure 18 shows the Nusslet number ratios for 90° ribs. Heat transfer is the highest on T2 surface and the lowest on L2 surface for 90° orthogonal ribs. The rotating heat transfer is mainly affected by the effect of rotation because there is no secondary flow along the rib orientation. Nusselt number ratio increases dramatically from 7.0 to 13.0 on T2 surface along the streamwise direction at Re=10000. It increases slightly on L1 and T1 surfaces from 7.0 to 8.4 along the streamwise direction at Re=10000. Nu ratio on L2 surface is the lowest and remains the same level along the streamwise direction. It is interesting that the Nusselt number ratio (Nu/Nu_o) is higher in L1 surface than T1 surface near the entrance of the channel. This is due to the staggered arrangement of the ribs near the entrance under rotating condition. Nu ratios on L1 and T1 surfaces converge when flow goes downstream. As the Reynolds number increases, the Nusselt number ratio (Nu/Nu_o) decreases and the difference between stationary and rotating results also decreases. Thus, the effect of rotation is reduced.

4.1.3 Rotation Number Effects

Rotation number is a ratio of Coriolis force to the bulk flow inertia force. By varying the rotational speed (Coriolis force) and the Reynolds number (flow inertia force), the contribution from these two factors should yield the same results. The rotation number is defined in Equation 10.

$$Ro = \frac{\Omega D_h}{V} \tag{10}$$

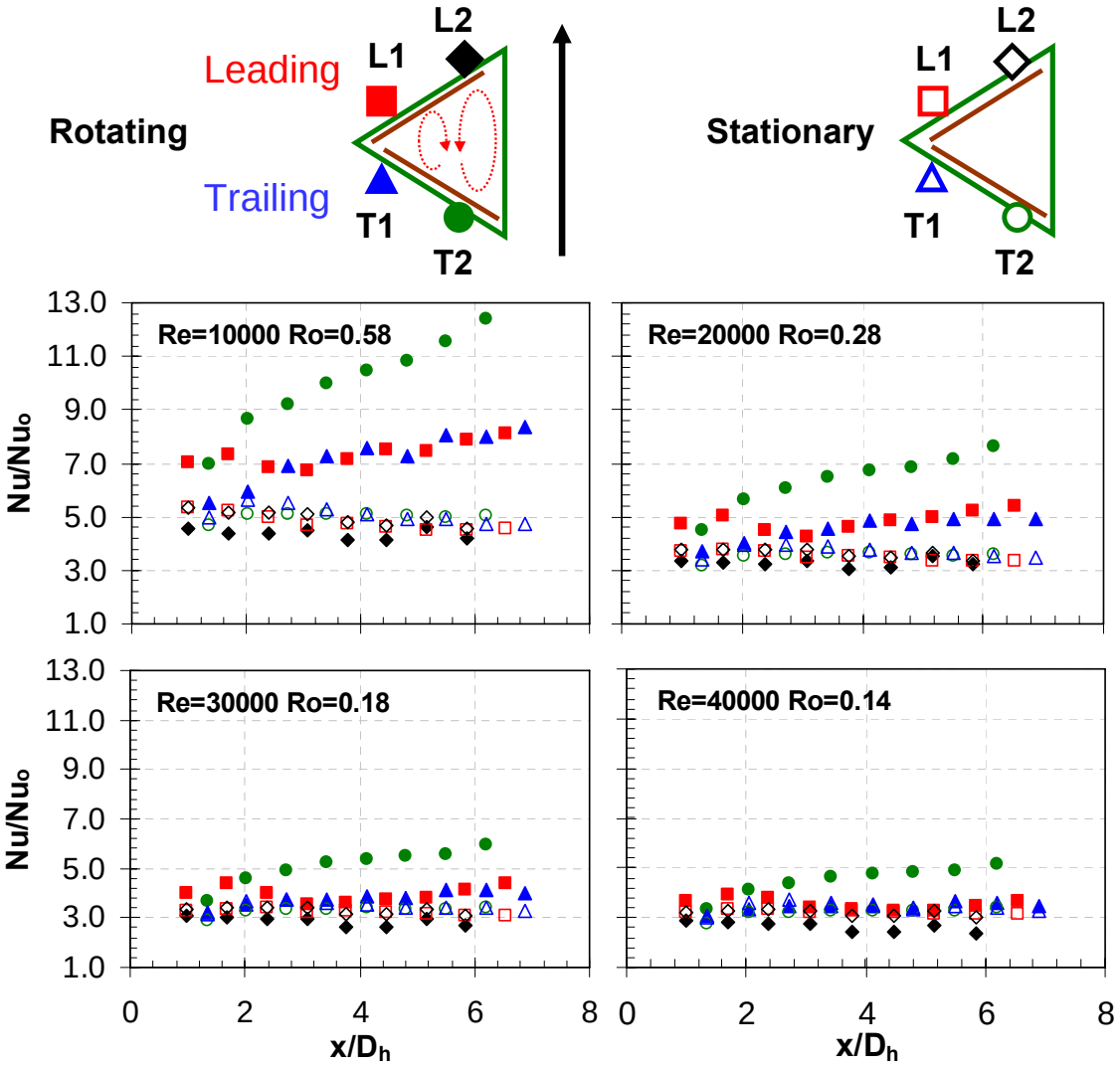

Figure 18: Nusselt Number Ratio Distribution in the Rotating Channel with 90° Rib

This non-dimensional parameter is widely used to quantify the effect of rotation in the industry and academia. Heat transfer enhancement due to effect of rotation is represented by the ratio of the rotational Nusselt number to the stationary Nusselt number (Nu/Nu_s). **Figure 19** shows this heat transfer enhancement (Nu/Nu_s) including Reynolds number from 10000 to 40000 and the rotational speed from 0 to 400 rpm. Three different regions (3, 6, and 9) in the streamwise direction (x/D_h=2.03, 4.11, and 6.19, respectively) are chosen to study the effect of rotation number for every rib case.

Smooth Channel

The discussion begins with the smooth cases. In region 3, the flow is developing due to the short entrance. The Nusselt number ratios (Nu/Nu_s) increase from 1.0 to 1.6 with the rotation number on the trailing surfaces. Both T1 and T2 surfaces have the similar heat transfer enhancement. However, on the leading surface, the Nusselt number ratios (Nu/Nu_s) on the L1 region didn't vary significantly until a rotation number of 0.3, and then gradually increase. The Nusselt number ratios on the L2 region decreases with the rotation number until a critical rotation number of 0.44, and then starts to increase. The Nu/Nu_s declination on the L2 surface is larger than the L1 surface. It shows that the rotation induced secondary flow has a greater impact on the L2 region and the heat transfer is low.

When the flow moves to region 6, the boundary layer grows thicker on the smooth wall. The highest Nusselt number ratio (Nu/Nu_s) on the trailing surfaces increase from 1.0 to 2.0 when rotation number increases. The Nusselt number ratios (Nu/Nu_s) on

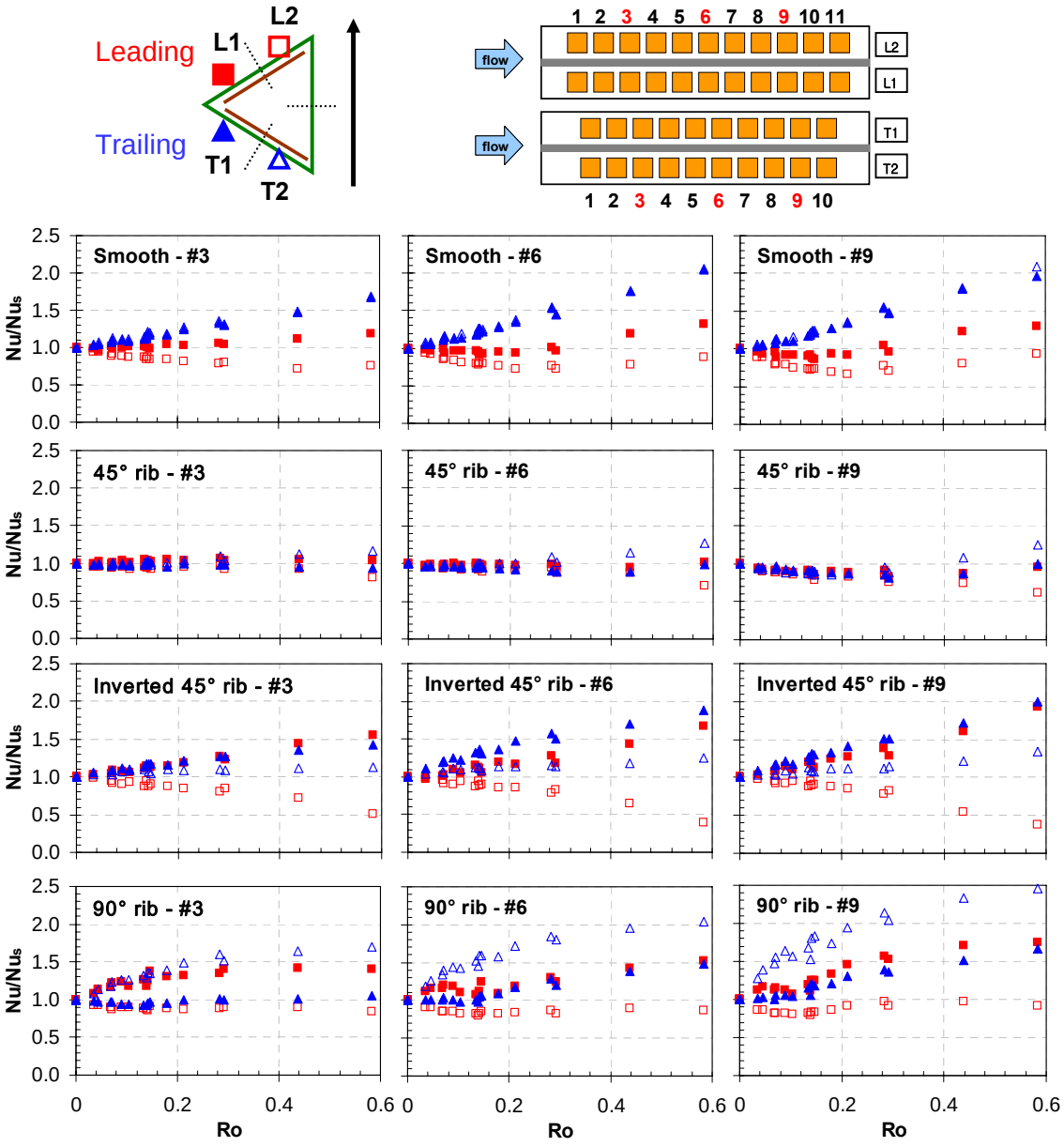

Figure 19: Effect of Rotation Number on Three Different Regions

the L2 region decrease until rotation number of 0.3, and then gradually increase with the rotation number. While on the L1 region, the Nusselt number ratios (Nu/Nu_s) didn't vary significantly until a rotation number of 0.3, and then gradually increase. As the flow goes further downstream to region 9, the trend and the level of Nusselt number ratios are very similar to region 6.

45° Angled Ribs

The Nusselt number ratios (Nu/Nu_s) with rotation number for 45° angled ribs are presented from region 3 to region 9. The heat transfer enhancements (Nu/Nu_s) on L1 and T1 surfaces are very similar which indicate the effect of rotation is small and rib induced secondary flow dominates. On region 3, Nusselt number ratio decreases gradually from 1.0 to 0.8 with the rotation number on L2 surface and gradually increases from 1.0 to 1.2 with the rotation number on T2 surface. When the flow moves downstream to region 6 and 9, the difference between L2 and T2 surfaces becomes larger than region 3. For 45° angled ribs, heat transfer enhancement/declination due to effect of rotation is smallest among all the cases.

Inverted 45° Angled Ribs

For inverted 45° angled ribs, heat transfer variation due to rotation is more obvious. Heat transfer enhancements on all surfaces increase with Ro except for L2 surface. On L1 and T1 surfaces, Nusselt number ratio (Nu/Nu_s) increases from 1.0 to 1.5 in region 3 and from 1.0 to 2.0 in region 9 with rotation number. Heat transfer

enhancement due to rotation decreases near the entrance of the channel because of entrance effect. The Nusselt number ratio (Nu/Nu_s) on L1 and T1 surfaces is high due to low Nusselt number at stationary condition (Nu_s).

On T2 surface, heat transfer enhancement increases slightly with rotation number. Nu/Nu_s increases up to 1.1 in region 3 and 1.35 in region 9. Heat transfer enhancement due to rotation is smaller compared to L1 and T1 surfaces. Heat transfer on T2 surface is already high at stationary condition and thus enhancement due to rotation is limited. On L2 surface, Nu/Nu_s decreases gradually down to 0.5 in region 3 and 0.4 in region 6 and 9 with rotation number.

90° Orthogonal Ribs

For 90° orthogonal ribs, heat transfer enhancement is the highest on T2 surface and lowest on L2 surface. On T2 surface, Nu/Nu_s increases with rotation number up to 1.7 in region 3 and 2.5 in region 9. It also shows that heat transfer enhancement is smaller near the entrance region. For L2 surface, heat transfer enhancement maintains the same level of 0.8 as rotation number increases and the effect of rotation in this region is minimal. L2 surface has the lowest Nusselt number ratio due to rotation among all the ribbed cases. In region 3, Nu/Nu_s maintains the same level with rotation number on T1 surface but increases with the rotation number on L1 surfaces. It is noted that Nu/Nu_s on T1 surface is lower than L1 surface due to staggered ribs near the entrance under rotating condition in region 3. In region 6 and 9, Nu/Nu_s increases gradually with rotation number for L1 and T1 surfaces in region 6 and 9. For 90° orthogonal ribs, there is no

significant heat transfer declination as rotation number increases; therefore, overall heat transfer gradually increases with rotation.

4.1.4 Buoyancy Parameter Effects

The buoyancy parameter is also a widely used non-dimensional parameter to quantify the effect of rotation inside the gas turbine blade. The buoyancy force due to the centrifugal force and temperature difference is important due to the high rotating speed and large temperature difference in the actual engines. The buoyancy parameter considers all factors affecting the effect of rotation: the density ratio (temperature difference), the rotation number, and the rotating radius. It is shown in Equation 11.

$$Bo_x = \left(\frac{\Delta\rho}{\rho}\right)_x (Ro)^2 \frac{R_x}{D_h} = \frac{T_{w.x} - T_{b,x}}{T_{f,x}} (Ro)^2 \frac{R_x}{D_h} \tag{11}$$

The local film temperature is defined as the average of the local wall temperature and the local bulk temperature as shown in Equation 12.

$$T_{f,x} = (T_{w,x} + T_{b,x})/2 \tag{12}$$

In the current study, three regions (x/D_h=2.03, 4.11, and 6.19, respectively) along the streamwise direction are also chosen to study the effect of buoyancy parameter on Nusselt number ratios (Nu/Nu_s). All the cases were conducted with density ratio of 0.11.

Smooth Channel

Figure 20 shows the Nusselt number ratios (Nu/Nu_s) with the buoyancy parameter in region 3, 6, and 9. Since the density ratio is maintained the same value of

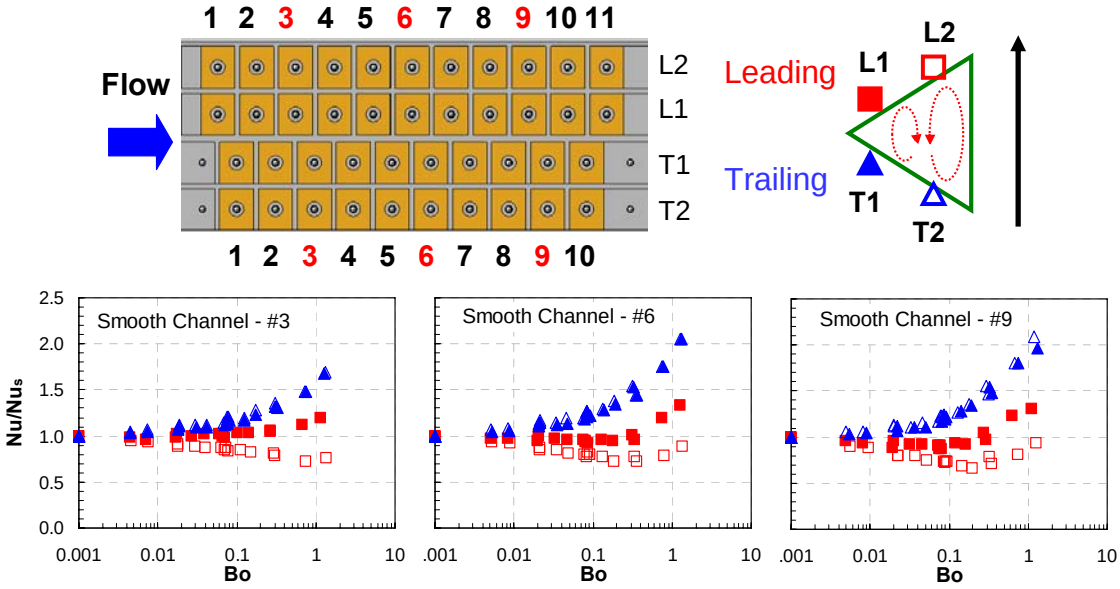

Figure 20: Effect of Buoyancy Parameter on Heat Transfer Enhancement (Nu/Nu_s) for Smooth Surface

0.11, the buoyancy parameter is mainly dominated by rotation number. Similar trends can be observed in the rotation number plots. It also shows that the Nusselt number ratio increases with the buoyancy parameter on the trailing surface. For the L1 region in region 3 and 6, the Nusselt number ratio maintains the same level until buoyancy parameter of 0.3 and then gradually increases with the buoyancy parameter. While for the L1 region on region 9, the Nusselt number ratio decreases with the buoyancy parameter until a critical buoyancy parameter of 0.3 and then increases. On the L2 region, the Nusselt number ratios decreases with the buoyancy parameter and then gradually increases. The entrance effect dominated over effect of rotation on region 3. For region 6 and 9, effect of rotation is more obvious.

45° Angled Ribs

Figure 21 shows the Nusselt number ratio (Nu/Nu_s) for 45° angled rib at the density ratio of 0.11. Nusselt number ratio (Nu/Nu_s) remains the same level on L1 and T1 surfaces as the buoyancy parameter increases. Heat transfer is enhanced slightly on T2 surface while declined slightly on L2 surface. As the flow moves downstream to region 6 and 9, the trend is similar to region 3 except heat transfer enhancement/declination is more obvious. Nusselt number ratio (Nu/Nu_s) increases up to about 1.2 in T2 region while decreases down to about 0.6 in L2 region at the maximum buoyancy parameter of 1.9.

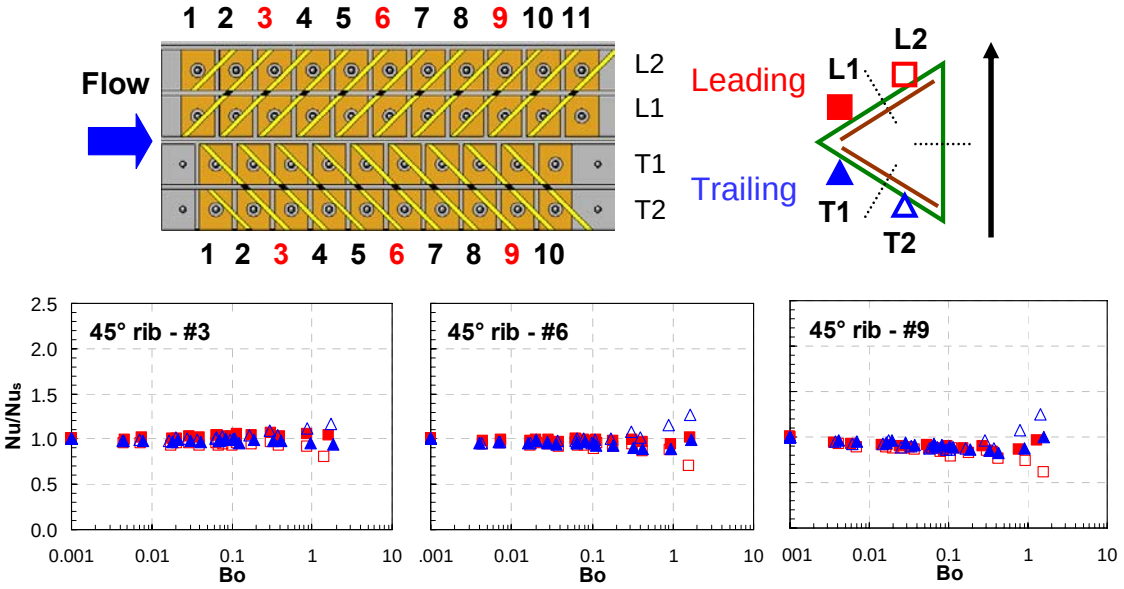

Figure 21: Effect of Buoyancy Parameter on Heat Transfer Enhancement (Nu/Nu_s) for 45° Angled Rib

Inverted 45° Angled Ribs

Two additional density ratios of 0.13 and 0.15 were tested specifically for inverted 45° rib case to study the density ratio effects. Total of three different density ratios (0.11, 0.13, and 0.15) are plotted in **Figure 22**. On the leading surface, L1 increases with buoyancy parameter while L2 decreases with buoyancy parameter. The heat transfer enhancement/declination due to rotation is more obvious as flow goes downstream to region 6 and 9. For the trailing surface, Nusselt number ratio (Nu/Nu_s) increases with the buoyancy parameter as shown in the figure. The heat transfer enhancement on T1 surface is higher than T2 region. The data with different density ratios fits nicely into the curve except only small deviation on region 3 and 9 of L1 surface due to different density ratios. It shows that the density ratio, Reynolds number, and rotational speed can be varied independently but the results still can be correlated into a single curve by buoyancy parameter.

90° Orthogonal Ribs

Figure 23 shows the results for 90° orthogonal ribs. In region 3, Nusselt number ratio (Nu/Nu_s) maintains the same level as buoyancy parameter increases on L2 and T1 surfaces. Nu/Nu_s increases with buoyancy parameter on T2 and L1 surfaces. When the flow moves downstream, the trend on the L1 and T1 surfaces is different from region 3. The Nu/Nu_s didn't vary significantly until buoyancy parameter of 0.06 and suddenly increases with buoyancy parameter on T1 surface. Heat transfer enhancement on T2 surface increases as the flow goes downstream. The Nusselt number ratio (Nu/Nu_s) still

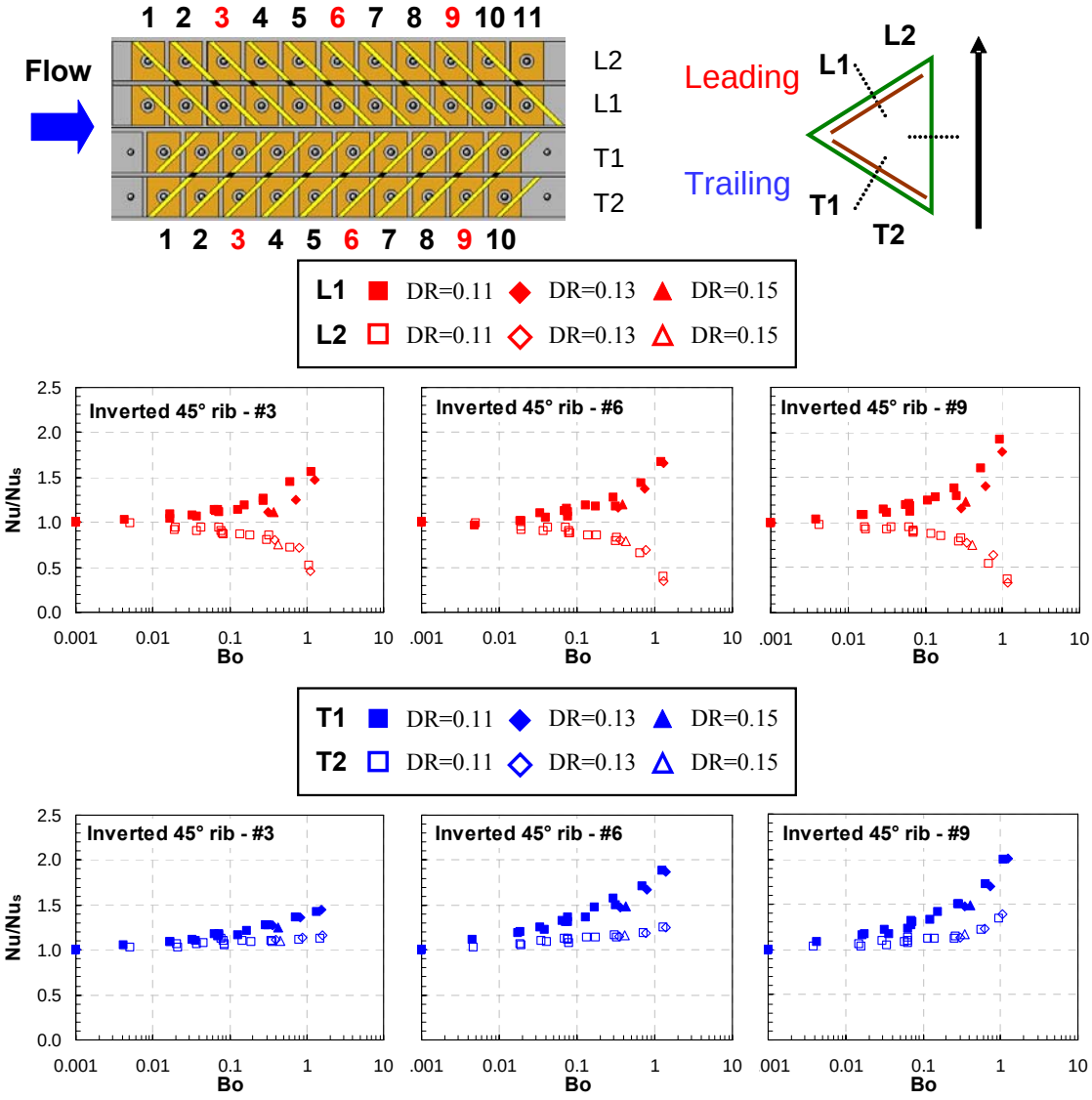

Figure 22: Effect of Buoyancy Parameter on Heat Transfer Enhancement (Nu/Nu_s) for Inverted 45° Angled Rib

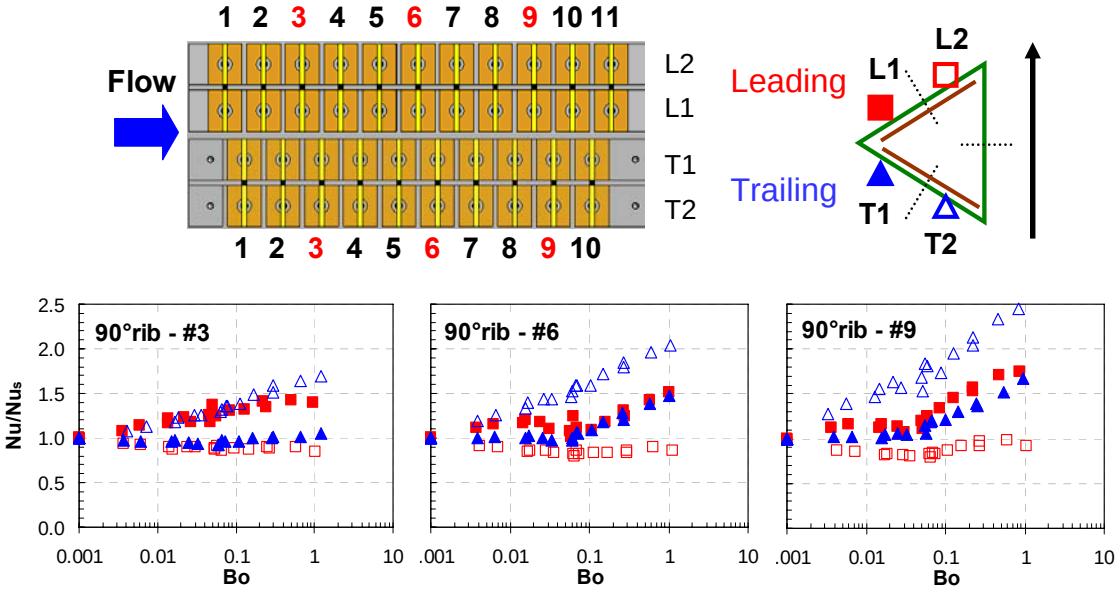

Figure 23: Effect of Buoyancy Parameter on Heat Transfer Enhancement (Nu/Nu_s) for 90° Rib

maintains the same level as buoyancy parameter increases on L2 surface at downstream location. It is noted that there is no significant heat transfer declination for all the regions. High heat transfer due to rotation can be expected at high buoyancy parameter for the 90° orthogonal ribs.

4.1.5 Average Heat Transfer

The results were averaged along the atreamwise direction for every surface as shown in **Figure 24**. Total of nine points were averaged for each data point. Nusselt number ratio (Nu/Nu_o) is chosen as the parameter so that the true heat transfer level can be compared. Results are compared between stationary the highest rotational speed (400 rpm) to investigate the effect of rotation. **Figure 24(a)** shows the surfaces (L1 and T1) close to the leading edge of the gas turbine blade where high thermal load exists. For the stationary case, 45° rib has the highest heat transfer while the inverted 45° rib has the lowest heat transfer for both L1 and T1 surfaces. For rotating case, 90° rib has the highest Nu ratio on L1 surface when rotation number is higher than 0.18 and is similar to 45° rib cases when rotation number is lower than 0.18. On T1 surface, 90° rib has highest Nu ratio at higher rotation number domain while 45° rib has the highest Nu ratio at lower rotation number domain. From this figure, we can conclude that although heat transfer for 45° rib is high at stationary case; however, the heat transfer enhancement by rotation for 45° rib is small. The heat transfer level of 90° rib will exceed 45° rib as Reynolds number decreases (rotation number increases).

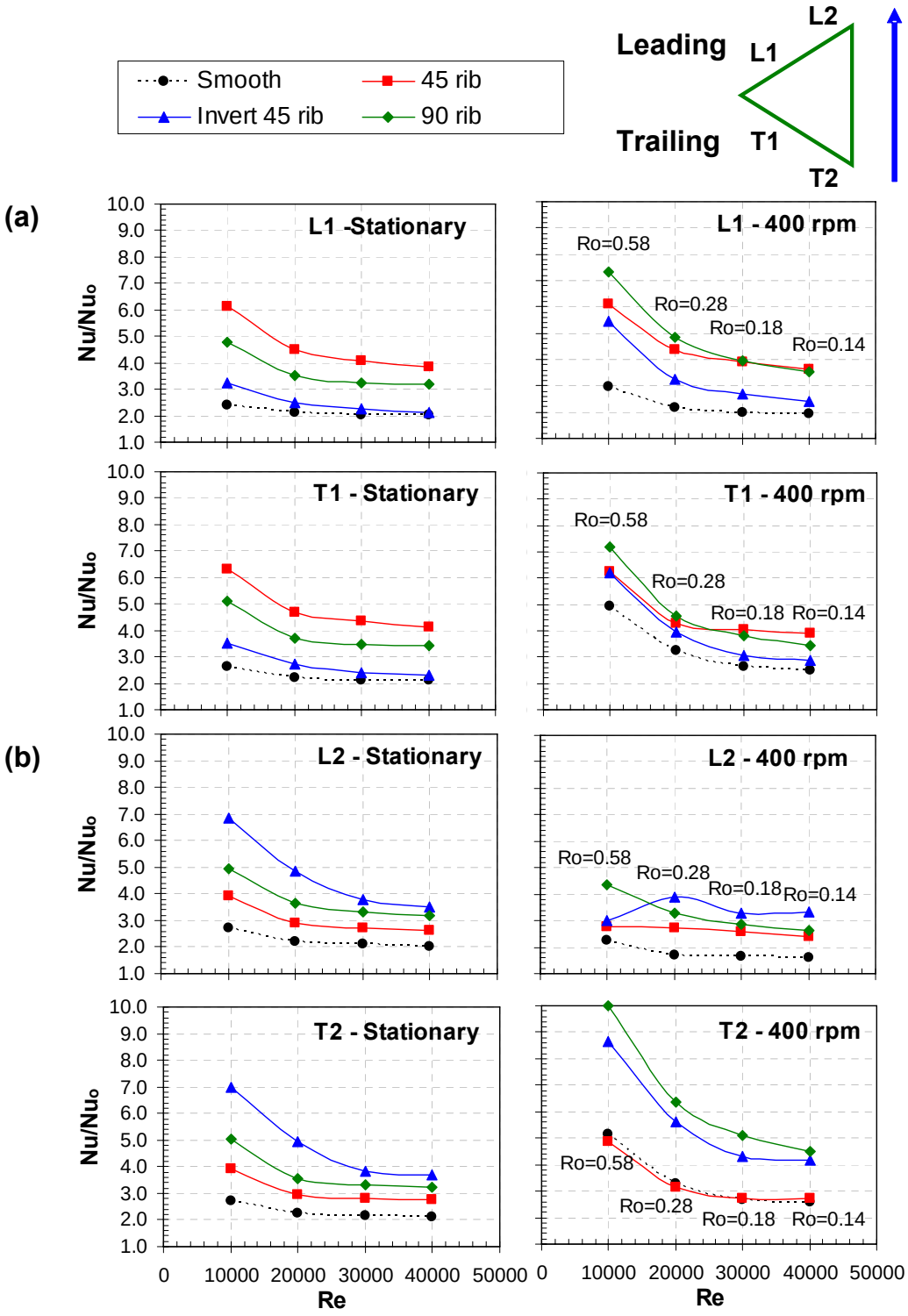

Figure 24: Average Heat Transfer Results of (a) L1 and T1 and (b) L2 and T2

Inverted 45° rib has the highest heat transfer at stationary condition for both L2 and T2 surfaces as shown in **Figure 24(b)**. For rotating condition, inverted 45° rib has the highest Nu ratio when rotation number is smaller than 0.28 while 90° rib has the highest Nu ratio at rotation number of 0.58 on L2 surface. 90° rib has the highest Nu ratio on T2 surface at rotating condition. It is noticed that Nu ratio for 45° rib is very small on this surface and is very close to the smooth case. 90° rib has the highest Nu ratio for all four surfaces (L1, L2, T1, and T2) at the highest rotation number due to strong heat transfer enhancement caused by rotation.

4.1.6 Friction Factor Ratio and Thermal Performance

One way to evaluate the performance of different ribs is to calculate thermal performance for each rib configuration. The friction factor ratio has been defined in Equation 5. In the current study, pressure drop is measured for all the cases at stationary condition. The friction factor ratios are shown in **Figure 25**. 90° rib has the higher friction factor ratio than the 45° and inverted 45° angled ribs.

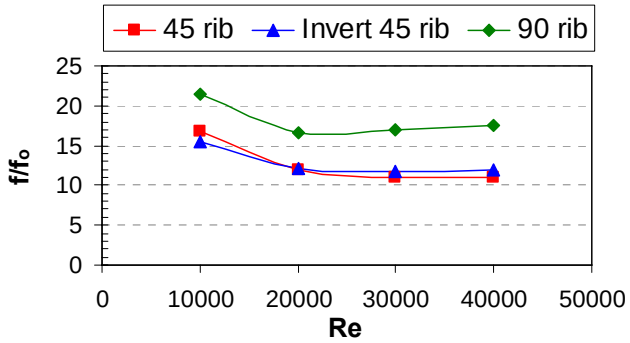

Figure 25: Friction Factor Ratio of Different Rib Configurations

Thermal performance near the leading edge of the turbine blade (L1 and T1 surfaces) and the total thermal performance are presented in **Figure 26**. In the current study, the stationary friction factor ratio is used for all the cases. For L1 surface, 45° rib has the best thermal performance at stationary condition. Angled ribs usually have higher thermal performance than the orthogonal ribs due to smaller pressure drop. However, when rotation is considered, the results are different. 90° rib shows the highest thermal performance at higher rotation number cases. Inverted 45° rib has the lowest thermal performance for all the cases on L1 surface. For T1 surface, 45° rib has the highest thermal performance both at stationary and rotating conditions with smaller rotation number than 0.28. When rotation number is larger than 0.28, all three rib configurations show similar thermal performance.

The total thermal performance is based on the average Nusselt number ratios (Nu/Nu_o) from the leading and trailing surfaces. Results show that 45° rib has the best thermal performance and 90° rib has the worst thermal performance at stationary condition. However, effect of rotation influences thermal performance. 90° rib and inverted 45° rib have similar performance when rotation number is smaller than 0.28. 90° rib has the highest thermal performance at highest rotation number of 0.58.

4.1.7 Correlations for Heat Transfer Enhancement

The average Nusselt number ratios (Nu/Nu_s) on the leading and trailing surfaces are plotted in **Figure 27**. Each data point is the average of 18 points over the entire leading or trailing surfaces. The results are plotted with the rotation number and the

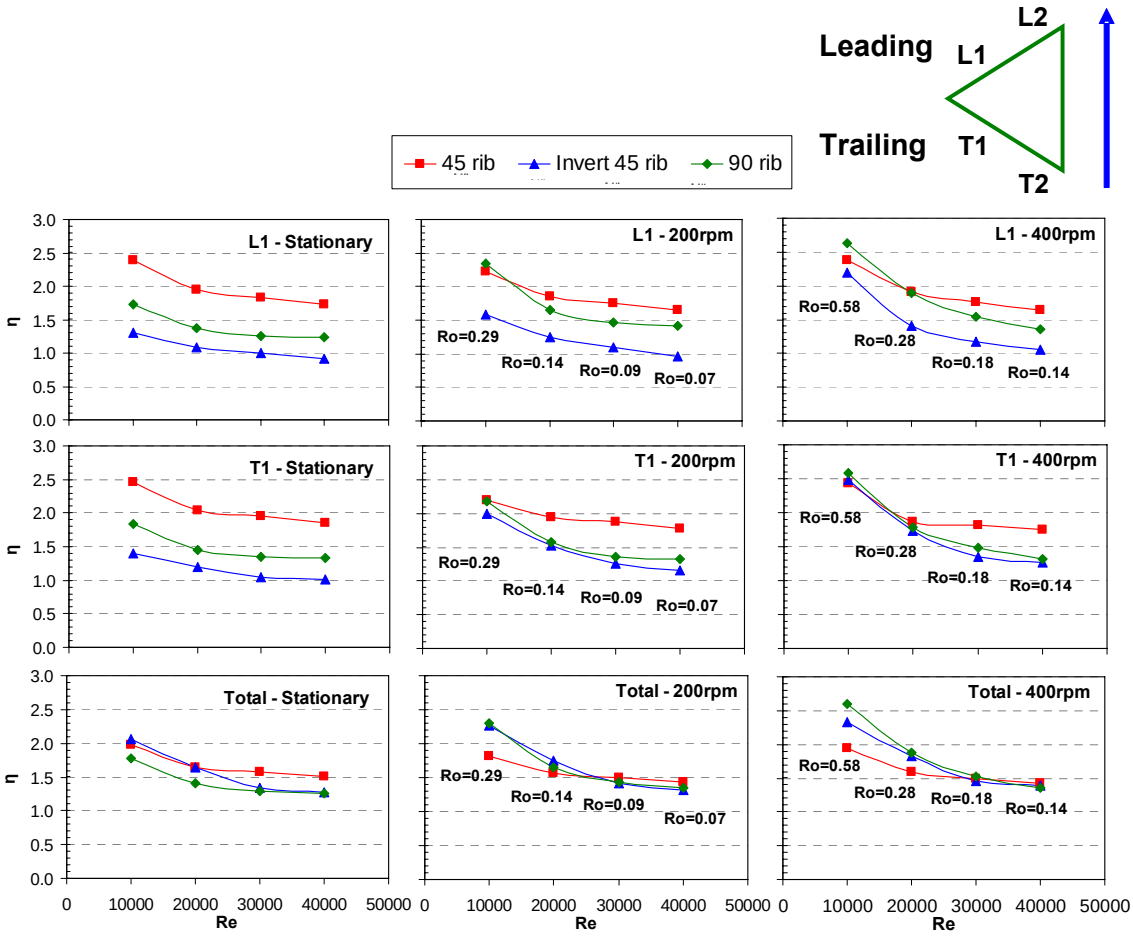

Figure 26: Thermal Performance Comparison of L1, T1, and Total Average

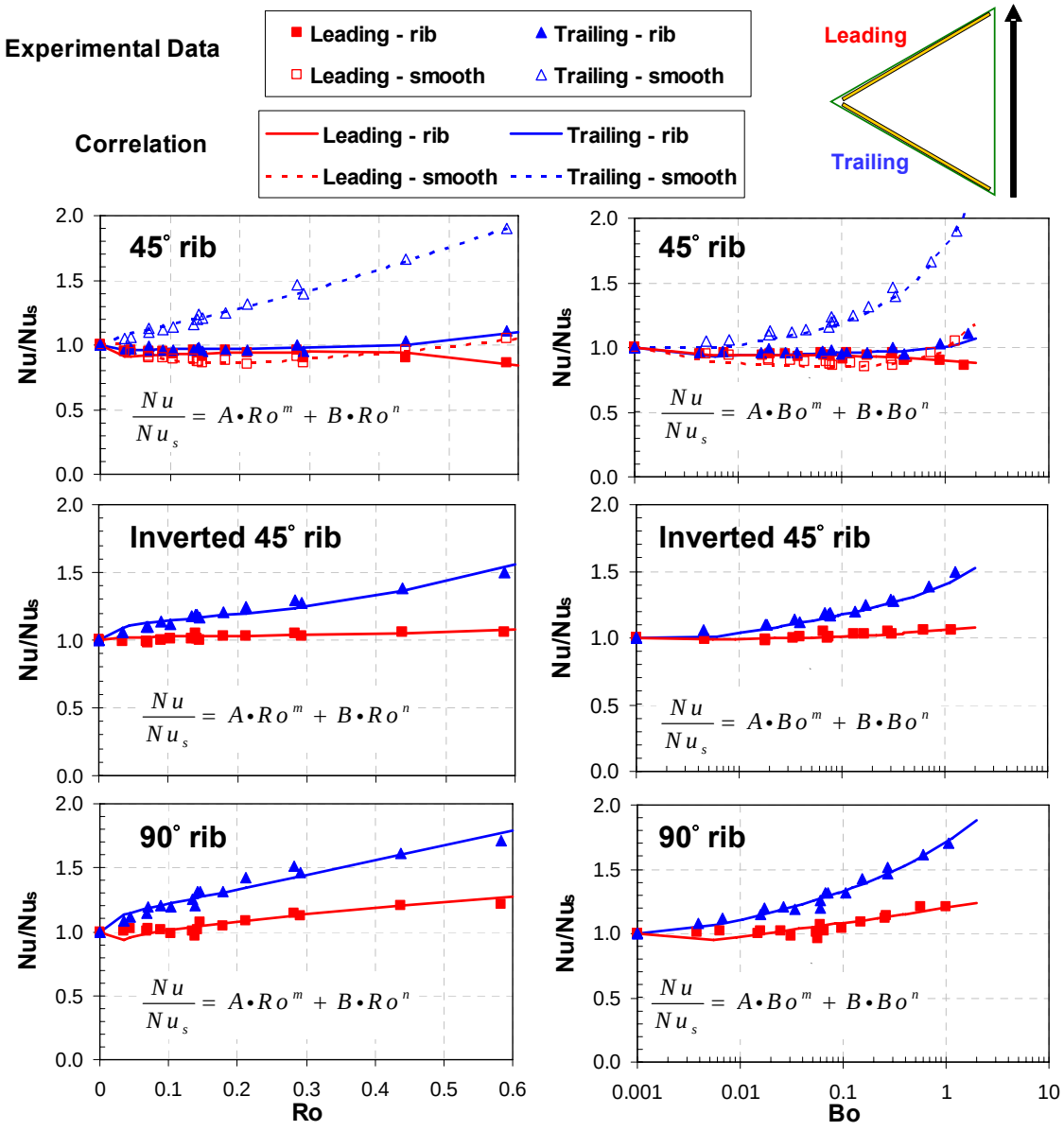

Figure 27: Correlations for Heat Transfer Enhancement

average buoyancy parameter. The well-correlated curve shows that rotation number and buoyancy parameter can be used to predict the heat transfer enhancement inside this triangular channel with smooth and ribbed surfaces. It is well-correlated for all the three rib cases by a power function with the maximum discrepancy within ±6.8%. The constants for the correlation functions are shown in **Table 1**.

The results for 45° angled ribbed case and smooth case were plotted together for comparison. The heat transfer enhancement due to rotation for the smooth case is higher than the 45° ribbed case. The heat transfer enhancement/declination for the smooth case occurs at a lower rotation number and buoyancy parameter than the ribbed case. For the ribbed case, the Nu/Nu_s values on the leading and trailing surfaces are very close when rotation number is smaller than 0.3. After that, the Nusselt number ratios on the leading and trailing surfaces begin to diverge. **Fig. 27** also shows the Nu/Nu_s with the average buoyancy parameters. The trends are very similar to the plots with the rotation number.

For the inverted 45° angled ribs, the average Nusselt number ratio (Nu/Nu_s) increases with rotation number and buoyancy parameter on both the leading and trailing surfaces. Nu ratio (Nu/Nu_s) increases up to 1.5 on the trailing surface while only increases up to 1.1 on the leading surface as rotation number and buoyancy parameter increases.

For 90° ribs, both the leading and trailing surface increase with rotation number and buoyancy parameter. Trailing surface has higher heat transfer enhancement than the leading surface. It shows that the heat transfer enhancement due to rotation for 90° rib is the highest among all the rib cases.

Table 1: Correlation Coefficients for Nu Ratio in Triangular Channel

Ro	A	m	B	n
Leading - Smooth	0.97	0.02	-5.5	7.5
Trailing - Smooth	0.5	-0.2	0.8	0.95
Leading - 45° rib	1.19	0.035	1.6	1.45
Trailing - 45° rib	0.99	0.01	1.9	5.5
Leading - Inverted 45° rib	1.05	0.01	0.5	5.5
Trailing - Inverted 45° rib	1.25	0.04	1.2	2.5
Leading - 90° rib	1.1	0.05	0.35	1.05
Trailing - 90° rib	1.22	0.028	1.05	1.15

Bo	A	m	B	n
Leading - Smooth	0.8	-0.02	0.18	1.1
Trailing - Smooth	1.1	0.02	-0.2	0.25
Leading - 45° rib	1.21	0.04	0.55	0.8
Trailing - 45° rib	0.98	0.01	0.02	2
Leading - Inverted 45° rib	0.9	-0.01	0.16	0.25
Trailing - Inverted 45° rib	1.3	0.05	0.1	0.8
Leading - 90° rib	1.41	0.055	-0.21	0.12
Trailing - 90° rib	1.21	0.04	0.5	0.35

4.2 Trailing Edge – Wedge Channel

4.2.1 Heat Transfer in Stationary Channel

Smooth Surface without Slot Ejection

The stationary channel provides baseline results before considering the effect of rotation. As shown in **Fig. 9**, these regions are the side wall, leading inner, leading mid-span, leading outer, trailing inner, trailing mid-span, and trailing outer surfaces. As previously noted, the channel is orientated 135° from the direction of rotation. The orientation is applicable to cooling channels typically encountered near the trailing edge of the turbine blades. It should be noted this orientation is defined with respect to the centerline of the channel. The current wedge-shaped channel used to model a typical trailing edge cooling channel combines several features, each of which has significant impacts on both the flow through the channel and the heat transfer within the channel. In the non-rotating channel, the level of heat transfer is influenced by the channel shape. With a much smaller cross-section, the flow encounters more resistance near the outer surfaces than the inner surfaces of the channel. The coolant flow enters the heated portion of the test section without being hydrodynamically developed. Increased heat transfer coefficients are expected due to the simultaneous development of both the hydrodynamic and thermal boundary layers. Due to the relatively short length of the channel (L/D_h =6.30), the flow likely never reaches a fully developed flow condition. An additional factor which cannot be ignored is the 180° turn used to return the flow out from the test section. Elevated heat transfer coefficients can be expected in the latter half of the channel due to the strong turn effect. The turn occurs on the outer edge of the

channel. The Nusselt number ratios for the stationary channel have been plotted in **Figure 28** to highlight the spanwise variation within the channel at a given Reynolds number. At the entrance of the channel, the heat transfer coefficients are elevated due to the simultaneous development of both the thermal and hydrodynamic boundary layers. The Nusselt number ratios gradually approach unity (coinciding with fully developed turbulent flow in a circular tube) near the end of the channel. It is also observed on this inner surface, the heat transfer coefficients are not influenced by the 180° turn on the opposite side of the channel. With the Nusselt number ratio, the Reynolds number effect on the heat transfer coefficients has been eliminated, and this is clearly shown by the collapse of the four curves together. At any given Reynolds number, the greatest heat transfer enhancement at the inlet of the channel occurs on the inner surface, and the Nusselt number ratios are the least on the outer surface. Moving streamwise through the channel, the side wall approaches the fully developed Nusselt number ratio of unity. Similar trends are present for the inner surface but the level of enhancement is elevated above the side wall. The Nusselt number ratios on the mid-span and outer surfaces follow different trends. The strong effect of the 180° turn is very obvious when directly compared to the side and inner surfaces.

Smooth Surface with Slot Ejection

In the actual turbine blade, the coolant is ejected through holes or slots to the mainstream flow near the trailing edge. In the current study, a second model with slot

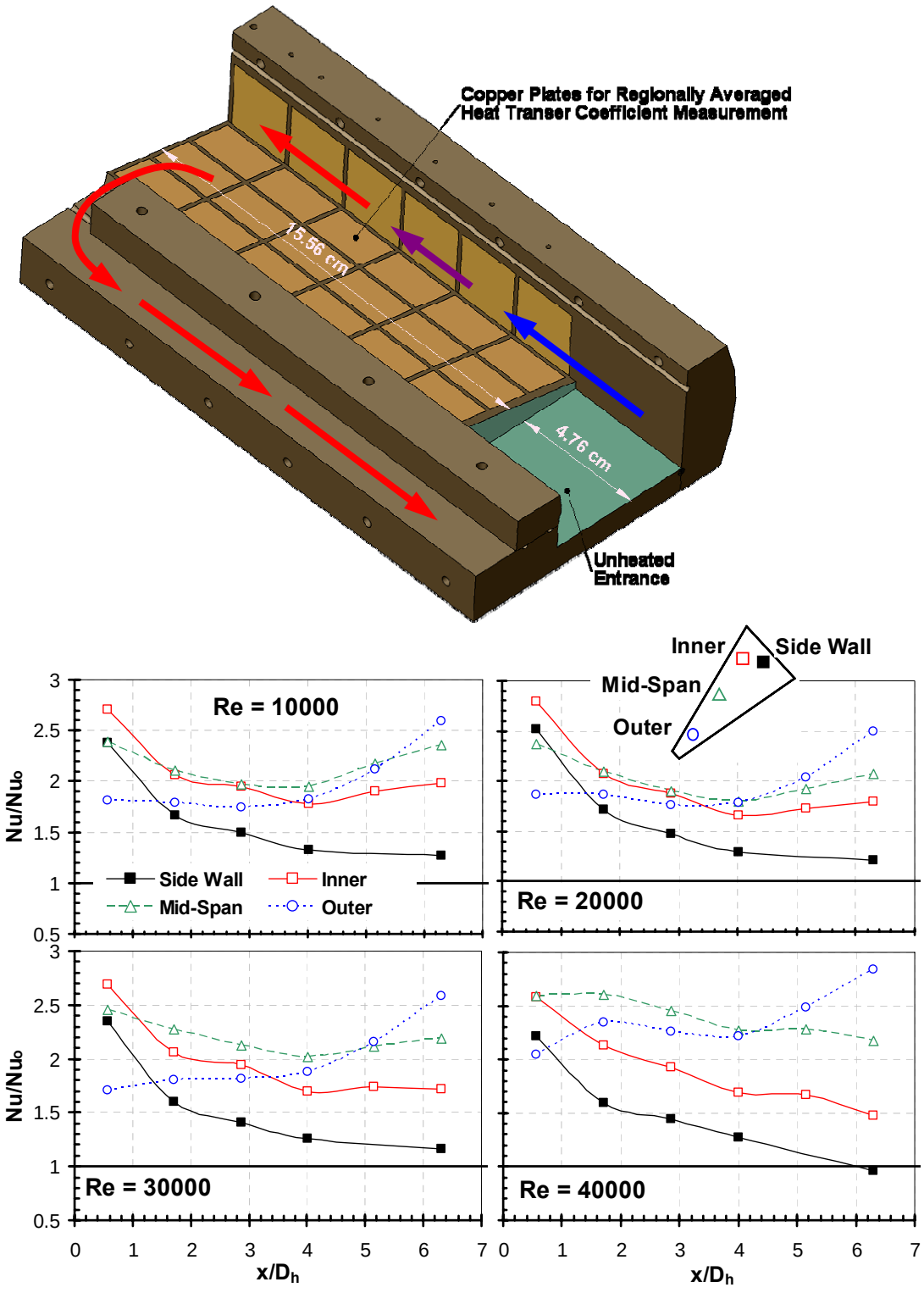

Figure 28: Nusselt Number Ratio for Smooth Channel without Slot Ejection at Stationary Condition

ejection was tested as shown in **Fig. 5(b)**. As the flow goes along the streamwise direction, it is discharged through the slot and the local mass flow rate decreases. The decrease of the coolant remaining in the channel leads to decrease of the heat transfer coefficient along the streamwise direction. **Figure 29** shows the Nusselt number distribution along the streamwise direction at four different inlet Reynolds numbers (Re_i=10000, 20000, 30000, and 40000). The local Reynolds number (Re_x) at the first region (x/D_h=0.57) and the last region (x/D_h=6.30) is also labeled in the figure. As the inlet Reynolds number increases from 10000 to 40000, the Nusselt number also increases. On the outer surface, the flow turns 90° from streamwise direction to the ejection slot and this turning induced secondary flow enhances the heat transfer. Furthermore, the slot ejection thins the boundary layer and strong turbulence mixing also occurs around this region. Therefore, heat transfer enhancement is the highest. In this region, the Nusselt number maintains the same level at the lowest Reynolds number case (Re_i=10000). However, the Nusselt number increases and then decreases for the other three Reynolds number cases. The coolant flow tends to go towards the narrow region (outer surface) due to slot ejection, and the wide region (side wall and inner surface) has less coolant. Therefore, the heat transfer decreases from the narrow side towards the wide side, and the wide side (side wall) has the lowest heat transfer. For the side wall, inner surface and the mid-span, the boundary layer is thicker than the outer surface due to less effect from the slot ejection. The Nusselt number decreases gradually along the streamwise direction due to the decrease of the local mass flow rate and the development of the boundary layer along the streamwise direction.

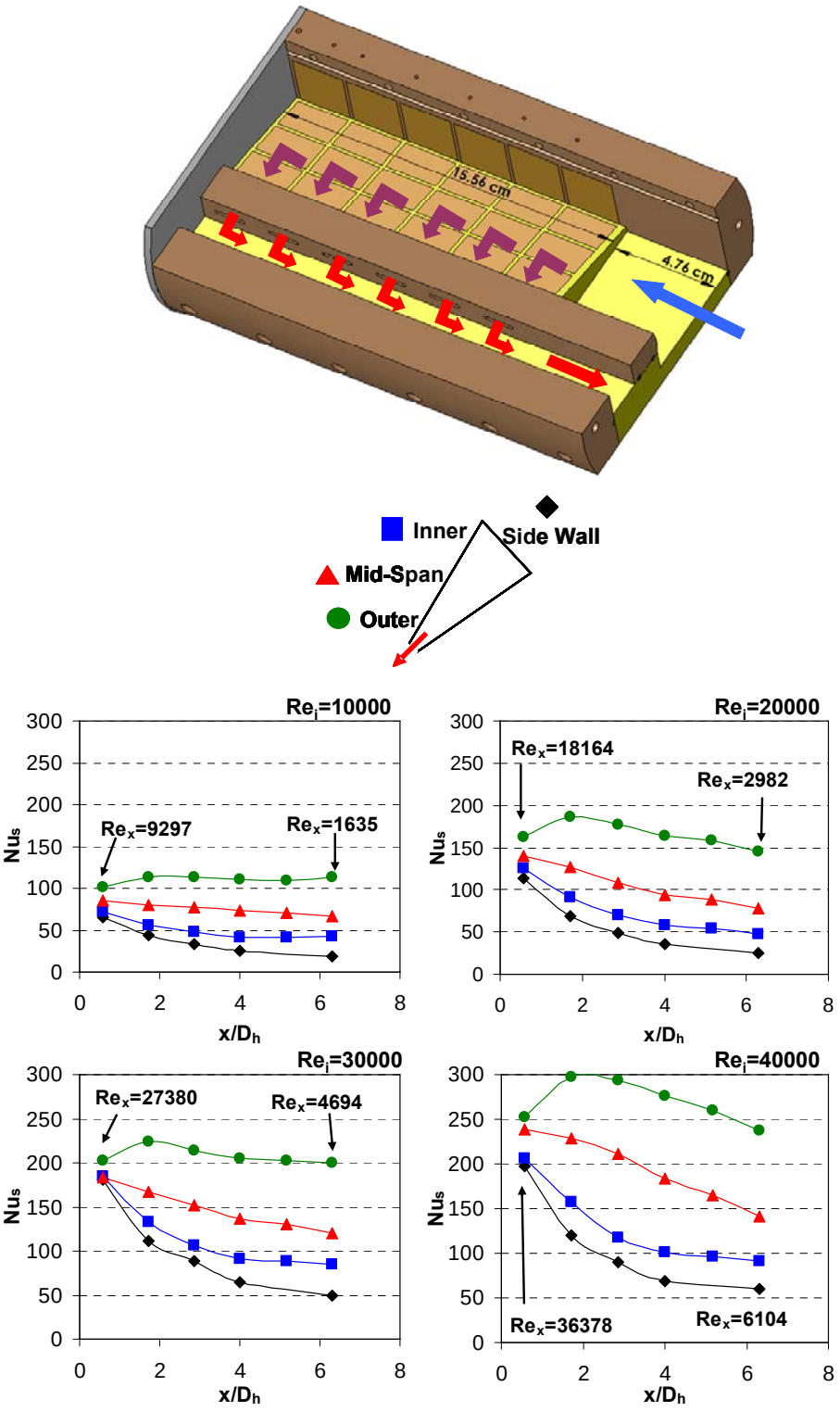

Figure 29: Nusselt Number for Smooth Channel with Slot Ejection at Stationary Condition

Smooth Surface without Returning Crossflow

The previous test model has the strong returning crossflow which influences fluid flow and heat transfer. The test section without returning crossflow has also been studied as shown in **Fig. 7(a)**. The local Reynolds number decreases as the flow goes downstream due to flow discharging through the slots as shown in **Figure 30**. The local Reynolds numbers for both the smooth and ribbed cases are presented. It decreases from 40000 down to 6500 at a Reynolds number of 40000 and decreases from 10000 down to 1700 at a Reynolds number of 10000. It shows that the local Reynolds number distributions are very similar for all the cases. The local mass flow distribution is affected by the slot configuration and neither rib nor rotation has significant effects on it. **Figure 31** shows the Nusslet number inside the stationary smooth channel at four different Reynolds numbers. The local mass flow rate decreases along the streamwise direction due to slot ejection and the local Reynolds numbers are labeled on the first point and last point of the figure. Heat transfer is enhanced near the entrance for all the cases due to sudden contraction. Heat transfer on these two symmetric surfaces is very close due to symmetric geometry. It only shows small difference on the last point at downstream due to higher uncertainty caused by stagnation and turn effects.

On the outer region, Nusselt number maintains the same level along the streamwise direction. The Nusselt number is 120 at a Reynolds number of 10000 and 250 at a Reynolds number of 40000. It has the highest heat transfer level over the entire channel because it is close to the strong slot ejection region. Slot ejection not only alters turbulent mixing but also produces turning effects from mainstream flow to the exit jet.

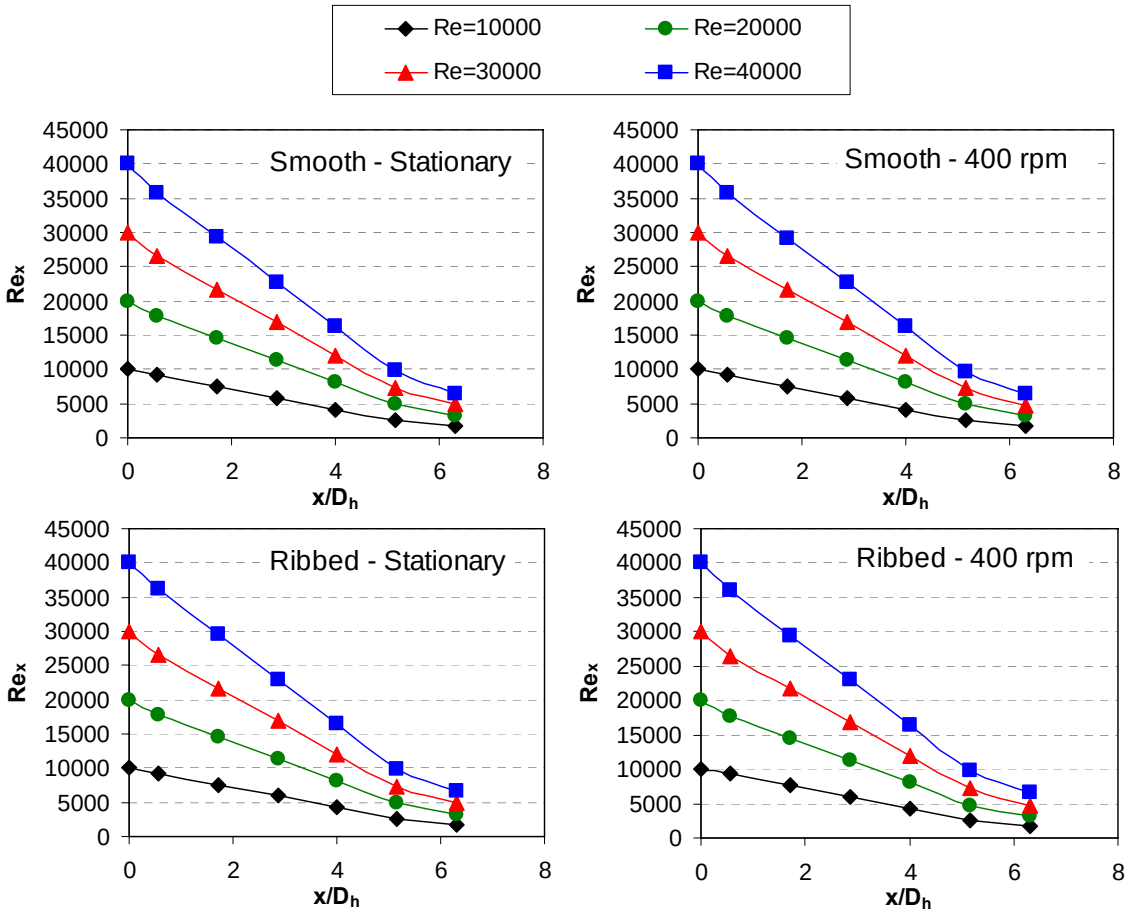

Figure 30: Local Reynolds Number Distribution inside the Channel

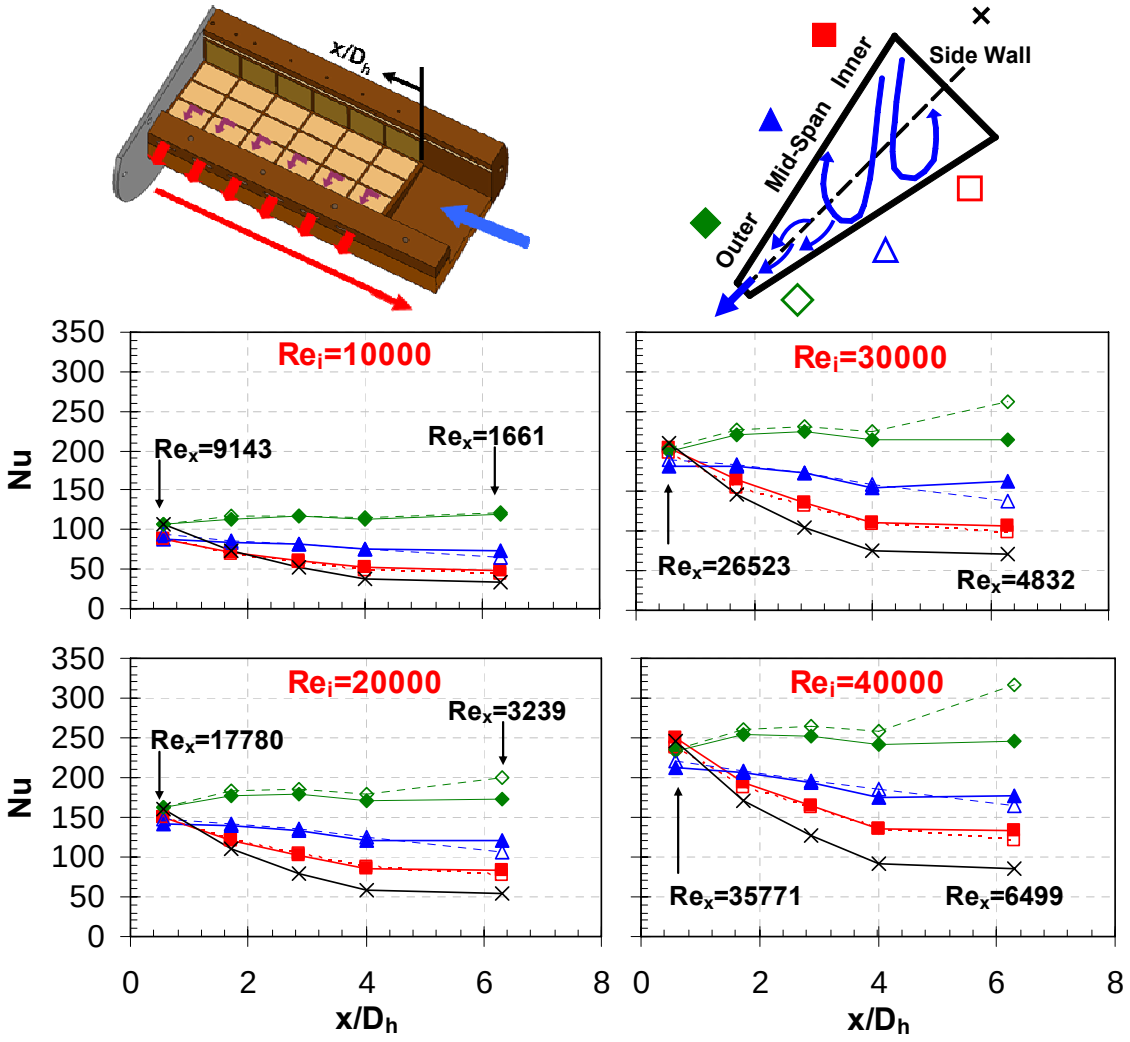

Figure 31: Nusselt Number for Smooth Channel at Stationary Condition without Crossflow Effect

This also shows that the slot ejection can enhance heat transfer even for the low Reynolds number region at downstream. The other regions (mid-span, inner, and side wall) show that Nusselt number decreases along the streamwise direction due to decreasing Reynolds number and boundary layer development. The Nusselt number declined due to diminished effect of slot ejection as the region moves towards the side wall. Slot ejection has minor effects near the side wall and heat transfer is the lowest due to thicker boundary layer. The Nusselt number decreases from 110 to 50 at Re=10000 and decreases from 250 to 80 at Re=40000 along the streamwise direction. As the Reynolds number increases, the Nusslet number also increases for all the regions.

Ribbed Surface without Returning Crossflow

From the smooth tests, heat transfer improvement is needed on the regions away from the slots. The ribs are put on the mid-span and inner regions to enhance heat transfer. There is no rib on the outer region because the slot ejection already enhances heat transfer tremendously. The 45° angled rib is chosen because this configuration helps heat transfer towards the inner region based on [8] and [11]. **Figure 32** shows the rib induced secondary flow which goes along the surface of inner region towards outer region and heat transfer enhancement is higher near the inner region than the mid-span region. It tends to continue flowing towards the outer region due to strong slot ejection without turning back towards the side wall.

The Nusselt number distribution inside the ribbed channel is shown in **Figure 33**. Similar trend can be observed while the heat transfer level is enhanced due to ribs. On

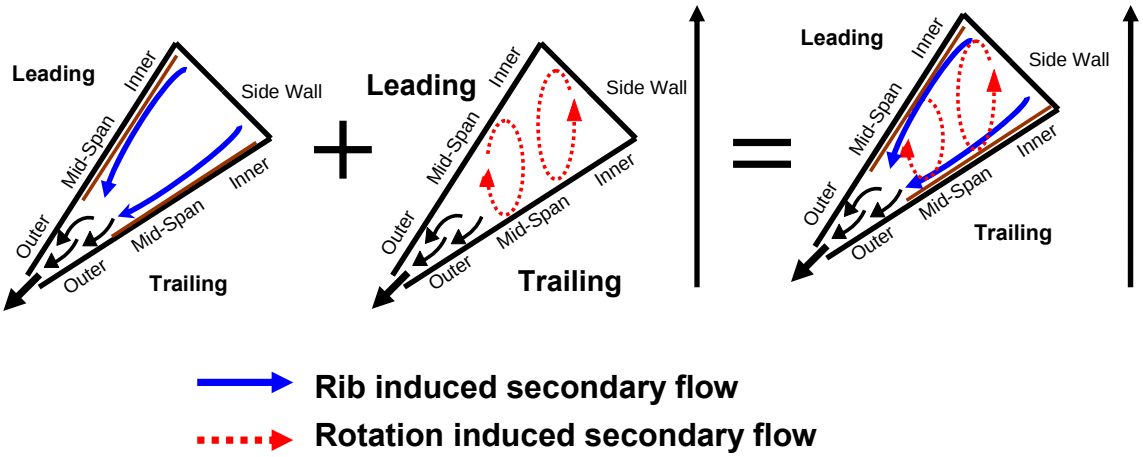

Figure 32: Secondary Flow Induced by the Rotation and Ribs inside the Channel

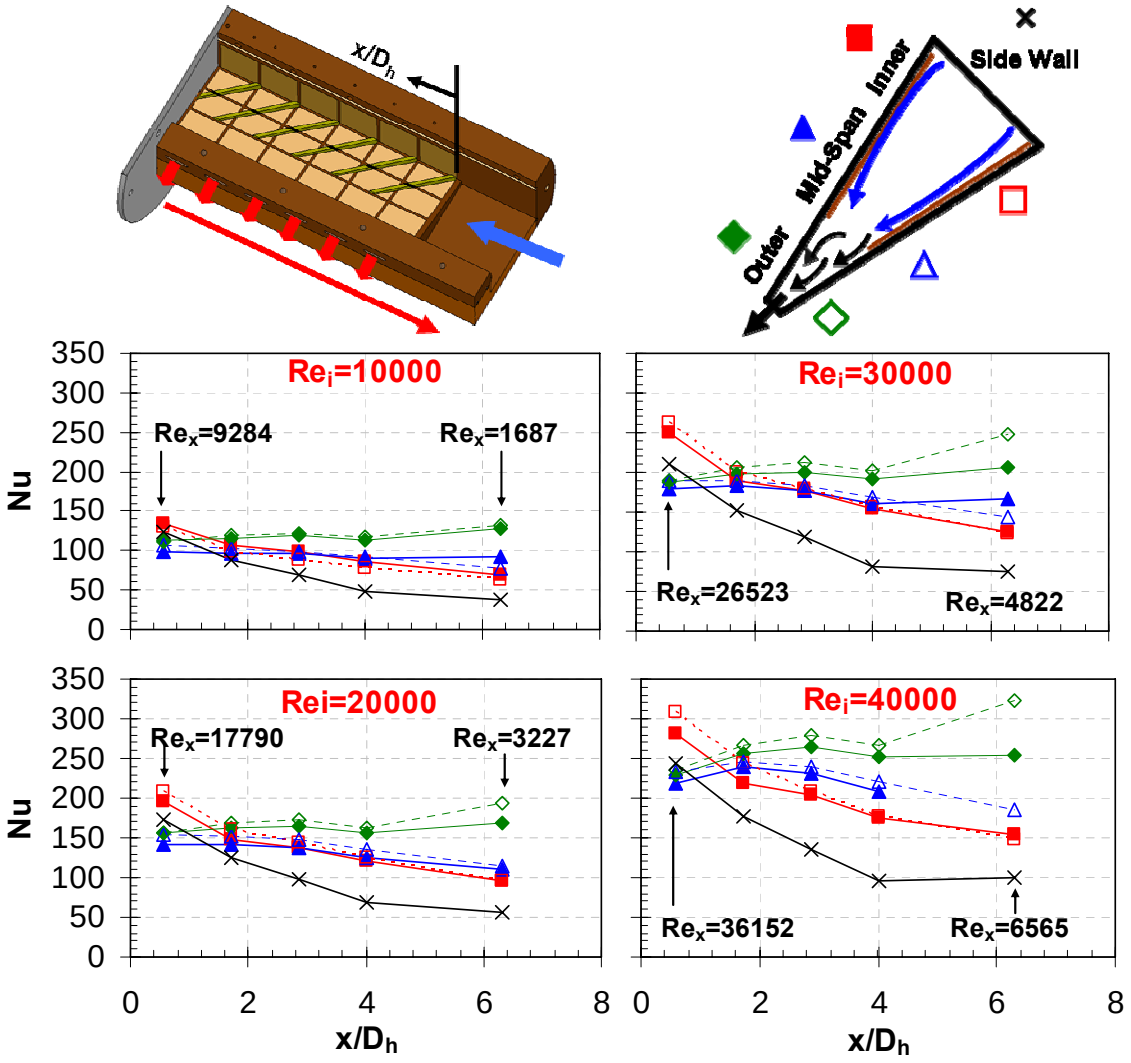

Figure 33: Nusselt Number for Ribbed Channel at Stationary Condition without Crossflow Effect

the inner region, Nusselt number decreases along the streamwise direction from 130 to 70 at a Reynolds number of 10000 and from 290 to 150 at a Reynolds number of 40000. The Nusselt numbers are higher compared to the smooth case. It is noted that near the entrance region (x/D_h=0.6), inner region has the highest heat transfer due to entrance effects in the ribbed channel. The heat transfer augmentation by the ribs diminished towards downstream because local mass flow is reducing. Slot ejection effects dominated over the rib effects at downstream regions. The heat transfer enhancement on the mid-span is smaller than the inner region because the Nu/Nu_o is similar for both regions in the middle of the channel. Highest heat transfer still occurs on the outer region as flow goes downstream for the ribbed case. There is no significant difference between the ribbed case and the smooth case on the outer region and side wall. The results show that even with the help from the ribs, inner and mid-span regions still have lower heat transfer than the outer region. Slot ejection has higher heat transfer enhancement than ribs in this channel.

4.2.2 Heat Transfer in Rotating Channel

Smooth Surface without Slot Ejection

In the present study, the wedge-shaped channel is rotating with β=135°. It has already been shown that this specific geometry has many features which combine to profoundly affect the heat transfer coefficients within the channel. However, it is necessary to consider how rotation affects the heat transfer through the channel. Traditional, conceptual descriptions of the rotation induced secondary flow involve the

formation of two counter-rotating vortices. The vortices form in the cross-section of the channel as the coolant is forced away from the leading surface to the trailing surface. Due to the wedge-shaped cross-section of the present study, it is anticipated, there is not a distinct formation of these counter-rotating vortices. This behavior is likely to occur within the wide half (near the side wall and inner surfaces) of the channel. In other words, the coolant is forced away from the leading inner surface toward the trailing mid-span and inner surfaces. In the very narrow region of the channel, these rotation induced vortices begin to breakdown, and no clear structure exists. In this configuration, it shows that the secondary flow structure deteriorates, and a second (or even more) set of counter rotating vortices form. This structure breakdown will result in more turbulent mixing, and thus increased heat transfer coefficients of both the leading and trailing surfaces in the narrow region of the channel. The presentation of the measured heat transfer coefficients begins with the streamwise distributions measured at each of the four Reynolds numbers at a set rotational speed of 500 rpm. As shown in **Figure 34**, the heat transfer enhancement on each surface can be compared at each Reynolds number. As previously described, the rotational speed combines with the Reynolds number of the flow to form the non-dimensional rotation number. Therefore, as the Reynolds number increases from 10000 to 40000, the rotation number decreases from 1.02 to 0.25. The isolated effect of these two parameters (Reynolds number and rotational speed) will soon be addressed. At the lowest Reynolds number of 10000 (Ro = 1.02), the expected trend of non-symmetrical heat transfer coefficient distributions is observed. In other words, more heat transfer enhancement is present on the trailing surfaces than the leading

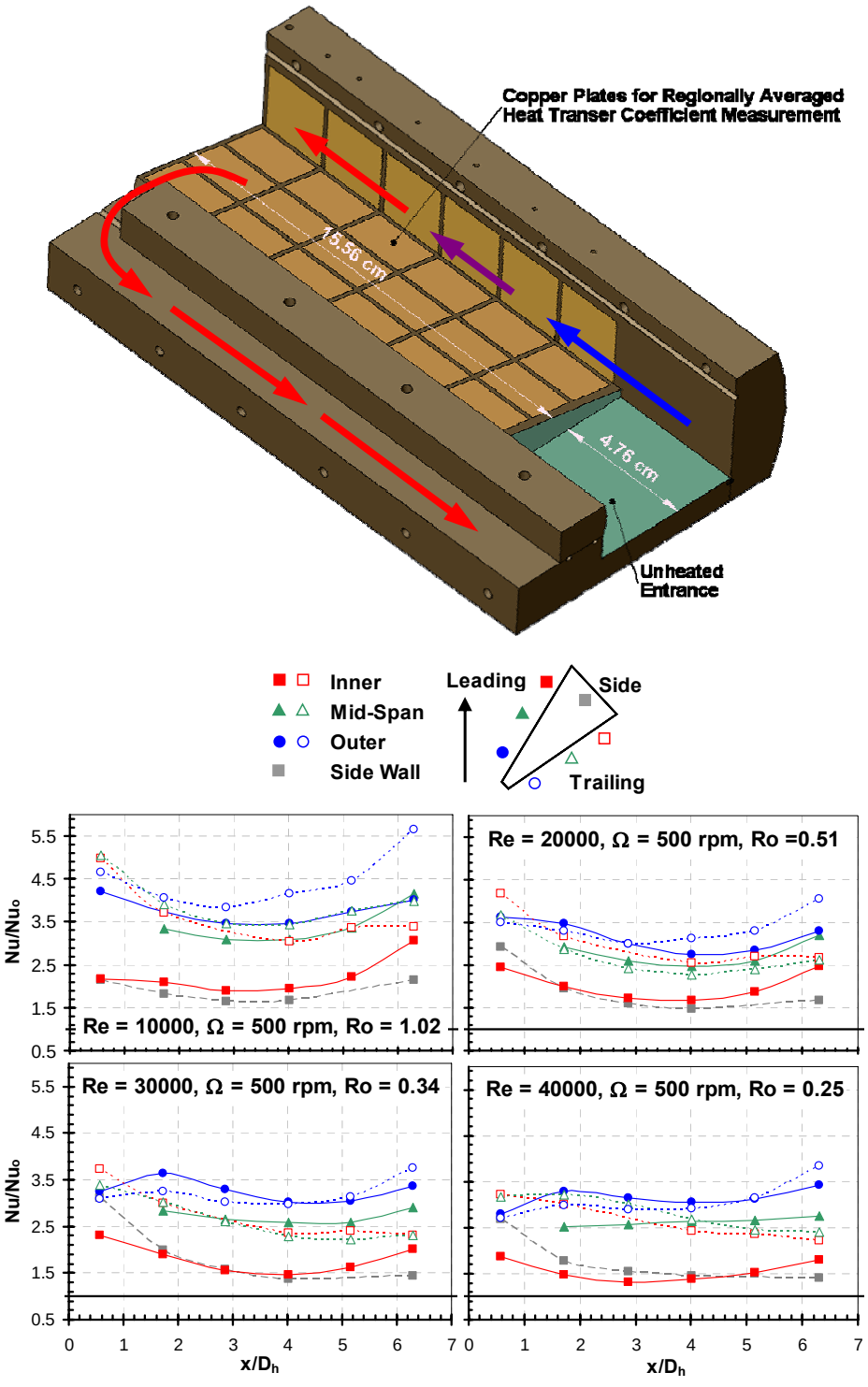

Figure 34: Nusselt Number Ratio for Smooth Channel without Slot Ejection at Rotating Condition

surfaces. In addition, the greatest difference between the leading and trailing surfaces occurs on the inner surfaces. In this wider area of the channel, the rotation induced secondary flow is much stronger, and organized, than in the more narrow section of the channel. In addition to the effect of rotation, the features inherent to the channel design are also present (entry region, 180° turn, and channel shape). As the Reynolds number increases (rotation number decreases), the Nusselt number ratios decrease. In addition, the difference between the leading and trailing surfaces decreases.

Smooth Surface with Slot Ejection

This specific geometry with slot ejection also has many features which combine to affect the heat transfer coefficients within the channel. However, it is necessary to consider how rotation affects the heat transfer through the channel. As stated previously, conceptual descriptions of the rotation induced secondary flow involve the formation of two counter-rotating vortices in the wider region. In the very narrow region of the channel, these rotation induced vortices begin to breakdown and no clear structure exists. Furthermore, strong turbulent mixing occurs at this region due to the slot ejection through the outer surface. The strong slot jet behavior tends to decrease toward the inner surface and side wall. In order to study the heat transfer enhancement (or declination) due to rotation, the ratio of rotating Nusselt number (Nu) to the stationary Nusselt number (Nu_s) distribution along the streamwise direction is plotted in **Figure 35**. Four different Reynolds number cases, each at the highest rotational speed (500 rpm), are presented to show the effect of rotation. The Nu/Nu_s value on the trailing surface is

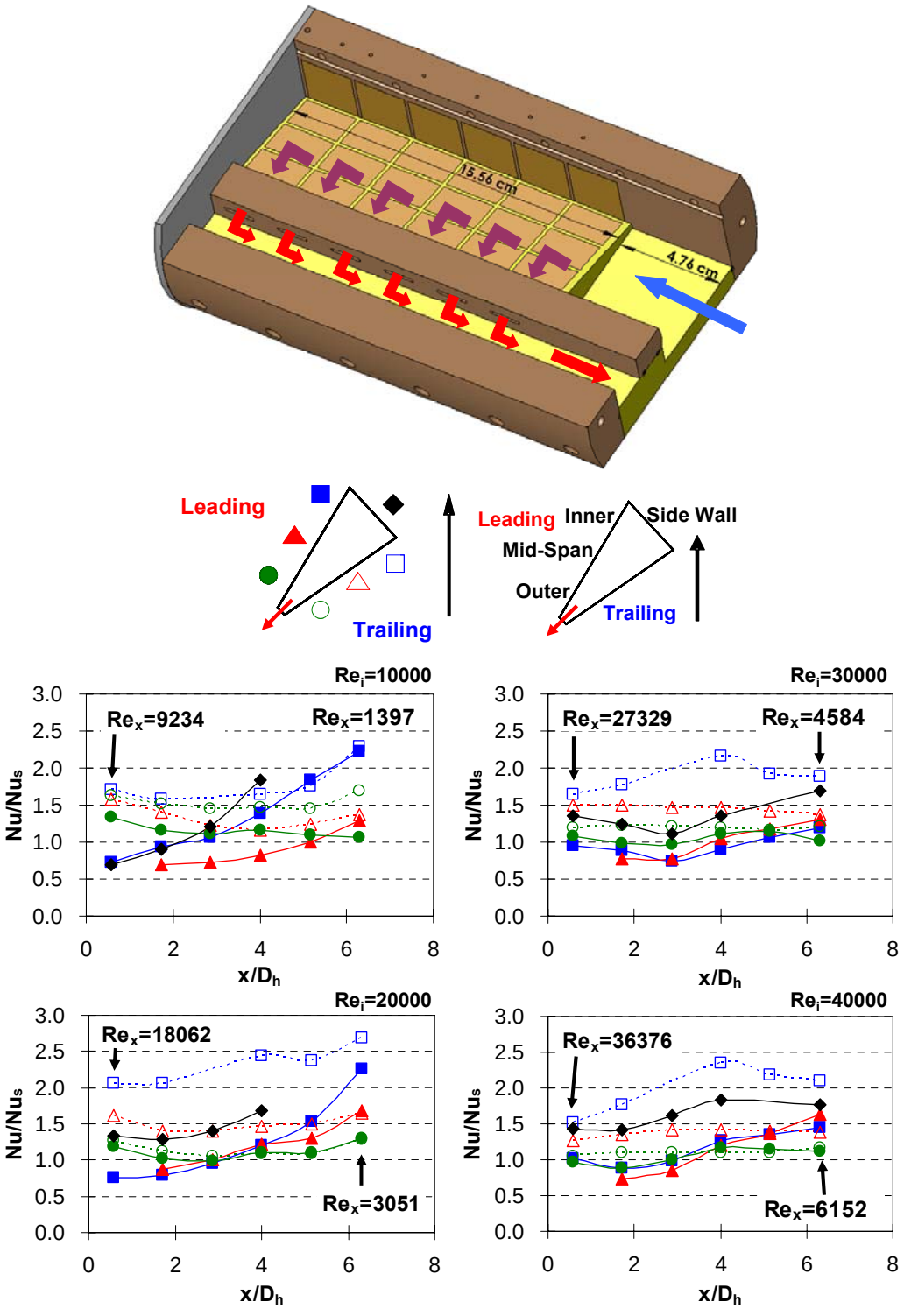

Figure 35: Nusselt Number Ratios for Ribbed Channel with Slot Ejection at Rotating Condition

higher than the leading surface for the inner, mid-span, and outer surfaces. In the inner surface, the effect of rotation is strong and the difference of Nu/Nu_s value between the leading and trailing surfaces is large. In the outer surface, the effect or rotation reduces and the difference between the leading and trailing surfaces is small. As the Reynolds number increases, the effect of rotation deceases. The heat transfer enhancement is the highest in the trailing inner surface at Re_i=20000, 30000, and 40000.

Smooth Surface without Returning Crossflow

When the channel is rotating, heat transfer is affected by the rotation induced Coriolis force and the buoyancy force. The channel orientation with respect to the direction of rotation also affects heat transfer. For a radially outward flow inside a square channel, heat transfer is enhanced on the trailing surface while declined on the leading surface. A pair of counter rotating vortices is formed inside the rotating channel due to Coriolis force. The structure of this counter rotating vortices is determined by this wedge-shaped geometry and the direction of rotation. The rotation induced vortices in the current study can be speculated in **Fig. 32**. The effect of rotation is more obvious near the mid-span and inner region and diminishes towards the outer region. There is no clear rotating vortex near the outer region due to strong turbulent mixing caused by the slot ejection. Therefore, the effect of rotation is minor near the narrow region. For the ribbed case, the ribs also induced secondary flow inside this channel. Heat transfer is affected by the combined secondary flow effects from ribs and rotation as shown in **Fig. 32**.

The Nusselt number distribution in the rotating smooth channel is shown in **Figure 36**. In the current setup, the slot ejection dominates and the effect of rotation is small near the outer region. With the channel orientation of 135°, heat transfer is enhanced on the trailing surface. On the inner region, the effect of rotation is most obvious because the larger space allows counter rotating vortices to develop freely. The Nusslet number on the trailing surface is much higher than the leading surface in this region. The difference between leading and trailing surface is the largest, especially near the entrance region. The heat transfer is the lowest on the leading inner region when $x/D_h<4.0$ and on the side wall when $x/D_h=6.3$. The Nusselt number on the trailing surface is about 2.5 times higher than the leading surface at the entrance of the inner region. The results on the leading and trailing surfaces converge as the flow goes downstream. On the mid-span region, the trend is similar to the inner region. However, the difference between the leading and trailing surfaces is smaller due to smaller effect of rotation. The Nusselt number on the trailing surface is only 1.5 times higher than the leading surface near the entrance. The Nusselt number on the leading and trailing surfaces also converges as flow goes downstream. It is interesting to see that the heat transfer is higher on the leading mid-span at the downstream region. On the outer surface, heat transfer on the trailing surface is only slightly higher than the leading surface. The strong slot ejection effect dominates over the effect of rotation and heat transfer enhanced due to rotation on both surfaces.

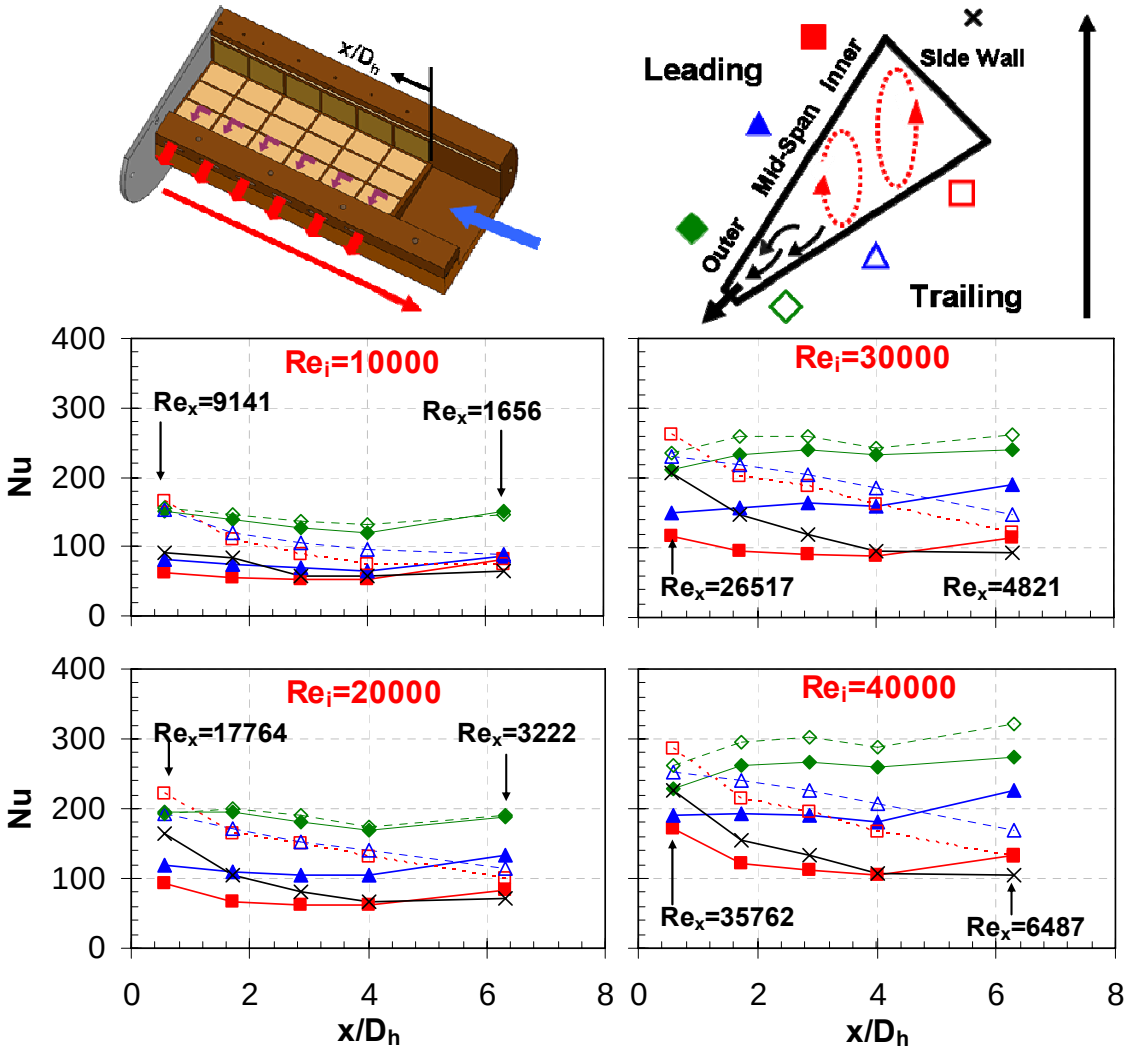

Figure 36: Nusselt Number for Smooth Channel at Rotating Condition without Crossflow Effect

Ribbed Surface without Returning Crossflow

When the ribs were put on the leading and trailing surfaces, the heat transfer distribution was affected by the combined effects from rib and rotation. The Nusselt number distribution for the rotating ribbed channel is shown in **Figure 37**. The Nusselt number is the lowest on the leading inner region near the upstream region and the side-wall near the downstream region. On the inner region, heat transfer also enhanced on the trailing surface. The Nusselt number on the trailing surface is 2.1 times higher than the leading surface at entrance. The difference between leading and trailing surface becomes smaller as flow goes downstream. Similar trends can also be observed on the mid-span region while the heat transfer is enhanced compared to the smooth rotating case. Highest heat transfer also occurs on the outer region. It shows that neither the rib nor rotation has significant effects on heat transfer because of the strong slot ejection. It is seen that rotation has larger enhancement near the entrance and effect of rotation is minor near the downstream region.

4.2.3 Rotation Number Effects

Rotation number is a ratio of Coriolis force to the bulk flow inertia force. The rotation number is defined in Equation 10. This non-dimensional parameter is widely used to quantify the effect of rotation in the industry and academia. By varying the rotational speed (Coriolis force) and the Reynolds number (flow inertia force), the contribution from these two factors should yield the same results. In the current setup, the local mass flow rate decreases along the streamwise direction due to mass flow loss

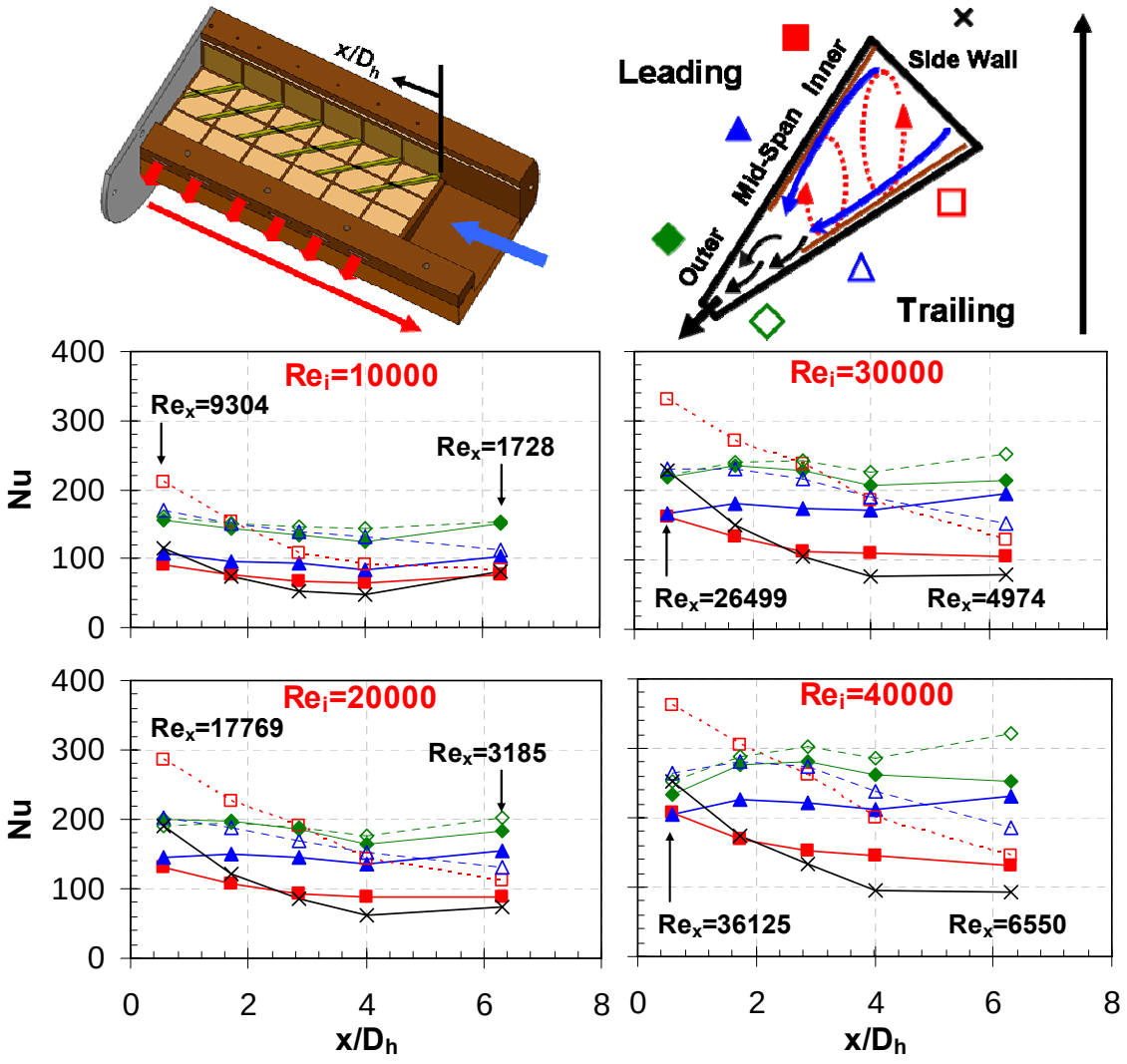

Figure 37: Nusselt Number for Ribbed Channel at Rotating Condition without Crossflow Effect

through slot. The local rotation number varies depending on the local Reynolds number as shown in **Figure 38**. It shows that the rotation number is relatively smaller near the entrance of the channel (region 2) than the end of the channel (region 6). The maximum local rotation number is up to 4.5 on region 6.

Heat transfer enhancement due to effect of rotation is represented by the Nusselt number ratio (Nu/Nu_o). It represents the true heat transfer enhancement compared to the turbulent flow inside the smooth tube. **Figure 39** shows the heat transfer enhancement (Nu/Nu_o) of the smooth case as well as the ribbed case. Three different regions (2, 4, and 6) along the streamwise direction (x/D_h=1.7, 4.0, and 6.3, respectively) are chosen to study the effect of rotation.

The Reynolds number effect has been eliminated and all the data points can be correlated into a curve. The discussion starts with region 2 where strong entrance effects exist. For region 2, Nu ratio is the highest on the leading and trailing surfaces of the outer wall and it increases with rotation number. The Nu ratio also increases with rotation number on the trailing mid-span and trailing inner region. However, Nu ratio decreases until a critical rotation number of 0.55 and then increases with rotation number on the leading mid-span and leading inner region. Leading inner region is the lowest Nu ratio region due to profound effect of rotation declines heat transfer. Nu ratio increases with rotation number on the side wall region.

The heat transfer level on region 4 is higher than region 2 due to smaller Reynolds number. For region 4, similar trend can be observed on outer surface and this region also has highest heat transfer. The entrance effect is reduced in this region. For

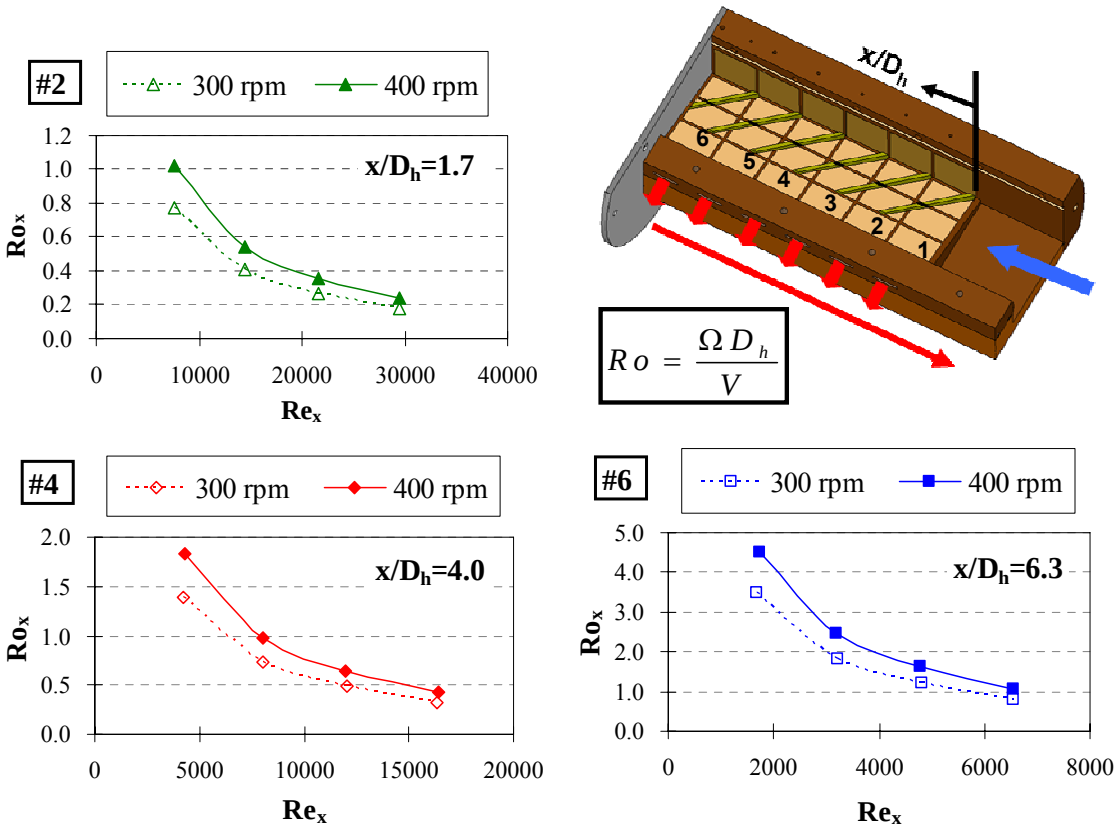

Figure 38: Local Rotation Number Distribution inside the Channel

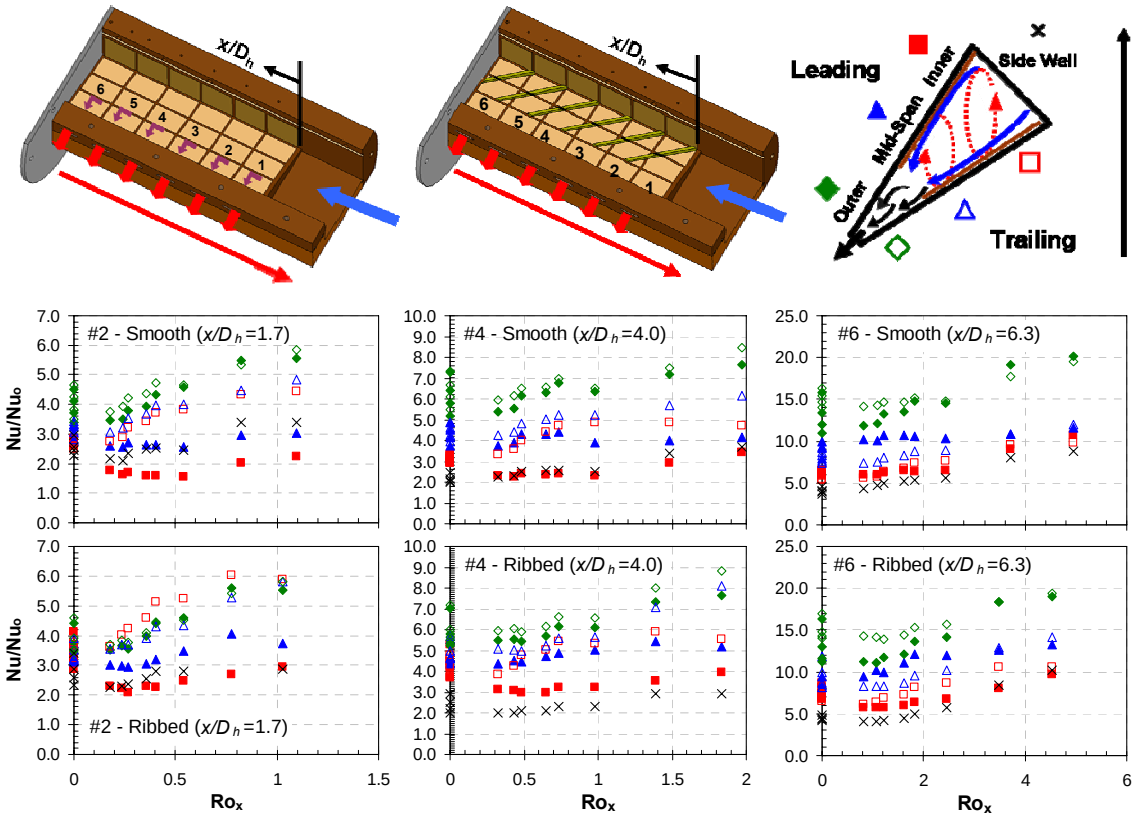

Figure 39: Effect of Local Rotation Number on Nusselt Number Ratios (Nu/Nu_o)

the mid-span region, Nu ratio maintains the same level on the leading surface and increase with the rotation number on the trailing surface. For the inner region, heat transfer increases with rotation number on the leading surface. Nu ratio increases with rotation number up to 1.0 and then remain similar level on the trailing surface of the inner region. On region 6, heat transfer increases with rotation number on every region except leading surface of the mid-span. It maintains the same level as rotation number increases. Side wall has the lowest heat transfer on region 6. The heat transfer level is extremely high due to lowest Reynolds number near this region. Nu/Nu_o increases up to 20 at the highest rotation number due to low Reynolds number of about 1700.

The Nusselt number ratio (Nu/Nu_o) distribution with rotation number for the ribbed surface is also plotted in this figure. For region 2, heat transfer increases with the rotation number on the trailing inner region and is the highest among all the surfaces. However, Nu/Nu_o decreases to 2.0 with rotation number until rotation number of 0.25 and then increases to 3.0 with rotation number on the leading inner region. This region has the lowest Nu ratio due to effect of rotation. Heat transfer increases with the rotation number on the mid-span and outer regions. On region 4, Nu ratio decreases and then increases with rotation number on leading inner region while the other regions increases with rotation number. However, on region 6, all the curves increases with rotation number and both have similar trends. Side wall has the lowest heat transfer on region 4 and 6.

4.2.4 Buoyancy Parameter Effects

The buoyancy parameter is also a widely used non-dimensional parameter to quantify the effect of rotation inside the gas turbine blade. The buoyancy force due to the centrifugal force and temperature difference is important due to the high rotating speed and large temperature difference in the actual engines. The buoyancy parameter considers all factors affecting the effect of rotation: the density ratio (temperature difference), the rotation number, and the rotating radius. The local buoyancy parameter is shown in Equation 11. The local film temperature is defined as the average of the local wall temperature and the local bulk temperature as shown in Equation 12. A constant density ratio of 0.11 was maintained for all the tests. In the current study, three regions (region2, 4, and 6) along the streamwise direction (x/D_h=1.7, 4.0, and 6.3, respectively) are also considered to study the effect of buoyancy parameter on Nusselt number ratios (Nu/Nu_o).

The Nusselt number ratio (Nu/Nu_o) with local buoyancy parameter for smooth case is plotted in **Figure 40**. The local buoyancy parameter is based on the local rotation number and rotating radius of each local point. The buoyancy parameter keeps increasing along the streamwise direction due to increased rotation number caused by decreased Reynolds number. For region 2, Nu/Nu_o decreases with buoyancy parameter until a critical buoyancy parameter of 1.0 and then increases with the buoyancy parameter on the leading surface of the inner region and mid-span. The other regions show heat transfer increases with the buoyancy parameter. For region 4, Nu ratio maintains the same level until buoyancy parameter of 3 and then starts to increases on

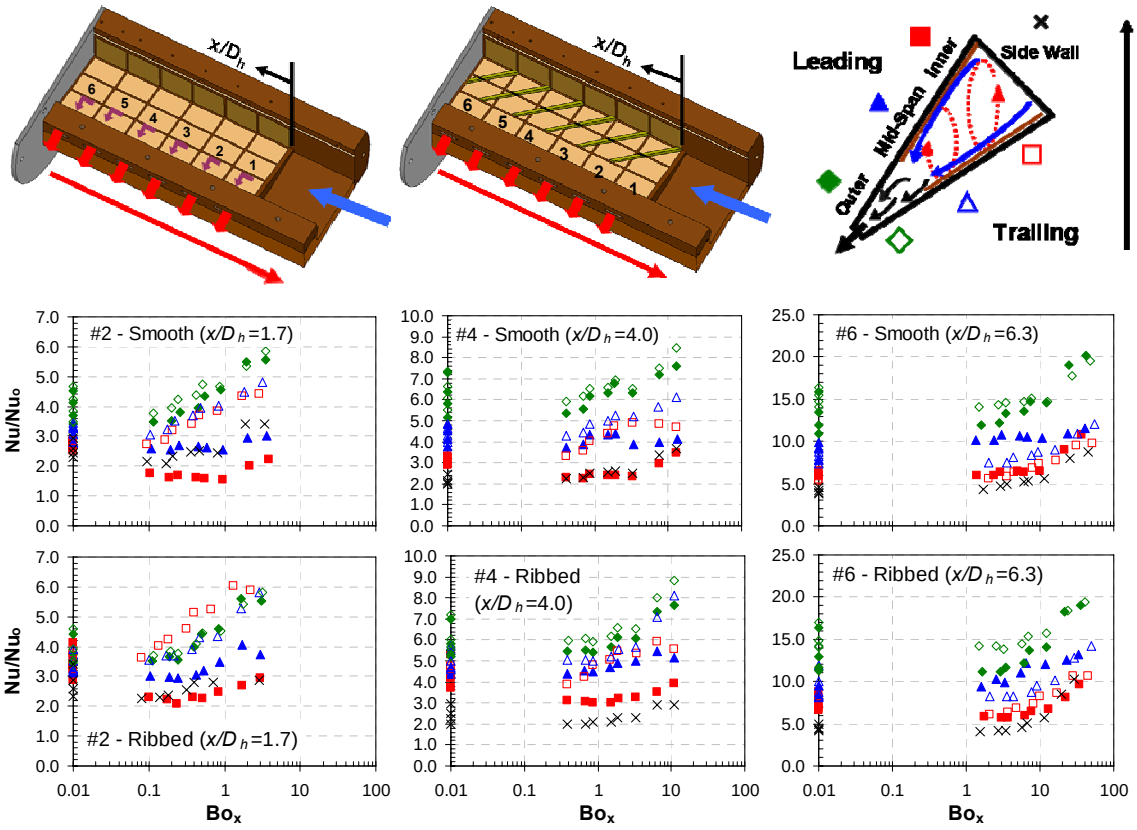

Figure 40: Effect of Local Buoyancy Parameter on Nusselt Number Ratios (Nu/Nu_o)

the side-wall and the leading surface of inner wall. It is interesting to see the Nu ration on the leading surface of the mid-span increases then decreases and increases again with buoyancy parameter. All the other regions show heat transfer increases with the buoyancy parameter. For region 6, heat transfer on the leading surface of the mid-span remains the same Nu ratio of 10.0 as the buoyancy parameter increases. All the other regions show heat transfer increases with the buoyancy parameter. The Nusselt number ratio (Nu/Nu_o) with local buoyancy parameter for ribbed case is also plotted in **Fig. 40.** The results are very similar to the rotation number plots. It also shows that the difference between the leading and trailing surfaces becomes smaller as flow goes downstream.

4.2.5 Average Heat Transfer

The average heat transfer results are based on the six points along the streamwise direction. Heat transfer enhancement (Nu/Nu_o) is presented to show the true enhancement level compared to the smooth tube as shown in **Figure 41**. The average rotation number and buoyancy parameter are also the average of six points in the streamwise direction. Both smooth results as well as the ribbed results are presented. For the smooth and ribbed cases, Nu/Nu_o gradually increases with rotation number on all regions. The Nu/Nu_o also presented with the average buoyancy parameter and it shows similar trend as rotation number plots.

A Nusselt number ratio of rotating Nusselt number to the stationary Nusselt number (Nu/Nu_s) is also presented in order to show the heat transfer enhancement/declination due to rotation as shown in **Figure 42**. For the smooth case,

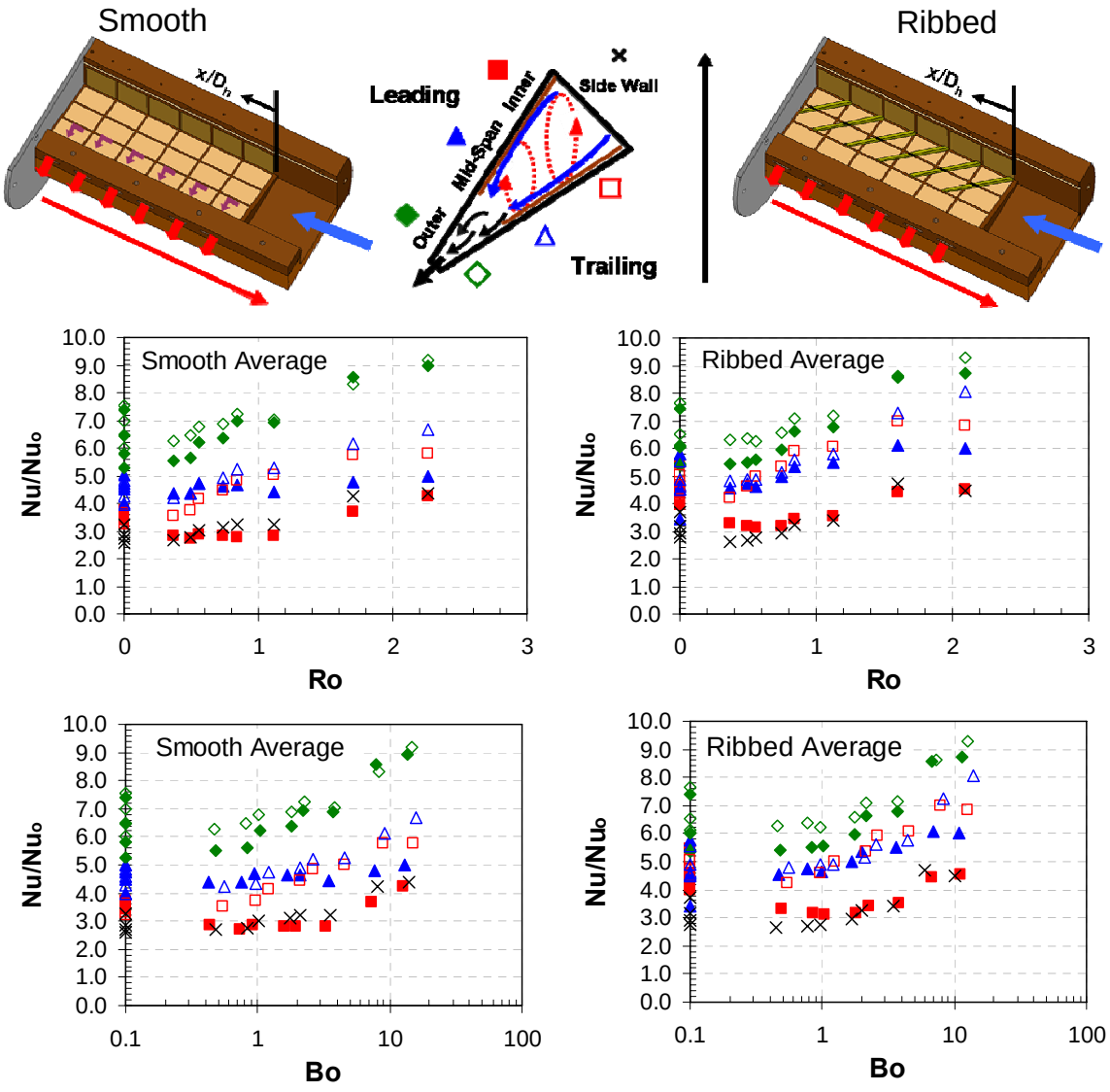

Figure 41: Average Nusselt Number Ratios (Nu/Nu_o) with Rotation Number and Buoyancy Parameter

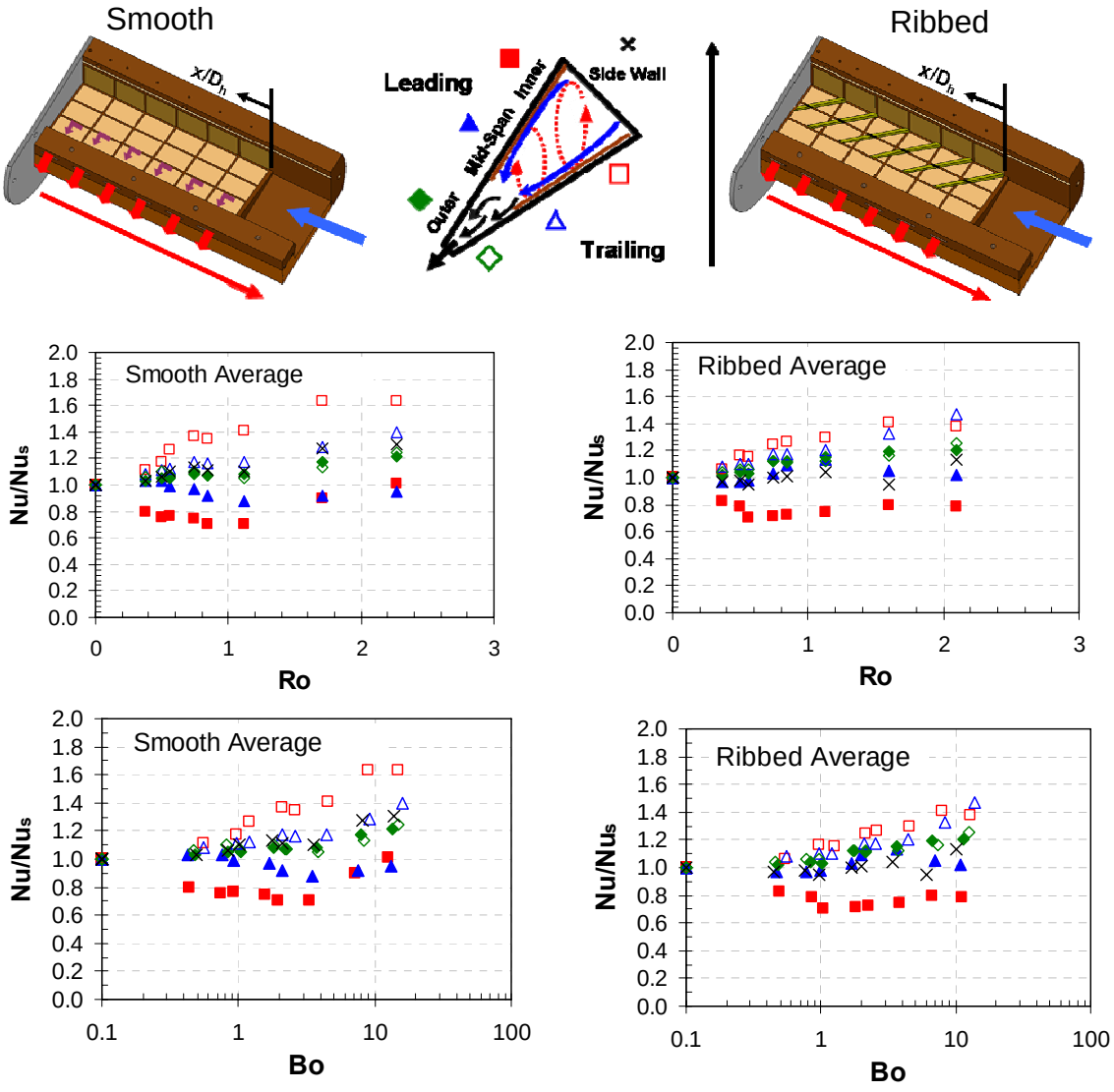

Figure 42: Average Nusselt Number Ratios (Nu/Nu_s) due to Effect of Rotation with Rotation Number and Buoyancy Parameter

begins to increase on the leading surfaces of the inner and mid-span. Nu/Nu_s increases with rotation number on all the other regions. The Nu ratio (Nu/Nu_s) is the lowest (0.7) on leading inner region and is the highest (1.6) on the trailing inner region. The Nusselt number ratios also plotted with the average buoyancy parameter as shown in the figure. There is also a critical buoyancy parameter of 3.5 where the heat transfer trend begins to change on the leading inner and mid-span region. The heat transfer enhancement due to rotation is most obvious in the inner region.

For the ribbed case, Nu/Nu_s decreases until a critical rotation number of 0.6 and then gradually increases only on the leading surface of the inner region. The Nu ratio with buoyancy parameter plot also shows similar trends as the rotation number plot. The highest Nu/Nu_s is 1.45 which is lower than the smooth case due to smaller effect of rotation on the ribbed surface. There is also a critical buoyancy parameter of 1.0 where the heat transfer trend begins to change on the leading inner surface.

4.2.6 Correlations for Heat Transfer Enhancement

The average heat transfer enhancements on the leading and trailing surfaces are averaged over the inner, mid-span, and outer regions. The spanwise and streamwise averaged Nusselt number ratios are shown in **Figure 43**. Each data point (on the leading and trailing surfaces) is now the average of the 18 points. It has been established that the heat transfer enhancement varies across the entire channel. Over the range of Reynolds numbers and rotational speeds, all the data points of these three surfaces can be fitted into a single curve. Most notably, the Nusselt number ratios increase as the rotation

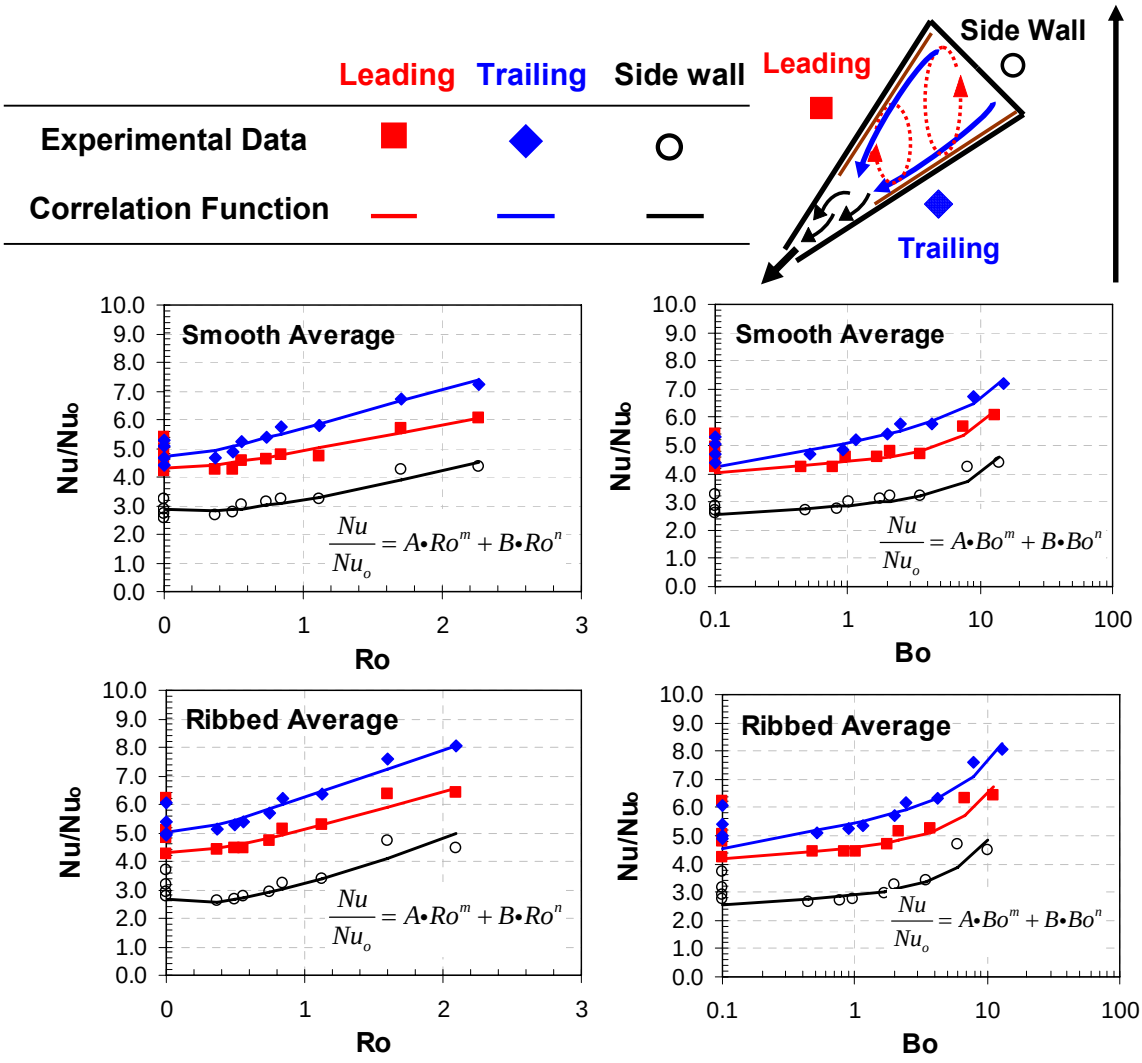

Figure 43: Correlations for Heat Transfer Enhancement with Rotation Number and Buoyancy Parameter

number and buoyancy parameter increases for all three surfaces. The correlations have been generated as a function of the rotation number and buoyancy parameter as shown in Equation 8. The constants for these correlation functions are shown in **Table 2**.

$$\frac{Nu}{Nu_o} = A \cdot Ro^m + B \cdot Ro^n \quad \frac{Nu}{Nu_o} = A \cdot Bo^m + B \cdot Bo^n \tag{13}$$

It shows that the heat transfer enhancement can be predicted by rotation number and buoyancy parameter in this wedge-shaped channel with smooth surface or ribbed surface.

Table 2: Correlation Coefficients for Nu Ratio in Wedge Channel

Smooth	**Ro**	A	B	m	n
	Leading	0.8	4.1	1.1	-0.01
	Trailing	1.4	4.3	1	-0.02
	Side wall	0.6	2.6	1.45	-0.02
	Bo				
	Leading	4.4	0.025	0.04	1.55
	Trailing	5.1	0.01	0.08	1.7
	Side wall	2.85	0.025	0.05	1.51
Ribbed	**Ro**	A	B	m	n
	Leading	1.02	4.1	1.2	-0.01
	Trailing	1.7	4.55	1	-0.02
	Side wall	0.9	2.3	1.5	-0.03
	Bo				
	Leading	4.56	0.04	0.04	1.55
	Trailing	5.45	0.02	0.08	1.7
	Side wall	2.85	0.05	0.05	1.51

5. SUMMARY AND CONCLUSIONS

5.1 Leading Edge – Triangular Channel

Heat transfer and pressure drop have been measured in a rotating equilateral triangular channel to model the cooling channel near the leading edge of the gas turbine blade. The results on the leading and trailing surfaces of the channel were reported. The performance of three different rib cases (45°, inverted 45°, and 90°) as well as smooth case was studied. Four Reynolds numbers (10000 to 40000) with five different rotational speeds (0 to 400 rpm) were tested for each case. The experiments were conducted under high rotation number and high buoyancy parameter to simulate the actual engine condition. The results can be correlated with different density ratios, Reynolds numbers, and rotational speeds by rotation number and buoyancy parameter. Based on the results reported, the following conclusion can be drawn:

In the rotating smooth channel, the heat transfer increases on the trailing surface, while the heat transfer decreases on the leading surface. However, heat transfer decreases and then increases with rotation number on L1 surface. The largest heat transfer declination occurred on L2 surface.

In the stationary channel, Nu/Nu_o is higher on the rib leading surfaces (L1 and T1) than the rib trailing surfaces (L2 and T2). This is a good design near the blade leading edge region only. When Reynolds number increases, the rib enhanced heat transfer decreases. 45° rib has the highest total thermal performance at stationary

condition. The effect of rotation in the ribbed channel is smaller than the smooth channel. Although 45° rib has the highest thermal performance at stationary condition, however, heat transfer enhancement due to rotation is small.

Inverted 45° angled ribs have reversed rib induced secondary flow pattern compared to 45° angled ribs. Therefore, Nu/Nu_o is higher on L2 and T2 surfaces than L1 and T1 surfaces at stationary condition. Nu/Nu_s gradually increases with rotation on L1, T1, and T2 surfaces while gradually decreases with rotation on L2 surface. Effect of rotation on heat transfer for inverted 45° angled ribs is stronger than 45° angled ribs.

Nu/Nu_o on all the surfaces is very similar at stationary condition. The lowest total thermal performance at stationary condition for 90° rib is due to higher pressure drop. However, heat transfer enhancement increases with rotation for 90° rib and the effect of rotation on heat transfer enhancement is the highest. Heat transfer is enhanced on L1, T1, and T2 surfaces while declined slightly on L2 surface due to rotation. 90° rib has the highest total thermal performance at highest rotation number of 0.58.

5.2 Trailing Edge – Wedge Channel

Heat transfer has been experimentally measured inside a wedge-shaped channel to simulate the trailing edge of the gas turbine blade. Smooth surface as well as the 45° ribbed surface was tested to see the heat transfer enhancement. Tapered ribs were used to improve the low heat transfer regions of the inner and mid-span. The coolant has been discharged through six slots and the local mass rate remaining in the channel has been determined. The experiments were conducted under high rotation number and high

buoyancy parameter to simulate the actual engine condition. The following conclusions can be drawn:

1. Based on the stationary results, Nusselt number is the highest near the narrow region due to slot ejection for both smooth and ribbed cases. Heat transfer decreased towards the wide region of the channel due to reduced slot ejection effect. Tapered ribs enhance heat transfer on the ribbed surface but still lower than the region with ejection.
2. Effect of rotation is stronger near the wider region (inner) than the narrow region (outer). Slot ejection dominates over rotation and heat transfer enhances due to rotation near the narrow region.
3. With the channel orientation of 135°, average Nusselt number ratio (Nu/Nu_o) gradually increases with rotation.
4. Both the rotation number and buoyancy parameter can be correlated to predict the heat transfer enhancement for the smooth case and ribbed case in the extended range.

REFERENCES

[1] Han, J. C., Dutta, S., and Ekkad, S. V., 2000, *Gas Turbine Heat Transfer and Cooling Technology*, Taylor and Francis, New York.

[2] Han, J. C., 1984, "Heat Transfer and Friction in Channels with Two Opposite Rib-Roughened Walls," ASME J. Heat Transfer, **106**, pp.774-781.

[3] Han, J. C., 1988, "Heat Transfer and Friction Characteristics in Rectangular Channels with Rib Turbulators," ASME J. Heat Transfer, **110**, pp. 321-328.

[4] Han, J. C., and Zhang, P., 1991, "Effect of Rib-Angle Orientation on Local Mass Transfer Distribution in a Three-Pass Rib-Roughened Channel," ASME J. Turbomach., **113**, pp. 123-130.

[5] Taslim, M. E., and Lengkong, A., 1998, "45 deg Staggered Rib Heat Transfer Coefficient Measurements in a Square Channel," ASME J. Turbomach., **120**, pp. 571-580.

[6] Taslim, M. E., and Spring, S. D., 1994, "Effects of Turbulator Profile and Spacing on Heat Transfer and Friction in a Channel," J. Thermophys. Heat Transfer, **8**(3), pp. 555-562.

[7] Liu, Y.H., Wright, L.M., Fu, W.L., and Han, J. C., 2007, "Rib Spacing Effect on Heat Transfer in Rotating Two-Pass Ribbed Channel (AR=1:2)," J. Thermophys. Heat Transfer, **21**(3), pp. 582-595.

[8] Metzger, D. E., and Vedula, R. P., 1987, "Heat Transfer in Triangular Channels with Angled Roughness Ribs on Two Walls," Exp. Heat Transfer, **1**, pp. 31-44.

[9] Ahn, S.W., and Son, K.P., 2002, "Heat Transfer and Pressure Drop in the Roughened Equilateral Triangular Duct," Int. Comm. Heat Mass Transfer, **29**, pp. 479-488.

[10] Haasenritter, A., and Weigand, B., 2001, "Heat Transfer in Triangular Rib-Roughened Channels," ASME Paper No. NHTC 2001-20245.

[11] Lee, D. H., Rhee, D. H., and Cho, H. H., 2006, "Heat Transfer Measurements in a Rotating Equilateral Triangular Channel with Various Rib Arrangements," ASME Paper No. GT 2006-90973.

[12] Dutta, S., Han, J.C., and Lee, C.P., 1996, "Local Heat Transfer in a Rotating Two-Pass Ribbed Triangular Duct with Two Model Orientations," Int. J. Heat Mass Transfer, **39**, pp. 707-715.

[13] Zhang, Y. M., Gu, W. Z., and Han, J. C., 1994, "Augmented Heat Transfer in Triangular Ducts with Full and Partial Ribbed Walls," J. Thermophys. Heat Transfer, **8**, pp. 574-579.

[14] Kays, W., Crawford, M., and Weigand B., 2005, *Convective Heat and Mass Transfer*, McGraw Hill, New York.

[15] Wright, L.M., Lee, E., and Han, J.C., 2005, "Influence of Entrance Geometry on Heat Transfer in Rotating Rectangular Cooling Channels (AR = 4:1) with Angled Ribs," ASME J. Heat Transfer, **127**(4), pp. 378 – 387.

[16] Liu, Y.H., Huh, M., Han, J. C., and Chopra, S., 2007, "Heat Transfer in a Two-Pass Rectangular Channel (AR=1:4) under High Rotation Numbers," ASME Paper, No. GT 2007-27067.

[17] Wright, L.M., Liu, Y.H., Han, J-C, and Chopra, S., 2007, "Heat Transfer in a Trailing Edge, Wedge-Shaped Cooling Channels under High Rotation Numbers," 2007, ASME Paper No. GT 2007-27093.

[18] Wagner, J. H., Johnson, B. V., and Hajek, T. J., 1991a, "Heat Transfer in Rotating Passage with Smooth Walls and Radial Outward Flow," ASME J. Turbomach., **113**, pp. 42–51.

[19] Wagner, J. H., Johnson, B. V., and Kopper, F. C., 1991, "Heat Transfer in Rotating Serpentine Passages with Smooth Walls," ASME J. Turbomach.*,* **113**, pp. 321-330.

[20] Johnson, B. V., Wagner, J. H., Steuber, G. D., and Yeh, F. C., 1994b, "Heat Transfer in Rotating Serpentine Passage with Selected Model Orientations for Smooth or Skewed Trip Walls," ASME J. Turbomach., **116**, pp. 738–744.

[21] Fu, W. L., Wright, L. M., and Han, J. C., 2004, "Heat Transfer in Two-Pass Rotating Rectangular Channels (AR=1:2 and AR=1:4) with 45º Angled Rib Turbulators," ASME Paper No. GT 2004-53261.

[22] Zhou, F., Lagrone, J., and Acharya, S., 2004, "Internal Cooling in 4:1 AR Passages at High Rotation Numbers," ASME Paper No. GT 2004-53501.

[23] Liou, T.M., Chang, S.W., Hung, J.H., and Chiou, S.F., 2007, "High Rotation Number Heat Transfer of 45° Rib-Roughened Rectangular Duct with Two Channel Orientations," Int. J. Heat Mass Transfer, **50**, pp. 4063-4078.

[24] Dutta, S., and Han, J. C., 1996, "Local Heat Transfer in Rotating Smooth and Ribbed Two-Pass Square Channels with Three Channel Orientations," ASME J. Heat Transfer, **118**, pp. 578–584.

[25] Park, C. W., and Lau, S. C., 1998, "Effect of Channel Orientation of Local Heat (Mass) Distributions in A Rotating Two-Pass Square Channel with Smooth Walls," ASME J. Heat Transfer, **120**, pp. 624–632.

[26] Bons, J.P., and Kerrebrock, J.L., 1999, "Complementary Velocity and Heat Transfer Measurements in a Rotating Cooling Passage with Smooth Walls," ASME J. Turbomach., **121**, pp. 651-662.

[27] Azad, G. S., Uddin, M. J., Han, J. C., Moon, H. K., and Glezer, B., 2002, "Heat Transfer in a Two-Pass Rectangular Rotating Channel with 45-Deg Angled Rib Turbulators," ASME J. Turbomach., **124**, pp. 251-259.

[28] Griffith, T. S., Al-Hadhrami, L., and Han, J. C., 2002, "Heat Transfer in Rotating Rectangular Cooling Channels (AR=4) with Angled Ribs," ASME J. Heat Transfer, **124**, pp. 617-625.

[29] Acharya, S., Agarwal, P., and Nikitopoulos, D. E., 2004, "Heat/Mass Transfer in a 4:1 AR Smooth and Ribbed Coolant Passage with Rotation in 90-Degreee and 45-Degree Orientations," ASME Paper No. GT2004-53928.

[30] Fu, W. L., Wright, L. M., and Han, J. C., 2005, "Buoyancy Effects on Heat Transfer in Five Different Aspect-Ratio Rectangular Channels with Smooth Walls and 45-Degree Ribbed Walls," ASME Paper No. GT 2005-68493.

[31] Su, G., Chen, H.C., Han, J.C. and Heidmann, D., 2004, "Computation of Flow and Heat Transfer in Two-Pass Rotating Rectangular Channels (AR=1:1, AR=1:2, AR=1:4) with 45-Deg Angled Ribs by a Reynolds Stress Turbulence Model," ASME Paper No. GT 2004-53662.

[32] Lowdermilk, W.H., Weiland, W.F., and Livingood, J.N.B., 1954, "Measurement of Heat Transfer and Friction Coefficients for Flow of Air in Noncircular Ducts at High Surface Temperatures," NACA RM E53J07.

[33] Obot, N.T., 1985, "Heat Transfer in a Smooth Scalene Triangular Duct with Two Rounded Corners," Int. Comm. Heat Mass Transfer, **12**, pp. 251-258.

[34] Zhang, Y.M., Gu, W.Z., and Han, J.C., 1994, "Augmented Heat Transfer in Triangular Ducts with Full and Partial Ribbed Walls," J. Thermophys. Heat Transfer, **8**, pp. 574-579.

[35] Harasgama, S.P. and Morris, W.D., 1988, "The Influence of Rotation on the Heat Transfer Characteristic of Circular, Triangular, and Square-Sectioned Coolant Passages of Gas Turbine Rotor Blades," ASME J. Turbomach., **110**, pp. 44-50.

[36] Kumaran, T.K., Han, J.C., and Lau, S.C., 1991, "Augmented Heat Transfer in a Pin Fin Channel with Short or Long Ejection Holes," Int. J. Heat Mass Transfer, **34(**10), pp. 2617-2628.

[37] Taslim, M.E., Li, T., and Spring, S.D., 1995, "Experimental Study of the Effects of Bleed Holes on Heat Transfer and Pressure Drop in Trapezoidal Passages with Tapered Turbulators," ASME J. Turbomach., **117**, pp. 281-289.

[38] Hwang, J.J., and Lu, C.C., 2001, "Lateral-Flow Effect on Endwall Heat Transfer and Pressure Drop in a Pin Fin Trapezoidal Duct with Various Pin Shapes," ASME J. Turbomach, **123**, pp. 133-139.

[39] Lau, S.C., Han, J.C., and Kim, Y.S., 1989a, "Turbulent Heat Transfer and Friction in Pin Fin Channels with Lateral Flow Ejection," ASME J. Heat Transfer, **111**, pp.51-58.

[40] Lau, S.C., Han, J.C., and Batten, T., 1989b, "Heat Transfer, Pressure Drop, and Mass Flow Rate in Pin Fin Channels with Long and Short Trailing Edge Ejection Holes," ASME J. Heat Transfer, **111**, pp. 116-123.

[41] Lau, S.C., McMillin, R.D., and Kukreja, R.T., 1992, "Segmental Heat Transfer in a Pin Fin Channel with Ejection Holes," Int. J. Heat Mass Transfer, **35(**6), pp. 1407-1417.

[42] Kline, S.J., and McClintock, F.A., 1953, "Describing Uncertainty in Single-Sample Experiments," Mech. Eng., **75**, pp. 3-8.

VITA

Name: Yao-Hsien Liu

Address: 3123 TAMU, Department of Mechanical Engineering, Texas A&M University, College Station, Texas 77843

Email Address: yaohsien@neo.tamu.edu

Education: B.S., Mechanical Engineering, National Taiwan University, 2002

M.S., Mechanical Engineering, Texas A&M University, 2005

Ph.D.., Mechanical Engineering, Texas A&M University, 2008